UNIVERSIDAD EUROPEA DE MADRID

ESCUELA DE ARQUITECTURA, INGENIERÍA Y DISEÑO

DEGREE IN AEROSPACE ENGINEERING

FINAL PROJECT REPORT

PRELIMINARY DESIGN OF AN UAV FOR ISR

JAVIER COLOM GÓMEZ

YEAR 2023-2024

TITLE: PRELIMINARY DESIGN OF AN UAV FOR ISR

AUTHOR: JAVIER COLOM GÓMEZ

SUPERVISOR: JOSE OMAR MARTINEZ LUCCI

DEGREE OR COURSE: AEROSPACE ENGINEERING

DATE: 2024

ABSTRACT

This report presents the preliminary design of an Unmanned Aerial Vehicle (UAV) specifically for Intelligence, Surveillance, and Reconnaissance (ISR) missions. The UAV features a fixed-wing configuration with vertical take-off and landing (VTOL) capability and hybrid propulsion to facilitate operations in confined spaces and diverse environments. The fuselage integrates detachable wings to facilitate transportation and a high-wing configuration to improve stability.

Key components of the UAV include a payload bay capable of housing various ISR sensors, such as Electro-Optical/Infrared (EO/IR) cameras and Synthetic Aperture Radar (SAR), enhancing mission versatility. The UAV is also equipped with autonomous navigation systems and onboard processing units for real-time data analysis and decision-making.

The design process includes aerodynamic analysis using Computational Fluid Dynamics (CFD) with Ansys Fluent and Aeolus for aerodynamic optimization, as well as validation of the UAV's stability and performance. The UAV's structure has been designed to accommodate the necessary systems while maintaining aerodynamic efficiency. The structural design consists of a monocoque fuselage and the use of composite materials, primarily carbon fiber, optimizing the strength-to-weight ratio.

Keywords: UAV, ISR, VTOL, CFD, Preliminary design, Autonomous navigation

RESUMEN

Este informe presenta el diseño preliminar de un vehículo aéreo no tripulado (UAV) específico para misiones de inteligencia, vigilancia y reconocimiento (ISR). El UAV presenta una configuración de ala fija de despegue y aterrizaje vertical (VTOL) de motorización híbrida para facilitar las operaciones en espacios reducidos y entornos diversos. El fuselaje integra alas desmontables para facilitar el transporte y una configuración de ala alta para mejorar la estabilidad.

Los componentes clave del UAV incluyen una bahía de carga útil capaz de alojar varios sensores ISR, como cámaras electro-ópticas/infrarrojas (EO/IR) y radares de apertura sintética (SAR), mejorando la versatilidad de la misión. El UAV también está equipado con sistemas de navegación autónomos y unidades de procesamiento a bordo para el análisis de datos en tiempo real y la toma de decisiones.

El proceso de diseño incluye un análisis aerodinámico mediante dinámica de fluidos computacional (CFD) con Ansys Fluent y Aeolus para la optimización aerodinámica, así como la validación de la estabilidad y el rendimiento del UAV. La estructura del UAV ha sido diseñada para alojar los sistemas necesarios manteniendo la eficiencia aerodinámica. Para ello, el diseño estructural consiste en un fuselaje monocasco y en el empleo materiales compuestos, principalmente fibra de carbono, optimizando la relación resistencia-peso.

Palabras clave: UAV, ISR, VTOL, CFD, Preliminary design, Navegación autónoma

ACKNOWLEDGEMENTS

I would like to dedicate my deepest gratitude first and foremost to my TFG tutor, Omar Martínez. Whenever I sought his guidance, he always knew how to wisely impulse the project, and he never had any trouble finding time for me when I needed it.

I also want to express my most profound appreciation to my family, who have supported me unwaveringly throughout all my years of study. I cannot forget my colleagues, who have taught me so much and helped me during this final stage, assisting me with everything I needed to undertake this project.

Contents

Figures

.

Tables

.

Abbreviations

AESA	Agencia Estatal de Seguridad Aérea
BVLOS	Beyond Visual line of Sight
CAGR	Compound Annual Growth Rate
CFD	Computational Fluid Dynamics
DGAM	Dirección General de Armamento y Material
EASA	European Union Aviation Safety Agency
EMI	Electromagnetic Interference
EO/IR	Electro-optic / Infrared
FCAS	Future Combat Air System
GCS	Ground Control Station
GMTI	Ground Moving Target Indicator
ICE	Internal Combustion Engine
IMU	Inertial Measurement Unit
INTA	Instituto Nacional de Técnica Aeroespacial
ISAR	Inverse Synthetic Aperture Radar
ISIS	Islamic State of Iraq and Syria
ISR	Intelligence, Surveillance, and Reconnaissance
KTAS	Knots True Airspeed
MANET	Mobile Ad Hoc Network
MMTI	Maritime Moving Target Indicator
NED	North-East-Down
PDB	Power Distribution Board
PSE	Primary Structure Element
RPM	Revolutions Per Minute
RTH	Return To Home
SAR	Synthetic Aperture Radar
SFC	Specific Fuel Consumption
SIGINT	Signals Intelligence
SMR	Short to Medium Range
UAS	Unmanned Aerial System
UAV	Unmanned Aerial Vehicle
USD	United States Dollar
VTOL	Vertical Take-Off and Landing

Chapter 1. INTRODUCTION

Currently, the use of unmanned aerial vehicles has proven to be an extremely useful tool due to their versatility, cost and the reduced risk involved in their use, as they can be operated remotely or even autonomously.

Their use includes ISR missions, target acquisition and electronic warfare, among others. However, this project focuses on the development of a UAV for ISR missions. The demand for this type of UAVs has increased notably in recent years, which opens up a very interesting market opportunity for the manufacturers of these aircraft.

This project involves the development of a UAV equipped for ISR missions that aims to bring together all the elements necessary for its use in the short and medium term. These include target detection using EO/IR sensors, 3D surface mapping, SAR, high level of autonomy through artificial intelligence, MANET communication networks and satellite datalink.

Chapter 2. MARKET ANALYSIS

In recent decades, warfare strategies have undergone significant changes due to the emergence of new technologies and platforms. Additionally, major powers like the US, Russia, and China are concentrating on developing advanced and powerful weapons that can effectively destroy enemy targets using cost-efficient and reliable methods.

UAVs have demonstrated their utility in various scenarios. For example, drones have been heavily utilized in counter-terrorism efforts, especially in regions like the Middle East and South Asia. Conflicts such as the ISIS insurgency, the Indo-Pak conflict over Kashmir, Russian military actions in Ukraine, the Syrian civil war, the Lebanon conflict, and the tensions between the US and North Korea have heightened security concerns. These factors contribute positively to the market, thus driving its growth during the forecast period.

2.1 Market Forecast

The UAV Market is projected to grow by USD 20.40 billion, with a compound annual growth rate (CAGR) of 9.96% from 2023 to 2028. This market expansion is influenced by several factors, including increased defense budgets for unmanned technologies, cost-effectiveness compared to fighter jets, and the development of miniaturized electro-optical/infrared (EO/IR) systems. In recent years, technological advancements and new platforms have significantly altered warfare strategies. Aviation designers are focusing on enhancing performance while maintaining or reducing operational costs. The rapid growth of the market is driven by technological progress and the rising demand for aerial surveillance and reconnaissance.

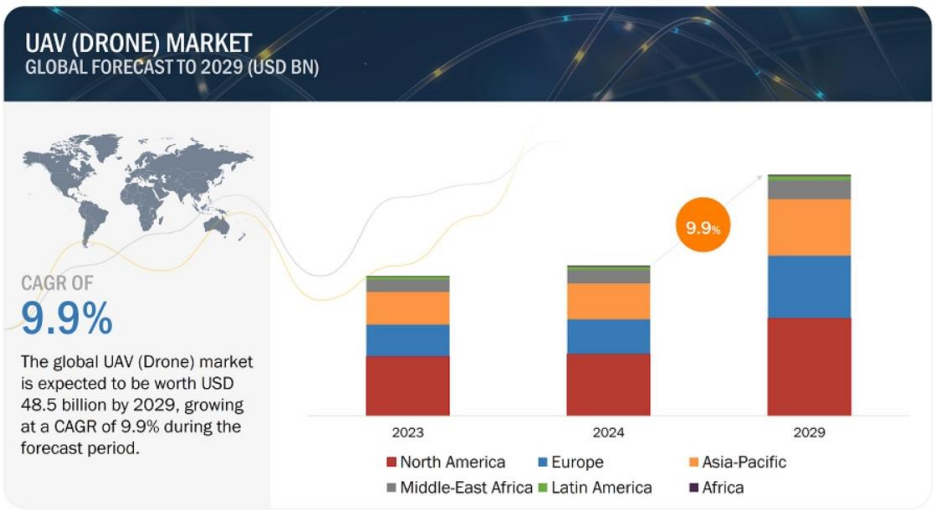

Figure 1. UAV (DRONE) Market global forecast to 2029. (MarketsandMarkets, 2022)

The defense and homeland security sector are projected to experience substantial growth over the forecast period. This is driven by rapid advancements in microelectronic components and other aerospace technologies, leading to the creation of modern tactical UAVs. These new UAVs offer superior performance compared to earlier models and are capable of being used in highly demanding combat missions.

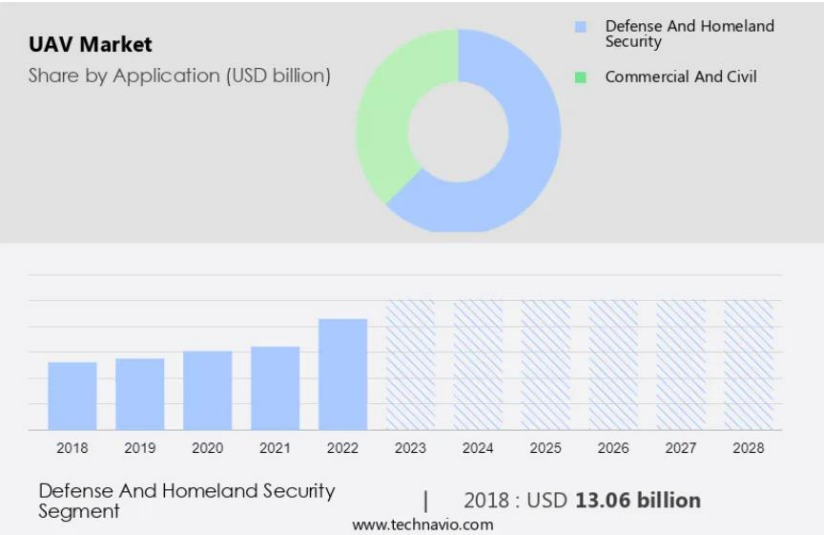

Figure 2. UAV Market, share by application. (Technavio, 2024)

2.2 Competitors

The UAV market has seen significant growth and technological advancements, leading to the emergence of specialized UAVs designed for various applications. Among these, the VTOL configuration stands out for its flexibility and efficiency in diverse operational environments. Two prominent players in this segment are AR3 Tekever and Koios UAVs, each offering unique capabilities and innovations in their VTOL UAV designs.

Tekever is a notable player in the UAV market, known for its innovative unmanned aerial systems designed for various applications including maritime surveillance, search and rescue, and environmental monitoring. Tekever focuses on integrating advanced technologies to enhance the capabilities and efficiency of their UAVs. Below is a detailed overview of these key competitors and their contributions to the VTOL UAV market.

Figure 3. AR3 Tekever VTOL UAV

AR3 Tekever main characteristics:

- MTOW: 25 kg
- Wingspan: 3.5 m
- Payload Capacity: 4 kg
- Flight Endurance: 8 hours
- Endurance: 8 hours
- Service Ceiling: 3,600 m AMSL
- Propulsion system: Hybrid

Koios is another key competitor in the UAV industry, recognized for its innovative VTOL UAV designs tailored for both commercial and defense applications. Koios focuses on delivering high-performance UAVs that meet the rigorous demands of modern aerial operations.

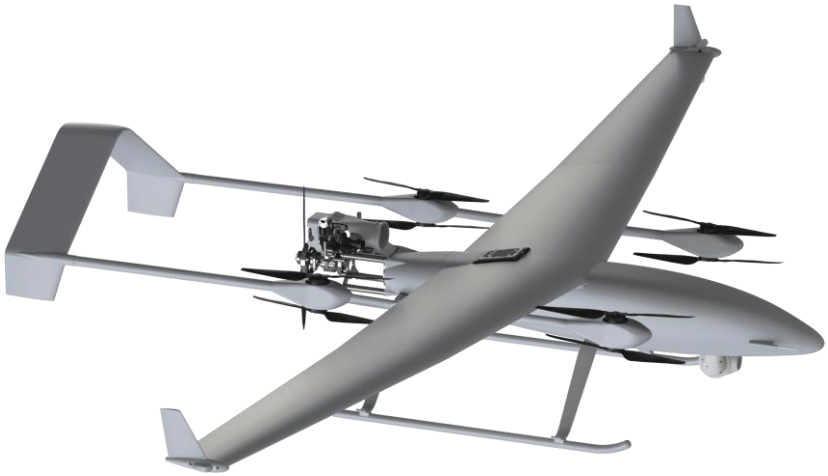

Figure 4. Koios VTOL UAV

Koios main characteristics:

- MTOW: 35 kg
- Wingspan: 4 m
- Payload + Fuel Capacity: 7 kg
- Endurance: 6-8 hours
- Cruise Speed: 25 m/s
- Propulsion system: Hybrid

Given the substantial growth projections for the UAV market, it is clear that investing in the development of a new UAV specifically designed for ISR missions is economically justified. The market is expected to expand significantly, with UAVs playing a critical role in both military and commercial applications due to their versatility and advanced technological capabilities. Companies like AR3 Tekever and Koios UAVs are already setting high standards with their VTOL configurations, offering impressive performance and operational flexibility.

Developing a new UAV that can compete with these existing models will not only tap into the growing demand for ISR capabilities but also leverage the ongoing advancements in UAV technology. With the market poised to grow by USD 20.40 billion at a CAGR of 9.96% between

2023 and 2028, as noted in multiple market reports, the potential for high returns on investment makes this a promising venture. Therefore, pursuing the development of a competitive ISR UAV is a strategic move that aligns with the market trends and future growth opportunities.

Chapter 3. CONCEPTUAL DESIGN

3.1 Mission analysis

3.1.1 Flight profile

UAVs have become integral to modern ISR operations. These UAVs, particularly short-to-medium range (SMR) models, are extensively used in both civil and military domains for tasks such as tactical reconnaissance, surveillance, and search and rescue missions. The aerodynamic design and mission topology of these UAVs play a crucial role in ensuring their efficiency and effectiveness. Next figure shows the flight profile for a VTOL ISR UAV.

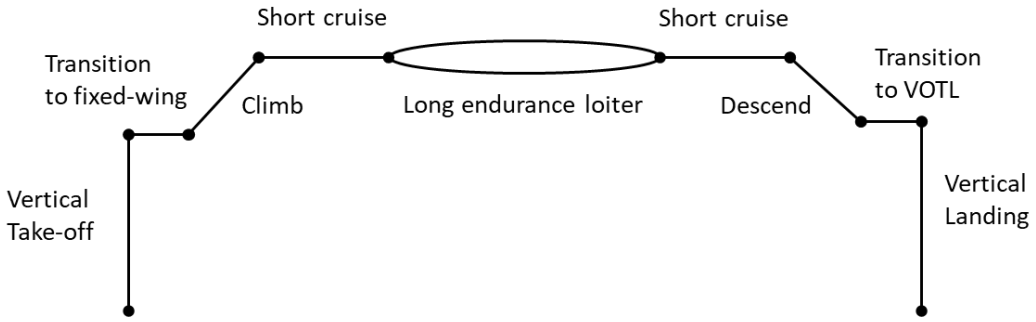

Figure 5. Flight profile for ISR UAV

Vertical Take-off

The mission begins with the UAV taking off vertically from a designated launch area. During this phase, the UAV's vertical propulsion system provides the necessary thrust to achieve lift-off, while the control systems manage the power to each engine to stabilize the UAV and to maintain the heading desired, always facing wind. Horizontal propulsion system may start working if wind pushes the UAV backwards, keeping the aircraft in a straight vertical path to the transition height.

Transition to fixed wing

When the transition altitude is reached, the horizontal thrust motor progressively increases power to move the UAV forward. As the speed relative to the wind increases, the power of the vertical thrust motors is progressively reduced until the speed required for the wing to fully support the aircraft is reached.

Climb

In this phase, UAV gains altitude by increasing the angle of attack and power to the main engine until the desired mission height is reached.

Ingress to Target Area

Once at the desired altitude, the UAV enters the ingress phase, cruising towards the target area. This phase ensures that the UAV positions itself over the area of interest, ready to commence its surveillance tasks.

Loiter

Upon reaching the target area, the UAV transitions into the loiter phase, where it circles or hovers over a specific location to perform its surveillance duties. This phase is optimized for long endurance. The loiter time is a crucial component, allowing the UAV to gather extensive data and maintain continuous surveillance over the target.

Egress from Target Area

After completing its surveillance operations, the UAV begins the egress phase, departing the target area and heading back towards its base. This phase ensures that the UAV safely exits the operational area and returns to a controlled airspace.

Transition to VTOL

This phase is the opposite of the transition from VTOL to fixed wing. In this case, the UAV progressively reduces speed by lowering engine power and increasing the angle of attack to remain airborne. When the transition speed is reached, the vertical thrust engines are activated and given the aircraft's positive angle of attack, produce sufficient thrust to maintain the aircraft's altitude and slow it down. The phase ends with the UAV flying at a fixed point using the vertical thrust engines to support its weight while the horizontal thrust engine is activated only to counteract the thrust produced by the wind, if necessary.

Landing

The final phase involves the UAV descending from its final transition point to land. The descent is managed carefully to ensure a smooth approach, minimizing the risk of damage upon landing. Landing phase finishes when the UAV touches ground with its landing gear.

3.1.2 Payload for ISR missions

UAVs designed ISR missions must be equipped with a variety of specialized payloads to effectively gather and transmit critical data. The payload for ISR UAVs typically includes sensors, communication equipment, and additional support systems, each serving a distinct purpose to ensure mission success.

Electro-Optical/Infrared (EO/IR) Sensors

EO/IR sensors are essential for capturing high-resolution imagery and video in both daylight and nighttime conditions. These sensors provide real-time visual intelligence, enabling operators to monitor areas of interest, identify targets, and assess situations. The infrared capability allows for thermal imaging, which is crucial for detecting heat signatures from vehicles, equipment, and personnel, even in low visibility conditions.

Synthetic Aperture Radar (SAR)

SAR systems are used for ground mapping and target detection, especially in adverse weather conditions. SAR can penetrate clouds, fog, and foliage, providing high-resolution radar images of the terrain below. This is particularly useful for mapping large areas and identifying changes or movements over time.

Signals Intelligence (SIGINT) Equipment

SIGINT payloads are used to intercept and analyze electronic signals, including communications and radar emissions. This equipment helps in gathering intelligence on enemy communications, electronic systems, and operational patterns.

Communication Relay Systems

These systems enable the UAV to act as a relay station, extending the communication range between ground forces, command centers, and other UAVs. This is critical in ensuring continuous and reliable communication during operations, especially in remote or hostile environments.

3.1.3 Top level requirements

Based on the market and ISR mission analyses carried out, the most relevant aspects to be taken into account for the preliminary design of the UAV are defined:

- **Long endurance**: The UAV should have extended flight endurance to conduct prolonged surveillance missions without frequent refueling or battery changes. This enables it to loiter over the area of interest for an extended period, collecting valuable intelligence.
- **Payload capacity**: Sufficient payload capacity is essential to carry a variety of sensors, cameras, and other equipment required for intelligence gathering. This includes electro-optical/infrared (EO/IR) sensors, synthetic aperture radar (SAR), signals intelligence (SIGINT) systems, and electronic warfare (EW) payloads.
- **Real-time Data transmission**: the UAV should be equipped with reliable communication systems for real-time transmission of sensor data and imagery to ground control stations or other command centers. This enables operators to receive timely intelligence and make informed decisions.
- **Autonomous operation**: Autonomous or semi-autonomous operation allows the UAV to execute predefined flight paths, conduct surveillance patterns, and perform tasks without constant manual control. This reduces the workload on operators and enhances mission efficiency.
- **Stealth and low observability capabilities**: Stealth features, such as reduced acoustic signature, help the UAV evade detection by enemy radar and air defense systems. Low observable characteristics enhance survivability and mission effectiveness in contested environments.
- **Adaptability and modular design**: An ISR UAV should have a modular design that allows for easy integration of different sensors and payloads to meet evolving mission requirements. This flexibility enables the UAV to adapt to various scenarios and operational environments.
- **Data fusion and analysis capabilities**: The UAV should have onboard processing capabilities for data fusion and analysis, enabling it to extract actionable intelligence from sensor data in real-time. This facilitates rapid decision-making and enhances the value of collected information. Also, it allows to process on board the data and transmit high value intelligence in a narrowed bandwidth.

- **Interoperability**: Interoperability with existing military networks and command and control systems allows the UAV to seamlessly integrate into broader intelligence-gathering operations and share information with other assets.
- **Easy to operate and maintain:** This means reduced pre-flight preparation and maintenance times, and takes into account logistic footprint and reliability.

Considering its versatility, it is interesting that it has the capability to be deployed in multiple environments, both on land and at sea (from ships). This characteristic means that it must be relatively easy to transport, so its maximum dimensions and weight must be limited.

In terms of payload, the ability of processing on board requires sufficient data from it sensors. To extend the UAV capabilities over time, it should carry out as much payloads as possible without scarifying performance.

In terms of range and autonomy, different UAV configurations must be considered. Multi-rotor configuration is ruled out, as the only sustaining element of these systems are their propellers, making them less propulsively efficient than fixed-wing aircraft, which employs the wing to generate lift. However, they have the advantage of being highly versatile in operation and do not require other systems for launch and recovery.

On the other hand, fixed-wing aircraft are more efficient in flight than multi-rotors. On the other hand, they need either a runway for take-off and landing or other systems for launch, such as a launcher and a net, which increases its logistic footprint.

Taking into account all the aforementioned, the UAV configuration will consist in a VTOL fixed wing, aiming to gather the benefits of both configurations. High-level requirements for the aircraft can be derived from the discussion above:

- Endurance: 8-10 hours
- Range: 350 km
- MTOM: 40 kg
- Max wingspan: 4 m
- Deployable from ships
- Payload: EO/IR, 3D mapping sensor, SAR, SIGINT

3.1.4 Certification Basis

The main market for the proposed UAV is the military, so airworthiness certification should come from the military rather than the civilian sector. However, the capabilities of the proposed UAV may fit for civilian applications, such as geographic monitoring, topographic surveying, fire detection and monitoring, and wildlife tracking, among others. Therefore, depending on the application, the certification should have a civilian or military basis.

Civil certification

Civil airworthiness is governed by EASA at European level, with AESA being the competent authority on national territory. In this respect, there are two regulations governing the use of UAVs:

- Regulation (EU) 2019/947: This regulation lays down detailed provisions for the operation of unmanned aircraft systems (UAS) and defines the requirements for their safe use. It includes rules for the different categories of UAS operations: Open, Specific, and Certified, each with specific operational limitations, requirements, and procedures. The regulation also covers aspects such as operator registration, remote pilot competence, and operational authorizations.
- Regulation (EU) 2019/945: This regulation sets the product requirements for unmanned aircraft systems and their accessories. It outlines the technical specifications and standards that UAS must meet to ensure safety and interoperability within the EU. This includes requirements for design, manufacturing, and environmental considerations, as well as the obligations for manufacturers, importers, and distributors to ensure that UAS placed on the market comply with these standards.

The proposed UAV would fall into the specific category, as the type of operation (BVLOS) and weight is outside the open category; and as it does not carry people, hazardous materials or fly over densely populated areas, it does not fall into the certified category.

EASA provides operational scenarios, called standard scenarios, which do not require a specific risk assessment as the operator is declaratively ascribed to this scenario. The intended operation would fall outside this category because it exceeds the weight of the UAV (maximum 25 kg) and the flight distance (greater than 2km). Therefore, it would be necessary to carry out a specific risk assessment following the SORA procedure, in order to assess and identify the risks of the operation and the necessary mitigations that must be implemented to achieve the required safety level.

Military certification

The airworthiness certificates for UAVs in the military sector in Spain are issued by INTA (Instituto Nacional de Técnica Aeroespacial). This procedure is governed by Royal Decree 866/2015. It is important to note in this regard that for INTA to grant the UAV certification, the DGAM (Dirección General de Armamento y Material) must first declare the project to be of national defense interest.

3.2 Systems definition

3.2.1 Payload

To fulfil the mission requirements, next is listed the payloads that the UAV will carry.

3.2.1.1 Gimbal EO/IR

State of the art multi-mission EO/LWIR surveillance system. Combining a global shutter EO sensor with FHD video featuring 90x super resolution zoom and cooled LWIR sensor with 30x optical zoom for super long-range tracking. The selected gimbal has the next characteristics:

- Weight: 1.27 kg
- Electro-Optical sensor: 1920x1080p
- vFOV for EO: 37.9º - 1.3º

- Max optical zoom: 30x
- Thermal Imager: LWIR 640x512p
- Thermal Imager vFOV: 30.9º - 6.7º
- Thermal Imager optical zoom: 5x
- Laser range finder
- Laser pointer
- Autotracking
- Autodetection
- Power supply: 30W

Figure 6. Gimbal EO/IR

3.2.1.2 3D Mapping sensor

A 3D mapping sensor is a device that captures depth information about its surroundings to create a three-dimensional representation of the environment. It allows a 3D representation from the image obtained by its 5 cameras. For ISR missions, it can provide key information of a designated area. Also, with data fusion onboard the UAV, it could be shared a real-time 3D map with enemies' position to the soldiers on the field, derived from the autodetection capability of the gimbal. The selected sensor has the next features:

- Weight: 1.3 kg
- Sensor: Full frame Exmor RCMOS
- Oblique lens angle: 45º
- Power supply: 60W

Figure 7. 3D Mapping sensor

3.2.1.3 SAR

SAR payload selected is an advanced radar imaging system used in satellites for earth observation. It utilizes synthetic aperture radar technology to produce high-resolution images of the Earth's surface regardless of weather conditions or daylight. The main capabilities of this payload are listed below:

- Weight: 3.04 kg
- Power supply: 81 W
- SAR Imaging Resolution: 0.3 m to 1 m
- Maximum Range: 10 km to 16 km
- GMTI Vehicle Detection and Tracking: 7 km
- Maritime Surveillance Detection and Geolocation: 104 NM (192 km)
- MMTI Detection and Tracking: 41 NM (75 km)
- ISAR Classification: 22 NM (40 km)
- MMTI Max Coverage: 1,900 NM^2/h (6,500 km^2/h) at 50 KTAS

Figure 8. SAR Payload

3.2.1.4 SIGINT Spectrum analyzer

A spectrum analyzer is a device used to analyze the frequency spectrum of signals. It displays signal amplitude versus frequency, allowing users to visualize and measure the characteristics of different frequency components within a signal. In this sense, it is an extremely useful tool for the detection of other unmanned vehicles or other communications of interest. The main features of the selected payload are listed below:

- Weight: 0.75 kg
- Frequency range: 9kHz to 6.2 GHz
- Power supply: 4W

Figure 9. Spectrum analyzer

3.2.2 Airframe

As described in the high-level requirements, the autonomy should be maximized while keeping logistical footprint to a minimum. Therefore, the proposed solution consists of a VTOL fixed-wing UAV. While it's true that the flight efficiency will never be superior to that of a purely fixed-wing equivalent, this configuration solution provides the UAV with great versatility, being able to take off and land in confined spaces without the need for auxiliary systems for takeoff and landing.

Regarding the landing gear, the proposed solution aims to improve upon its main competitor by characteristics, the UAV Koios. The Koios has fixed landing gear, which generates greater aerodynamic drag during flight. Therefore, the landing gear of the proposed UAV will be retractable and located in the arms, so that after VTOL mode takeoff, the landing gear will retract, reducing drag.

The payload has an approximate weight of about 7 kg, so a market review of VTOL UAV solutions with a similar range, autonomy, and payload weight is carried out to obtain a first approximation of the UAV's MTOM to be developed, as well as its wingspan. This results in a 40 kg MTOM aircraft with a wingspan of around 4 meters.

3.2.3 Propulsion system

Regarding the propulsion system, VTOLs typically have two: one for takeoff and landing and another for fixed-wing flight. While electric propulsion presents undeniable maintenance

advantages, gasoline engines currently outperform in terms of autonomy. Therefore, it is proposed that the vertical thrust propulsion be electric, while the horizontal thrust propulsion be thermal.

3.2.3.1 Vertical propulsion system

The electric motors must be capable of lifting the weight of the UAV, but they must also have a power margin to maneuver it, especially in strong wind conditions. Unlike a conventional multirotor UAV, aerodynamic surfaces such as wings and tail will exert greater forces on the aircraft than the multirotor equivalent. This mainly has implications for the yaw moment. Multirotor are able to generate this movement by increasing the speed of two motors that rotate in the same direction, producing a reaction moment on the center of mass of the multirotor in the opposite direction. Additionally, the motors must continue to provide lift equal to the weight, so while two motors increase their rotational speed, the other two must reduce it, ensuring that the resulting force equals the weight.

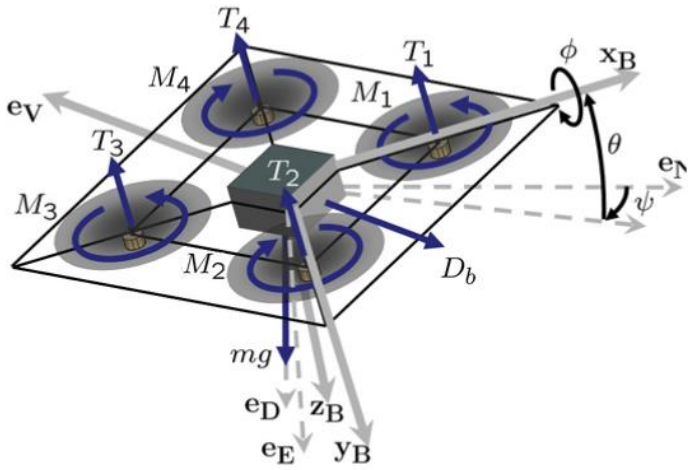

Figure 10. Illustration of quadrotor thrust and torque forces. Source: Beard, R. W., & McLain, T. W. (2012). Quadrotor Helicopter Flight Dynamics and Control: Theory and Experiment. Princeton University Press.

As Beard et al. state in his work, differential thrust between opposite motors provides roll and pitch torques. Differential thrust between the two pairs of counter-rotating motors provides yaw torque. Position control, with respect to the North-East-Down (NED) coordinate frame is accomplished by controlling the magnitude and direction of the total thrust. A drag force, D_b, also acts on the vehicle, opposite the velocity direction, e_v.[1]

Knowing the MTOM of the UAV defined by the requirements, the vertical thrust electric motors can now be selected. Due to the maneuverability issues mentioned earlier, the maximum thrust of the motors must double the MTOM, so each motor must be capable of generating 20 kg of lift. The motor selected has the next characteristics:

[1] Beard, R. W., & McLain, T. W. (2012). Quadrotor Helicopter Flight Dynamics and Control: Theory and Experiment. Princeton University Press.

- Weight:
- Working Voltage: 12S, 48V
- Max thrust: 20.997 kg
- Max current consumption: 151.70 A
- Average current consumption:42 A
- Propeller: 29x9.5 inches

Figure 11. Vertical thrust electric motor

Electrical motors are managed throw ESCs (Electronic Speed Controllers), which are on charge to provide the required voltage to motors to turn at the desired RPMs. These devices are dimensioned by the maximum output current that electric motors demand. The intended ESCs should at least provide 151.7 A each. Selected ESC can be seen in the next figure.

Figure 12. ESC 180 A selected

It is noticeable that these devices tend to over-heat if they are not properly dissipated. Therefore, the dissipater must be in contact with the airflow.

3.2.3.2 Horizontal propulsion system

As previously mentioned, to achieve the required autonomy, it is necessary to use an internal combustion engine. The energy density of the fuel is significantly higher. Although the thermal efficiency is lower than that of the electric motor, the energy density stored in batteries is much lower than that of fuel.

The specific selection of the horizontal thrust engine will be made later, once the aerodynamic drag of the UAV is known in detail. However, given the UAV's MTOM, by sizing the engine thrust to a quarter of the MTOM, the engine should be capable of producing at least 10 kg of thrust.

The power system definition will be addressed in the next section. However, considering the electrical consumption of the payload and the desired autonomy, supplying the energy demand solely with batteries would result in a significant weight penalty. Therefore, the combustion engine must be equipped with an alternator to produce the energy needed for the payload to function.

3.2.4 Power system

The function of the power system is to provide the necessary energy to all the equipment and systems of the UAV. For this purpose, batteries and an alternator will be used. The peaks in electrical consumption occur during takeoff and landing, which is when the vertical thrust motors are in operation. These motors are by far the equipment that will demand the most power during flight. Therefore, they are the ones that determine the sizing of the batteries.

Despite having an alternator, the power it would generate is insufficient to supply the vertical thrust motors. These motors require, at maximum and collectively, a power of 27.128 kW, while the alternators in internal combustion engines for these types of applications can provide a maximum of 300 W. Moreover, this power output by the alternator occurs at a specific RPM of the engine, which would produce unwanted thrust in VTOL flight mode.

Therefore, batteries capable of providing the required power and having sufficient capacity to supply the takeoff and landing phases must be selected. Additionally, the maximum discharge capacity of the batteries, measured in "C," must be considered. This "C" represents the number of times equal to the battery's maximum capacity that it can provide in current form. In other words, a 5C battery can deliver a maximum current equivalent to 5 times its nominal capacity. According to the motor manufacturer, their operating voltage is 48 V, so the batteries must be 12S. These types of batteries are quite large and may present future issues when positioning them inside the UAV. Therefore, it is proposed to use two 6S batteries connected in series.

With all this in mind, the average consumption of the vertical thrust motors must be estimated so that we can size the battery. To make this estimation, it will be assumed that the UAV ascends to 60 meters during takeoff and descends the same distance during landing. Additionally, the electric motors are also operating during transitions. Both takeoff and landing will be assumed to occur at a constant speed of 3 m/s, resulting in a total operation time of about 20 seconds for each phase. Adding 20 seconds for transitions, the total operation time is approximately 80 seconds. Assuming a thrust greater than necessary, generating a total thrust of 60 kg, the current consumption per motor according to the manufacturer's data is 72 A.

$$t_{Take-Off} = t_{Landing} = \frac{v_{vertical}}{h} = \frac{3\frac{m}{s}}{60m} = 20s$$

$$t_{transition} = 20s$$

$$t_{total} = t_{Take-Off} + t_{Landing} + 2t_{transition} = 80s$$

$$I_{total} = 4I_{motor} = 4 \cdot 72Ah = 288Ah$$

$$Capactity\ required = \frac{I_{total}t_{total}}{3600s/h} = 6.4Ah$$

$$Discharge\ Capacity = \frac{Max\ current}{Capacity\ required} = \frac{4 \cdot 151.7Ah}{6.4Ah} = 94.81C \cong 95C$$

The required capacity is 6.4 Ah for the batteries. This would mean a battery with a discharge rate of 95C is necessary. Such high discharge rate batteries are not available on the market. The highest discharge rate batteries are Lithium-Polymer (Li-Po) batteries, with a maximum discharge rate of around 30C for 12S. Semi-solid-state or Lithium-ion batteries offer better energy density than Li-Po. However, their discharge rate is around 10C. Therefore, the determining factor for selecting the battery capacity is its discharge rate.

$$Battery\ Capacity = \frac{Max\ current}{Discharge\ rate} = \frac{606.8Ah}{30} = 20.23Ah$$

Therefore, the selected batteries will be two 6S batteries in series with a 30C discharge rate. The capacity will be 22 Ah, increasing the margin slightly for safety.

Given the high power that the main batteries must deliver during the takeoff and landing phases, to avoid potential operational issues due to voltage spikes that the electric motors may produce, a smaller battery will be used to power both the avionics and the payload during these phases. Once in fixed-wing flight mode, the alternator will be responsible for powering these systems.

To manage the power system, all power sources will be connected to a power distribution board (PDB), which will efficiently distribute these power sources to all equipment. In Figure 13, a schematic of the UAV's power system can be seen.

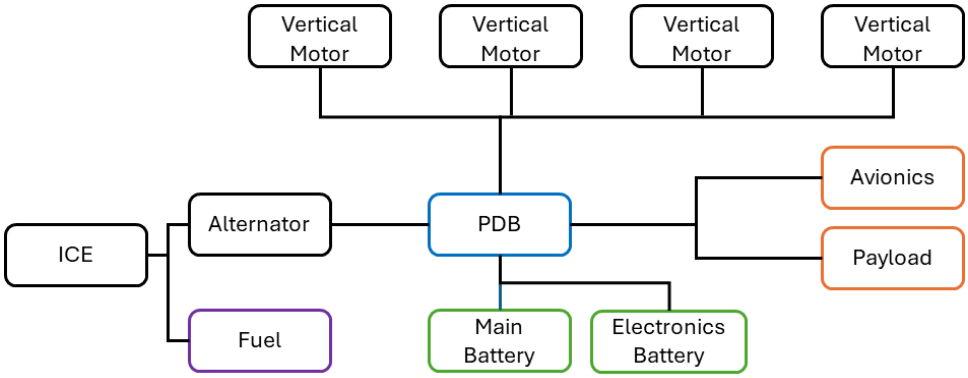

Figure 13. Power system scheme

3.2.5 Avionics

The avionics comprise the set of equipment and sensors necessary to safely perform the flight. Below is the list of components that the aircraft will be equipped with for this purpose:

- **Autopilot**: enables the aircraft to fly and navigate autonomously or semi-autonomously without direct human intervention. Essentially, it serves as the "brain" of the UAV, responsible for controlling its flight path, altitude, speed, and other parameters to execute predefined missions or tasks. It incorporates various important sensors: Inertial Measurement Unit (IMU), composed by accelerometers and gyroscopes; Barometric altimeter, to estimate altitude; and Magnetometer, to measure heading direction.

- **GPS**: provides accurate location, velocity, and time information, enabling precise navigation, waypoint following, and absolute positioning during flight. Some GPSs works using two antennas, which allows the UAV to know its heading. This is useful in environments where there are an important quantity of metallic materials and typical magnetometers does not work properly, such operations in military ships.
- **Airspeed**: measures the speed of an UAV relative to the air, providing crucial data for flight control and navigation. This sensor is connected to a Pitot tube for measuring airspeed.
- **Rangefinder**: measures the distance between the UAV and nearby objects or terrain, aiding in obstacle detection, terrain following, and altitude control. Its main objective for this aircraft is to detect the distance to the floor in landing phase, where errors from barometer and GPS are too high to be a reliable source of information, mostly when landing in ships or surfaces that are not loaded in their terrain height data.
- **Onboard Computer**: Given the importance of AI today, a UAV for ISR missions expected to be used in the medium term must have, if not the current capacity, the necessary means for the use of AI. This computer should be designed to be able to execute artificial intelligences based on neural networks, as industry trends point in this direction (FCAS).

3.2.6 Control surfaces

The control surfaces will consist of ailerons, elevons, and rudder. All of them will be actuated by servo motors connected to the autopilot. These servomotors will be powered from PDB.

3.2.7 Communication system

As required for the communication system, it must have a high degree of interconnection, as well as a significant range given the range described in the high-level requirements. There are solutions in the market that address this problem, as they allow the creation of a virtual local network where many devices can exchange information. This allows both the execution of the command and control of the aircraft and the transmission of UAV sensor information to other equipment, such as the GCS or soldiers deployed in the field.

Figure 14. Radio communication module

The radio communication system selected is optimized for mesh configuration, allowing several devices to be connected at the same network and share information. Also, it has a

MANET (Mobile Ad-Hoc Network), which allows communication between all the nodes while they are moving at a considerable speed. Also, it has encrypted communications as well as some features such as power control (that allows the module to work at the lowest power possible, making more difficult radio frequency detection) and beam forming technologies that helps to have a robust datalink. It is also resistant to EMI (Electro-Magnetic Interference) attacks.

In addition to the above, regarding detectability, the conflict in Ukraine has shown that radiofrequency emissions are a source of enemy detection. To carry out intelligence missions, it is necessary to reduce the radiofrequency footprint to the minimum possible. Therefore, it is proposed to use a small-sized satellite communications module that allows telemetry to be sent. This way, silent radio missions can be conducted, where the communication module does not send a signal, and the UAV can be visualized in the GCS through discreet transmission of its position and other relevant data via a satellite link.

In summary, the communication system would consist of:

- Communication module and antennas onboard for command and control and payload exploitation
- Satellite module for telemetry transmission in low radiofrequency footprint missions
- Ground antenna to transmit and receive from GCS

3.2.8 Ground Control Station (GCS)

The Ground Control Station serves as the command center from which operators control and monitor the UAV during its mission. Its main functions are as follows:

Command and control (C2)

- **Remote Piloting**: Allows operators to control the aircraft in real-time, including flight maneuvers such as ascent, descent, turns, and speed adjustments.
- **Mission Planning**: Operators can plan and upload preprogrammed missions to the UAV, including waypoints and specific routes.
- **Telemetry**: Receiving and monitoring real-time critical data from the aircraft, such as altitude, speed, GPS position, battery status, and other vital parameters.
- **Emergency Management**: Enables operators to make quick decisions in emergencies, such as activating return-to-home (RTH) procedures or emergency landings.

Payload exploitation

- **Sensor and Camera Control**: Allows operators to manage and configure onboard cameras and other sensors, including focus adjustments, zoom, and orientation.
- **Data Collection and Analysis**: Receiving and processing data and images captured by the payload.
- **Data Transmission**: Sending the collected data to other stations, analysis centers, or storage for further review and analysis.

In summary, the GCS is a vital component that allows for complete control and efficient exploitation of UAVs, ensuring missions are conducted safely and effectively while maximizing the utilization of data collected by the UAV's payload. Next is show the proposed GCS.

Figure 15. Ground Control Station

Also, GCS must be equipped with a set of antennas capable to set the datalink required. In order to maximize range, a tracking antenna should be selected. This kind of antennas, in opposition to omnidirectional antennas, allows the radiofrequency beam to be concentrated in a sector that increases gain.

Figure 16. GCS tracking antenna

Apart from the main UAV control station, from which the aircraft is intended to be controlled most of the time, the use of another portable control station is also proposed. The reason is that deployed soldiers can take control of the UAV if needed, to obtain information from a place of interest. The proposed portable control station is shown in the following figure:

Figure 17. Portable Ground Control Station

3.3 General arrangement

Taking into account all the information mentioned above and after several design iterations, the general arrangement of the UAV is shown in the following Figure 18.

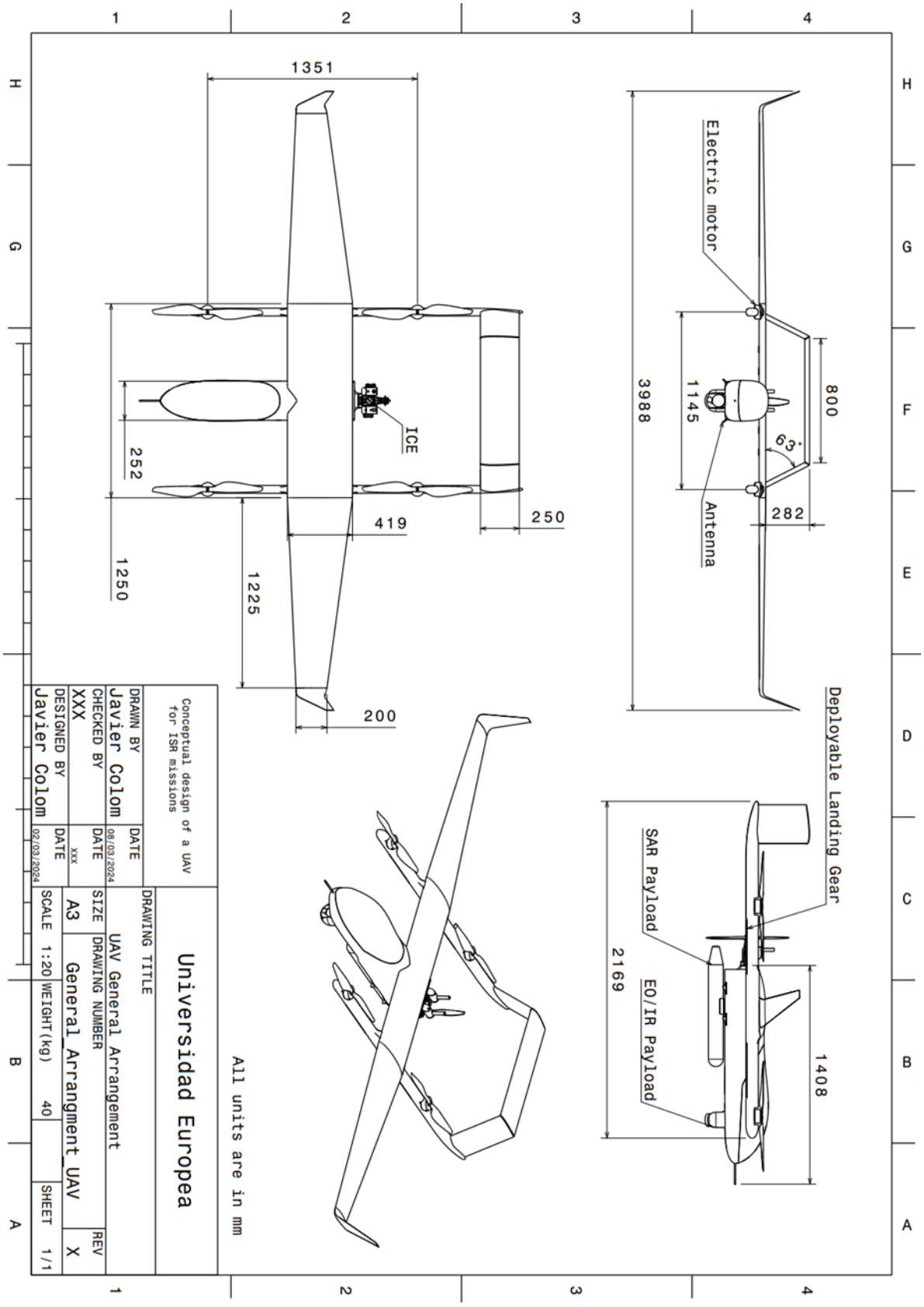

Figure 18. UAV general arrangement

In the following Figure 19, an approximate distribution of the equipment inside the fuselage can be seen. This configuration is subject to changes as the position of the center of gravity is not yet known. However, the equipment has been distributed taking their mass into account.

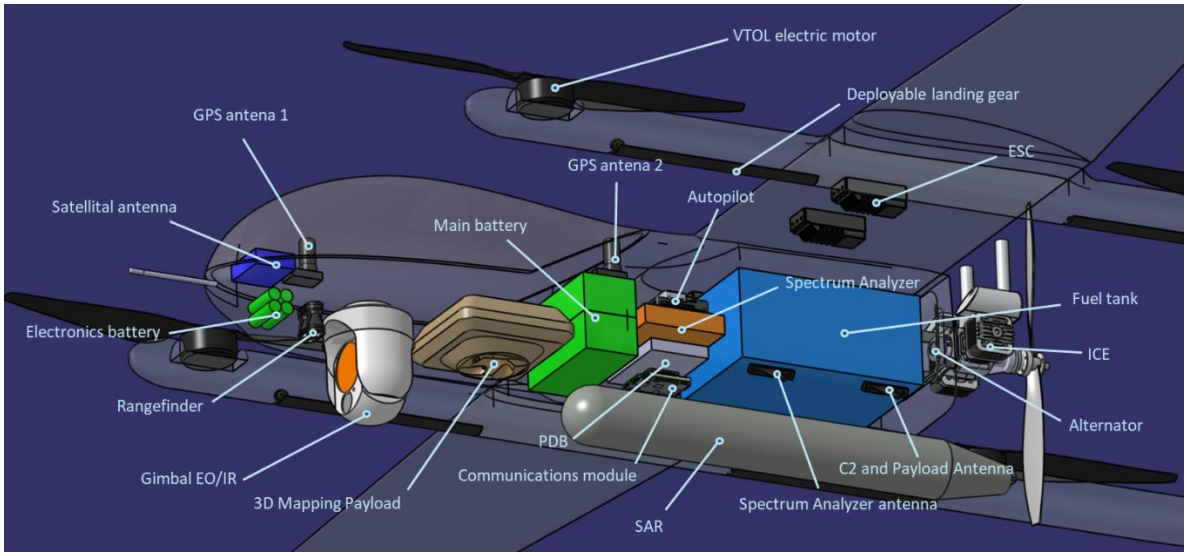

Figure 19. Internal equipment distribution

3.4 Wing arrangement

Regarding the wing configuration, several functional requirements must be considered in addition to the fundamental requirement of providing the UAV with the necessary lift to support its weight. These requirements are as follows:

- The wing must be detachable into several parts so that it can be transported in a ruggedized case.
- The wing must be able to be relatively easily attached to the arms that support the vertical thrust motors.
- The wing must be able to house the necessary systems for flight within its structure, such as the servomotors that operate the ailerons, as well as their wiring and the wiring of the vertical thrust motors housed in the arms. These cables must be able to pass from the wing to the arm.

To meet these requirements, the following design decisions have been made:

- The wing will be divided into three parts: a central section, which allows the wing-to-fuselage and wing-to-arm connections; and two sections that extend from the end of the central wing to the wingtips.
- To withstand the bending stresses caused by the wing's lift, as well as to meet the requirement of being detachable, the front spar will be a tube that runs along the central wing section and extends into part of the lateral wing sections, allowing these loads to be effectively transmitted. The rear spar will also have this configuration, but its length and cross-section will be smaller, as the majority of the bending load will be borne by the front spar, as the resultant lift force is applied at 25% of the chord length measured from the leading edge.

- This configuration also has implications for the wing planform. Since the spars are straight tubes, the wing sections, at least those intersected by the spars, must have enough space to accommodate them. This means that the sections of the wing intersected by the spar will have their 25% chord points aligned along the same X-coordinate of the aircraft's axes. That is, all these points will lie on the same Y-axis. This condition eliminates the possibility of incorporating sweep into the wing, which should not pose significant aerodynamic issues since sweep is primarily used to delay the critical Mach number when flying at speeds close to the transonic regime. This is far from the incompressible operating regime of the UAV.
- Regarding the wing-to-fuselage and wing-to-arm connections, sufficient space must be provided to install supports and fastening systems that are strong enough to withstand flight loads.
- As mentioned earlier, due to the spar structure to withstand wing bending stresses, dihedral angle will also not be available. This may affect the lateral stability of the aircraft, so a high-wing configuration will be chosen to improve this stability criterion.
- Due to the VTOL characteristics of the aircraft, i.e., the use of arms to accommodate vertical thrust motors, the overall efficiency of the aircraft will be reduced compared to an equivalent aircraft lacking these capabilities. Therefore, to reduce induced drag caused by the three-dimensional effects of a finite wing, winglets will be employed at the wingtips.

3.5 Tail arrangement

The tail of the aircraft must provide longitudinal stability as well as longitudinal and directional controllability while generating minimal resistance. There are numerous tail configurations available, so to narrow down the solution, specific characteristics of the UAV must be considered.

In this regard, since it will be necessary to use arms to support the vertical thrust motors, they can also be utilized as the structure to support the tail. The other option would be to utilize the fuselage, but this would result in an increase in weight compared to using the arms.

In the following images, different tail configurations and their associated drag can be seen. As shown in these images, the configuration with the lowest resistance is the "inverted V." However, despite being the most efficient in this regard, its configuration places the control surfaces in a suboptimal position, as they are inclined and coupled with both yaw and pitch controls. Therefore, a configuration more similar to that of UAV 2 in Figure 20 has been chosen.

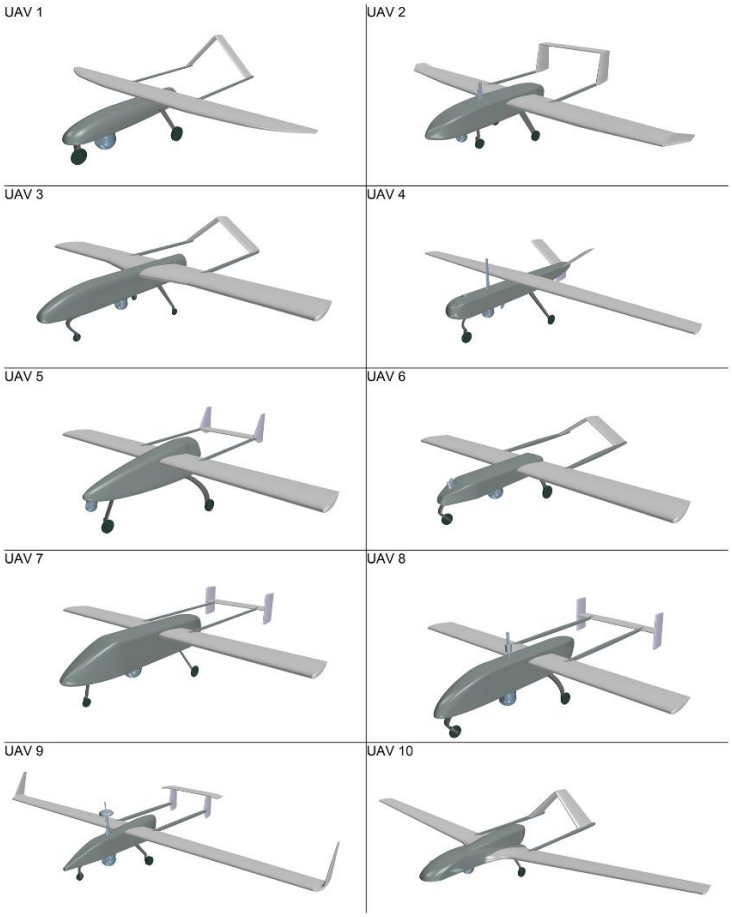

Figure 20. UAV tail configurations.

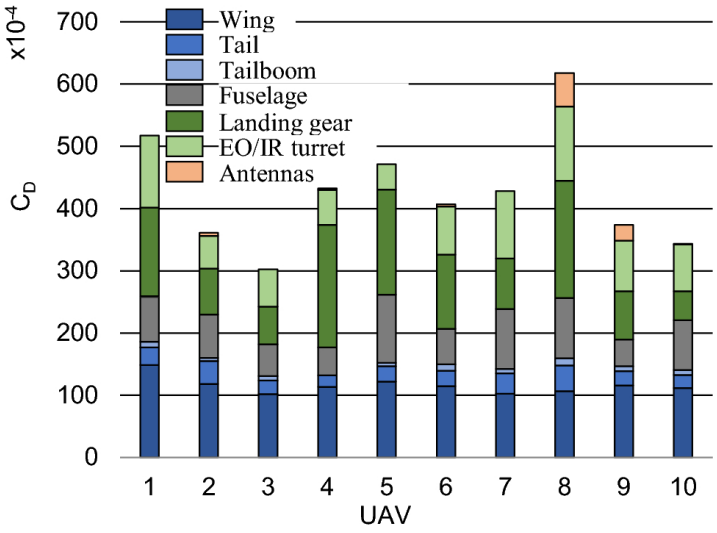

Figure 21. Drag Coefficients comparison for tail configurations. [2]

[2] F. Götten, D. F. Finger, M. Havermann, C. Braun, M. Marino, and C. Bil, "Full configuration drag estimation of short-to-medium range fixed-wing UAVs and its impact on initial sizing optimization," *CEAS Aeronautical Journal*, vol. 12, pp. 589–603, 2021.

In summary, the tail would have the following characteristics:

- The tail structure will be supported by the arms that support the vertical thrust motors.
- The tail configuration will consist of twin vertical stabilizers in an "H" shape with a high-mounted horizontal stabilizer.

Chapter 4. PRELIMINARY DESIGN

4.1 Aerodynamics

This chapter will address the aerodynamic aspect of the UAV. Bearing in mind that the objective of this project is a preliminary design of the UAV, the scope of this chapter will include the selection of the aerodynamic profile, the wing design, and the determination of the aerodynamic coefficients of the UAV. The designs obtained will be justified through validation using CFD analysis of the UAV.

4.1.1 Airfoil selection

Choosing the right aerodynamic airfoil is key when designing an aircraft, especially in the case of UAVs where mission configurations can vary significantly. In the specific context of a UAV where takeoff and landing phases are accomplished using vertical thrust engines, with the wing solely responsible for sustaining the UAV during cruise, the selection of the aerodynamic airfoil becomes even more critical. Unlike traditional aircraft where wings bear the weight throughout the flight, in this scenario, the airfoil must be optimized specifically for the cruising condition. This optimization ensures efficient lift generation with minimal drag, maximizing the UAV's endurance and overall performance. Therefore, the aerodynamic airfoil chosen plays a crucial role in determining the UAV's capabilities, efficiency, and mission success.

To carry out the selection, it has been decided to search for reference aerodynamic profiles optimized for low Reynolds number flights and gliders form UIUC Airfoil Database[3]. The candidate airfoils to be chosen must also have sufficient internal space to accommodate the servomotors and the spar section, allowing them to be inserted into the UAV's assembly.

To obtain a sufficiently representative result for the preliminary design, the number of airfoils to be studied will be 50.

The procedure for testing the qualities of the airfoils will involve using the Aeolus software. This software allows for aerodynamic analysis based on the panel method, which has demonstrated high fidelity. The following Figure 22 and Figure 23 shows comparisons with other aerodynamic analysis programs[4].

[3] M. Selig, "UIUC Airfoil Coordinates Database," University of Illinois at Urbana-Champaign, 2024. https://m-selig.ae.illinois.edu/ads/coord_database.html

[4] U. Schuster, "Comparison of Aeolus ASP for a Boxwing aircraft," Aeolus Aero, 2024. [Online]. Available: https://aeolus-aero.com/asp/benchmark-study/.

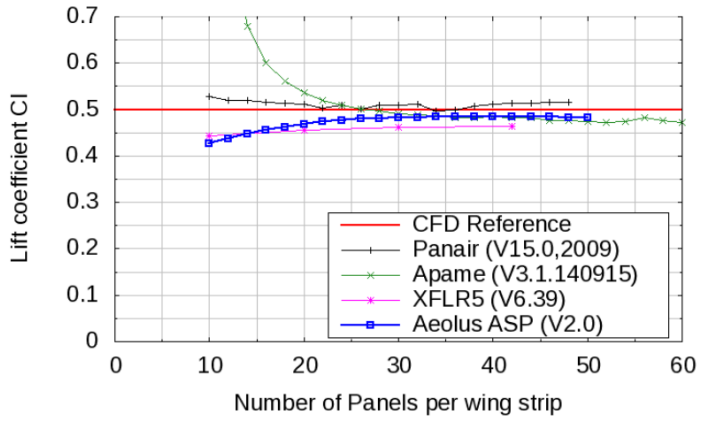

Figure 22. Comparison between aerodynamics software for Lift coefficient obtained.

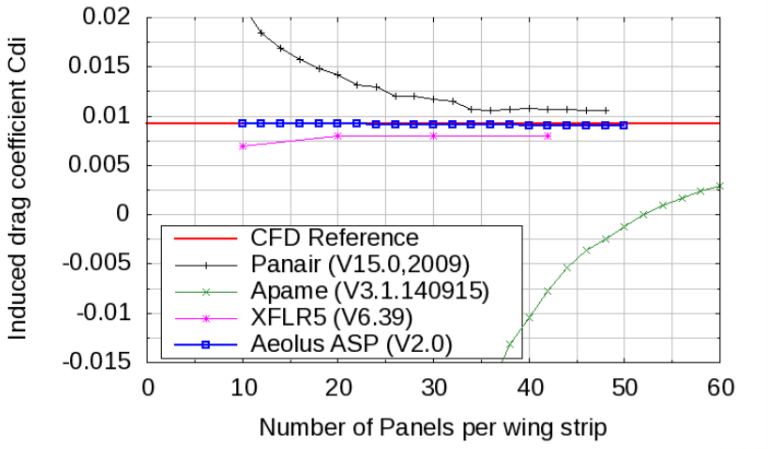

Figure 23. Comparisson between aerodynamics softwares for Drag coeffcient obtained

To obtain results closer to the proposed design, a wing will be constructed in Aeolus with an approximate planform of the final solution for the comparison of airfoils. In this way, the aerodynamic efficiency of the wing and the angle of attack at which it reaches cruise speed will be primarily measured. This is because we could obtain airfoils with very high efficiency for the flight condition but with very high angles of attack. Thus, even if this angle of incidence were given to the wing when it is attached to the fuselage, the angle of attack at which the aircraft enters into a stall would be very low, affecting the maneuverability of the UAV.

The flight conditions under which the simulations were conducted in Aeolus are as follows:

- Flight speed: 25 m/s
- Density: 1.167 kg/m3
- Mach: 0.074
- Altitude: 500 m
- UAV weight: 40 kg

The proposed wing geometry can be seen in Figure 24:

With the flight condition data and the wing geometry provided, Aeolus can determine the angle of attack at which balanced flight is achieved, as well as the drag produced by the wing in that flight condition to calculate efficiency. Note that for a given lift coefficient, determined by the weight and flight condition(density and velocity), knowing the airfoil geometry the angle of attack can be obtained.

$$\alpha = \frac{C_L - C_{L0}}{\frac{dC_L}{d\alpha}}$$

Below is the wing defined in Aeolus. As can be seen, three distinct sections have been defined: a central section, an intermediate section, and a lateral section. In each section, a geometry (airfoil), chord length, sweep angle, dihedral angle, and twist angle can be defined.

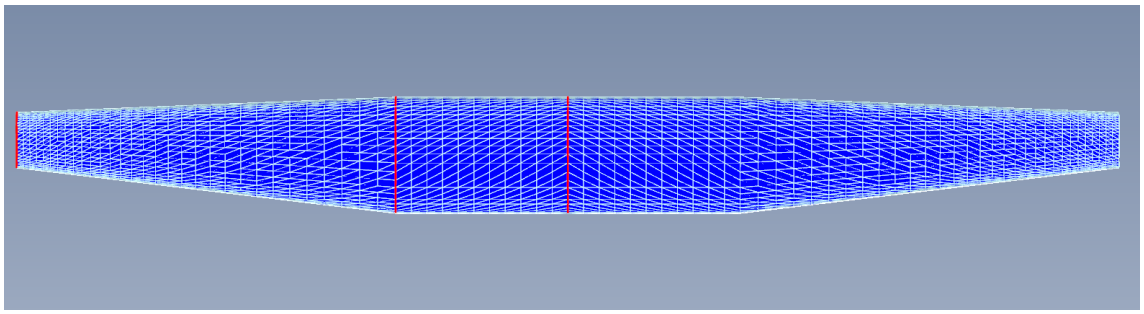

Figure 24. Wing designed to be tested in Aeolus

▼ Sections

Id	Airfoil	S-pos [m]	Chord [m]	Twist α [deg]	Sweep φ [deg]	Dihedral δ [deg]
0	E407	0.0	0.42	1.5	0.0	0.0
1	E407	0.625	0.42	1.5	0.0	0.0
2	E407	2.0	0.2	1.5	0.0	0.0

Figure 25. Parameters of the wing to be tested in Aeolus

The results obtained are shown in the next figure:

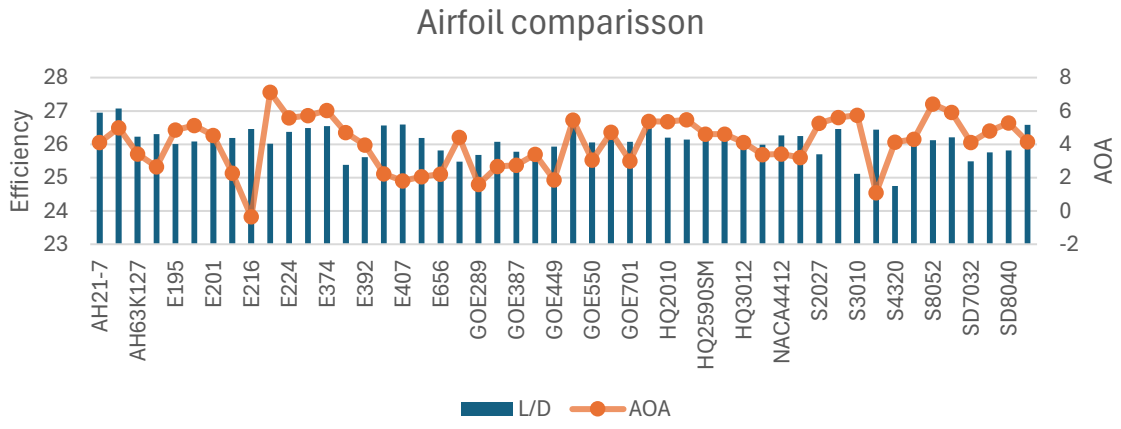

Figure 26. Airfoil comparison results

The results show several airfoils that stand out in efficiency compared to the rest:

Airfoil	Efficiency (L/D)	Angle of attack (º)
AH21-7	26.95	4.1
AH21-9	27.07	5
E403	26.56	2.2
E407	26.59	1.8
GOE563	26.52	5.5
GOE795	26.7	5.4
YS930	26.58	4.1

Table 1. Airfoil Efficiency and Angle of attack comparison

From this initial selection of airfoils, the two from the Andrew Hollom family show the highest efficiency. However, both have a high angle of attack (between 4 and 5 degrees). The AH21-9 airfoil is thinner than the AH21-7, which makes it more challenging to include the internal structure of the wing as well as the servomotors.

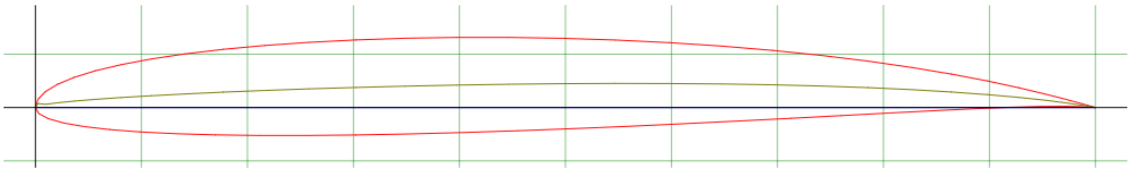

Figure 27. AH21-7 Airfoil

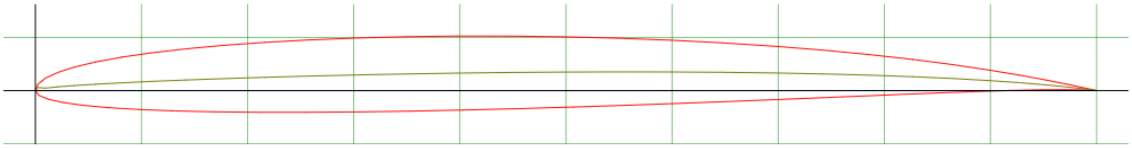

Figure 28. Airfoil AH21-9

For all these reasons, the selected airfoil is the AH21-7. The following images show the aerodynamic coefficient curves for a Reynolds number from 200,000 to 1,000,000:

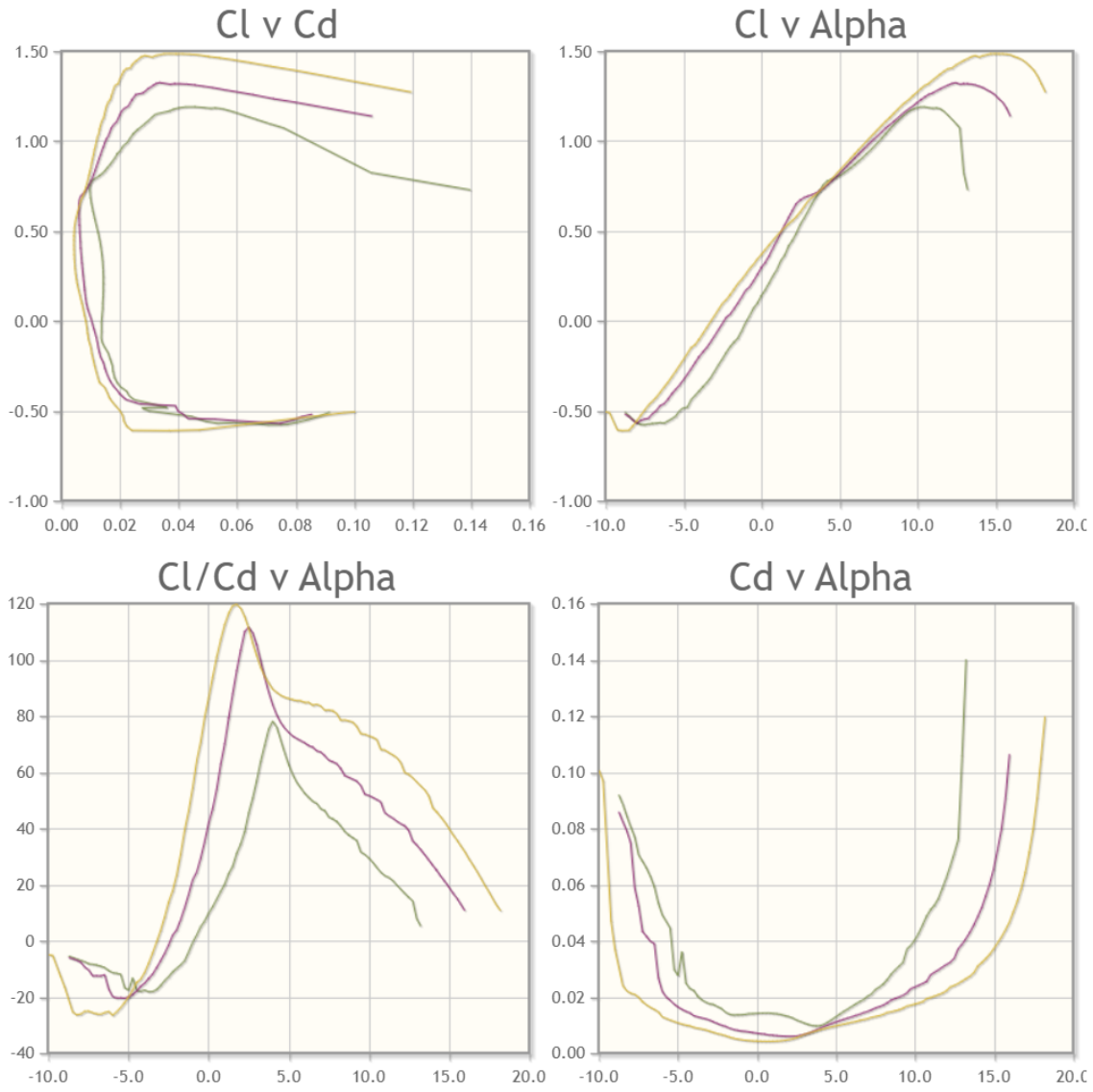

Figure 29. AH21-7 Aerodynamic coefficients. (Re 2e5 in green; Re 5e5 in purple; Re1e6 in yellow)

The AH21-7 airfoil has shown great efficiency for the chosen flight condition, but the angle of attack is too high. In response to this issue, two possible solutions are proposed:

- Based on the pressure profile of the AH21-7 airfoil under the flight condition, design a new airfoil that achieves the same distribution but at a lower angle of attack.
- Modify the AH21-7 airfoil to achieve the same lift and similar efficiency at a lower angle of attack.

Designing an airfoil based on the pressure distribution is an extremely complex task that could easily be a final degree project in itself. There are numerous airfoils that can achieve a specific pressure distribution, so additional pressure distributions at different angles of attack would be needed to narrow down the number of potential airfoils. Furthermore, it is possible that pressure distributions for different angles of attack may be incompatible with a specific airfoil, resulting in no feasible solution. Nevertheless, this approach would be the most efficient for the final result and would best align with the intended mission of the UAV.

On the other hand, modifying the airfoil is a much simpler and faster process, which can be accomplished using Xfoil software. Therefore, this approach to the problem is chosen.

To achieve a lower angle of attack while maintaining the same lift coefficient, the parameter to modify in an airfoil is the camber, which is the primary cause of lift generation in an airfoil. By increasing the camber, the lift coefficient vs. angle of attack curve shifts upwards. However, this modification can also affect the stall angle, as increasing the camber makes it easier for the boundary layer to separate from the airfoil surface due to the increased curvature required to stay in contact with the airfoil surface.

Given that it is necessary to modify the airfoil, it has been decided to take advantage of this opportunity to increase the maximum thickness of the airfoil to facilitate the integration of the structure and necessary equipment.

The effects that both the curvature and the thickness of the profile have on the aerodynamic coefficient curves are described below.

Thicknes	**Lift Coefficient**	• Increased Thickness: Thicker airfoils can generate more lift up to a certain angle of attack due to a larger surface area. • Stall Characteristics: Thicker airfoils tend to have a gentler stall and can sustain higher angles of attack before stalling.
	Drag Coefficient	• Airfoil Drag: Thicker airfoils generally have higher airfoil drag, especially at higher speeds, due to increased form drag. • Wave Drag: At transonic speeds, thicker airfoils experience higher wave drag due to shock wave formation. This does not affect the airfoil because the flight condition is under incompressible regime.
	Moment Coefficient	• Pitching Moment: The thickness of an airfoil can affect the pitching moment, but this effect is usually less significant than that of camber.

Figure 30: Influence of thickness in Aerodynamic Coefficients.

Camber	**Lift Coefficient**	• Increased Camber: Adding camber to an airfoil generally increases the lift coefficient for a given angle of attack. A more cambered airfoil produces more lift at lower angles of attack compared to a symmetric airfoil. • Zero-Lift Angle: The zero-lift angle of attack shifts to a negative value for cambered airfoils, meaning they generate lift even when the angle of attack is zero.
	Drag Coefficient	• Induced Drag: Higher camber usually increases induced drag because of the higher lift generated. • Airfoil Drag: Cambered airfoils may have higher profile drag at higher angles of attack due to increased surface area and flow separation tendencies.
	Moment Coefficient	• Nose-Down Moment: Cambered airfoils typically experience a more pronounced nose-down pitching moment. This is due to the asymmetric pressure distribution along the chord line..

Figure 31. Influence of chamber in Aerodynamic Coefficients

The influence on the polar curves can be summarized in the next sentences:

- Lift Curve: Cambered airfoils will have a shifted and typically steeper lift curve, indicating higher lift at lower angles of attack. Thicker airfoils may show a broader curve with a delayed stall.
- Drag Polar: Cambered airfoils will generally exhibit higher drag at a given lift coefficient compared to symmetric airfoils due to increased induced drag. Thicker airfoils will show higher drag across the curve due to increased profile drag.
- Moment Curve: Cambered airfoils will show a more negative (nose-down) pitching moment across the angles of attack. The effect of thickness on the moment curve is less pronounced but still present.

The procedure to follow consists of increasing the maximum thickness up to 10% and progressively increasing the curvature until achieving an angle of attack for the flight condition of at least one degree.

After several iterations, the modified airfoil is as follows:

- Max thickness: 0.1
- Max camber: 0.035592

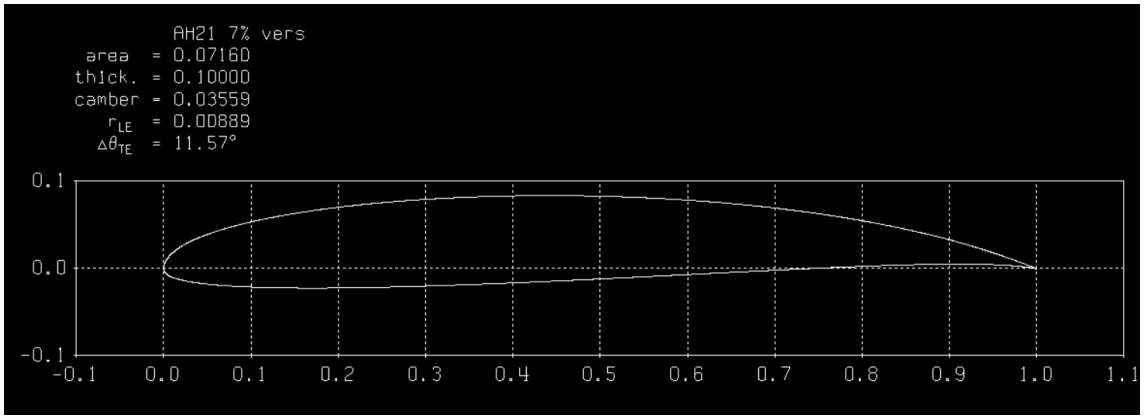

Figure 32. Modifyed airfoil in Xfoil

With the modified airfoil, the simulated wing in Aeolus presents the following results:

- Efficiency (L/D): 27
- Angle of attack: 1 º

In the following image, it can be seen the comparison of the geometries of the original AH21-7 airfoil and the modified one.

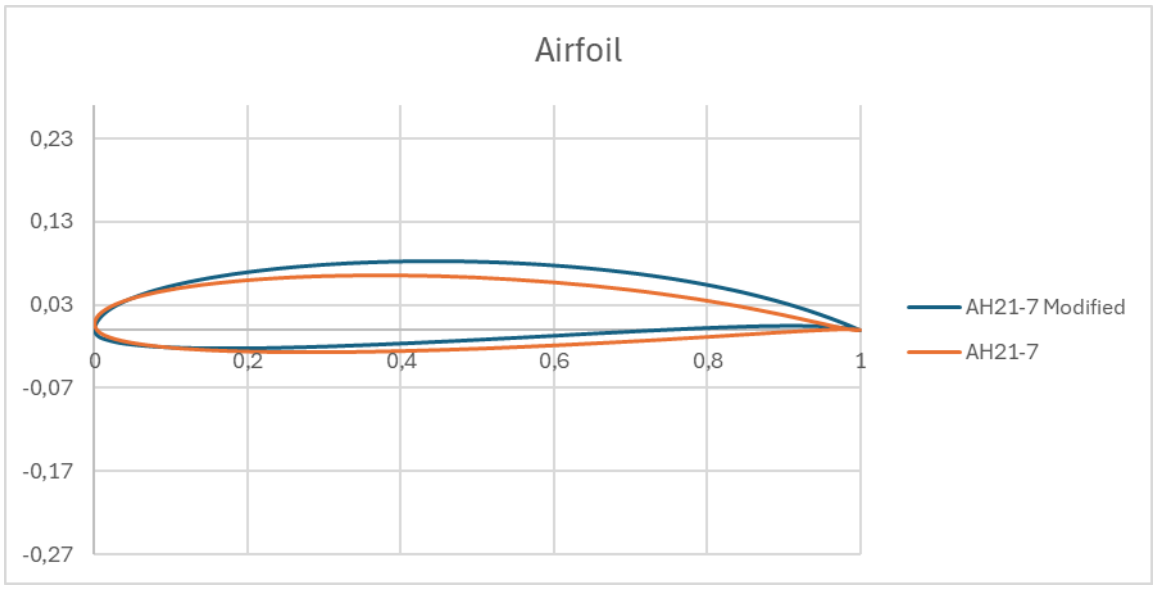

Figure 33. Geometry comparisson between the AH21-7 airfoil and the modified one

4.1.2 Wing planform design

The planform wing design is a critical aspect of UAV development, significantly impacting aerodynamic efficiency, structural integrity, and overall performance. For the UAV in question, the wing is designed without sweep due to the incorporation of stiffeners, ensuring robust structural support. Additionally, the wing is divided into three segments, facilitating easy disassembly and transport in a rugged case, making the UAV highly portable. To enhance aerodynamic efficiency, the lateral sections of the wing are tapered, increasing the aspect ratio and reducing induced drag. This thoughtful design balances performance with practicality, optimizing the UAV for both operational effectiveness and ease of transportation.

To improve aerodynamic efficiency, it was decided to add winglets to the wing. In Aeolus, winglets are defined by adding new sections to the wing with a high dihedral angle. Four sections were added after the previous wingtip section used for testing and selecting an appropriate airfoil for the intended mission. This addition increases the wingspan, as the previous wingtip section was located 2 meters from the plane of symmetry. Therefore, the position of this section was reduced to 1.85 meters to provide enough space for the winglet and meet the maximum wingspan requirement of 4 meters.

Regarding the winglet airfoil, a symmetrical NACA 0012 airfoil was chosen. The reason for this criterion is that being symmetrical, the lift generated will be less than that of a cambered airfoil. Therefore, the pressure difference, which is the main cause of wingtip vortex generation, will be reduced, minimizing its effect.

It is true that a cambered airfoil in that section could also increase the overall efficiency of the wing by producing more lift than drag. However, this would also require a more robust structure for the winglet. Given that the section progressively reduces significantly towards the winglet tip, introducing structural reinforcements in that area could be quite complex, as the winglet's skin would reduce the available space for the internal structure. In this regard, given the small size of the winglet sections, the design intent is for the winglet's skin alone to be structurally sufficient to withstand the flight loads.

As previously mentioned, Aeolus has been used for the detailed definition of the wing airfoil. This software has a wing geometry optimization function to maximize or minimize a specific parameter. It achieves this by using other user-defined parameters as degrees of freedom to iterate and optimize the parameter of interest.

For this case, the parameter to maximize is:

- Current Lift to Drag ratio.

The degrees of freedom to iterate over are:

- S-position of the winglet sections
- Chord length of the winglet sections
- Dihedral angle of the winglet sections
- Sweep angle of the winglet sections
- Twist angle of the wingtip section

After the iterative process for optimizing the wing geometry, the results can be seen in the following figures:

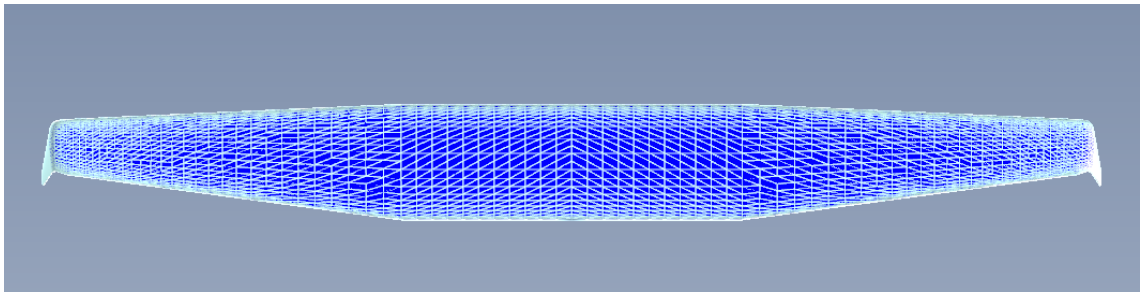

Figure 34. Optimized wing planform in Aeolus

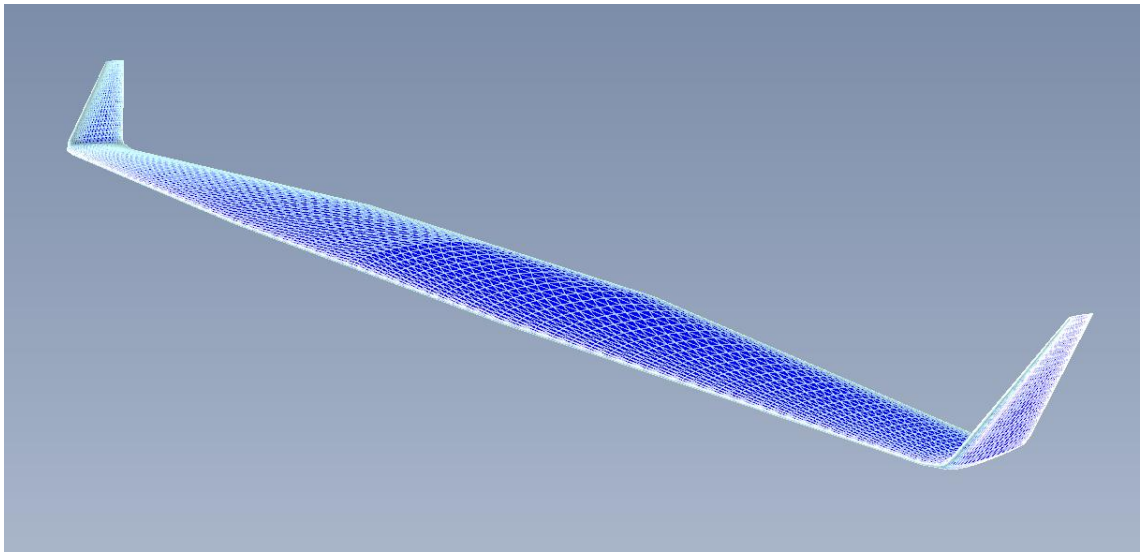

Figure 35. Optimized wing in Aeolus

Id	Airfoil	S-pos [m]	Chord [m]	Twist α [deg]	Sweep φ [deg]	Dihedral δ [deg]
0	AH217_0.1TH_0.35CH	0.0	0.42	1.2	0.0	0.0
1	AH217_0.1TH_0.35CH	0.625	0.42	1.2	0.0	0.0
2	AH217_0.1TH_0.35CH	1.85	0.2	3.0	0.0	11.666666666666666
3	NACA0012	1.892	0.18330989576176854	0.0	20.0	35.0
4	NACA0012	1.905433137555922	0.168	0.0	20.0	58.33333333333333
5	NACA0012	1.9256548947891257	0.16387085487251848	0.0	30.0	70.0
6	NACA0012	2.2	0.05	0.0	0.0	0.0

Figure 36. Geometrical characteristics of the optimized wing

4.1.3 Aerodynamic validation using Aeolus

Once the wing has been optimized, it is time to incorporate the tail design. The configuration will be as described in section 3.4, with a twin vertical stabilizer and an elevated horizontal stabilizer.

Despite the previously mentioned penalty for the inverted V tail configuration due to the coupling of pitch and yaw controls, the proposed vertical stabilizers will not be completely vertical. They will have a less pronounced angle than the inverted V configuration but will not be as upright as those in an H configuration. This approach reduces the wetted surface of the tail while maintaining independent pitch control.

For the tail sections, the use of symmetrical NACA 0012 airfoils is proposed. As for the dimensions of the horizontal stabilizer, it is proposed to iterate based on a projected area of 10% of the wing's surface area. Subsequently, to define its position, the longitudinal stability of the UAV will be evaluated in Aeolus based on the Moment coefficient vs angle of attack curve, aiming for a negative slope.

Finally, it will be necessary to define an angle of attack for the horizontal stabilizer. Aeolus has a function that allows studying the variation of one parameter based on another. In this case, the parameter to study will be the static margin. It should be noted that carrying a fuel tank that empties out will cause the UAV's center of gravity to shift as the fuel is consumed. The variation of the static margin has two main effects: increasing it enhances the stability of the aircraft but penalizes maneuverability; decreasing it enhances maneuverability but reduces stability.

Given the intended mission of the UAV, most of the time it will be flying in cruise mode, describing wide-radius circles to obtain sensor data more effectively. In other words, it will not perform acrobatic flights or risky maneuvers involving rapid changes in pitch and roll angles. Therefore, the design objective is for the UAV to be primarily stable. With this in mind, the static margin target will be between 10% and 15% of the mean aerodynamic chord.

In the following figure, it can be observed the wing and tail of the UAV in Aeolus after defining the position and angle of attack of the latter.

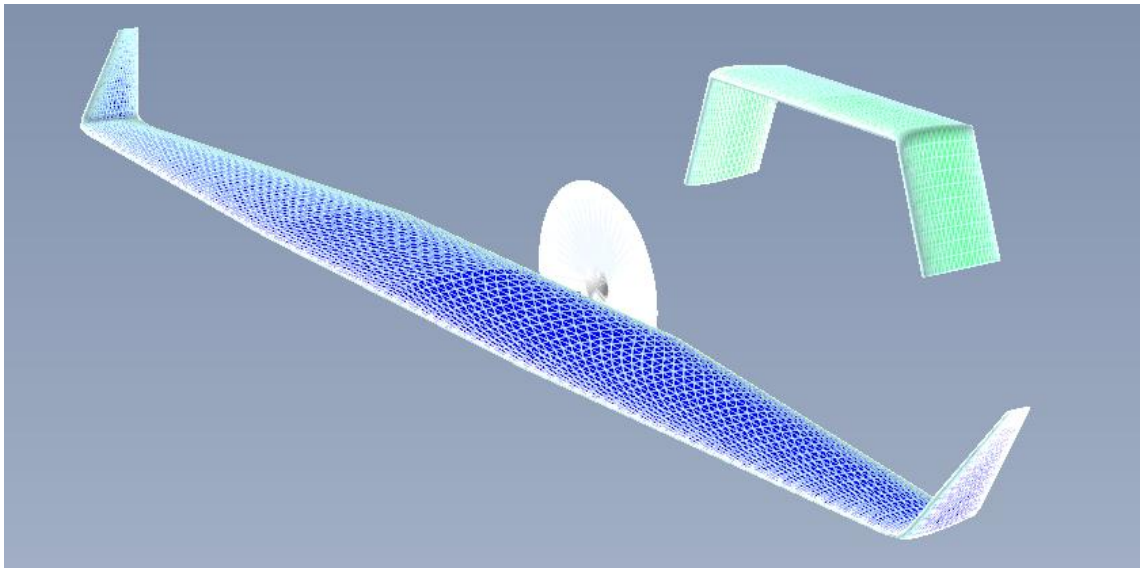

Figure 37. Wing and tail distribution in Aeolus

In Figure 38 can be observed the geometry of the tail, where an angle of attack of 1.4 degrees has been set to meet the static margin target.

Id	Airfoil	S-pos [m]	Chord [m]	Twist α [deg]	Sweep φ [deg]	Dihedral δ [deg]
0	NACA0012	0.0	0.25	1.4	0.0	0.0
1	NACA0012	0.4	0.25	1.4	0.0	-70.0
2	NACA0012	0.75	0.25	0.0	0.0	0.0

Figure 38. Tail sections defined in Aeolus

The flight condition for the simulation can be seen in the Figure 39.

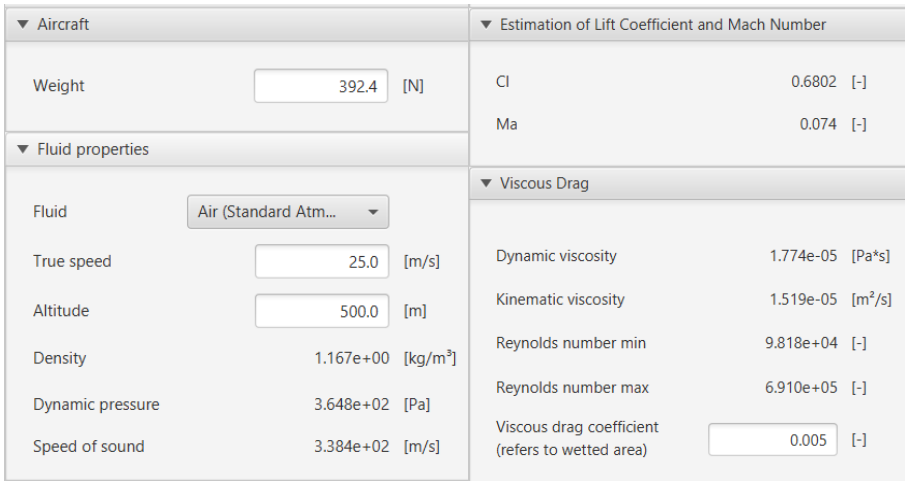

Figure 39. Flight condition details for Aeolus analysis

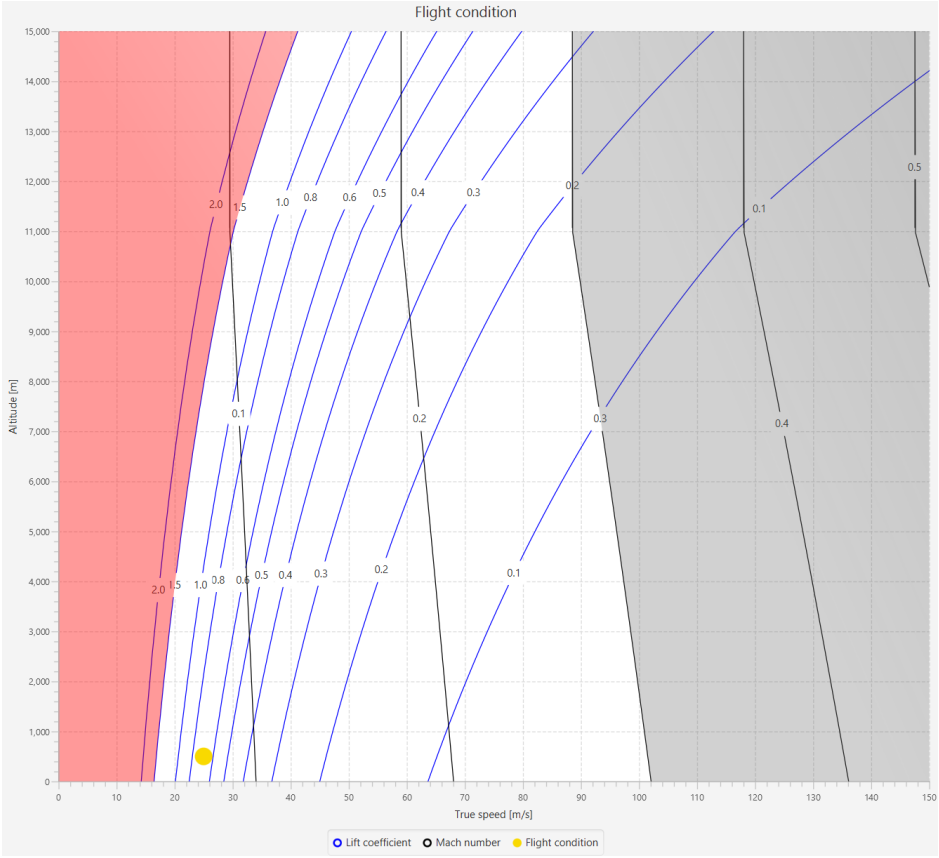

Figure 40. Flight condition as a function of true speed and altitude

In Figure 40 can be seen the flight condition regarding true speed and altitude. It is also shown the Mach number and lift coefficients. This graph also shows how it would evolve true speed when gaining altitude to remain in the same range of lift coefficient.

The aerodynamic results obtained for the UAV with this configuration can be seen in the following figures.

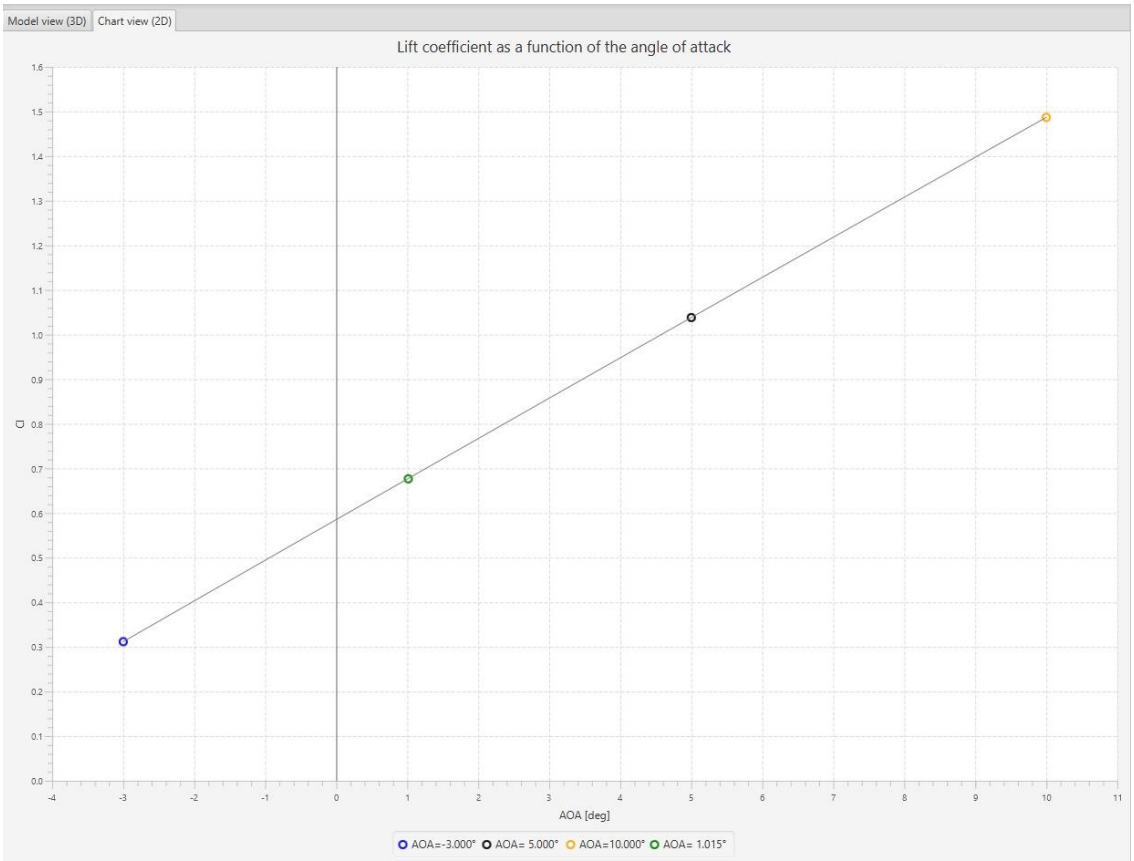

Figure 41. Lift Coefficient vs AOA for the UAV obtained in Aeolus

The results obtained for the lift coefficient as a function of angle of attack show that the optimal flight point of the UAV is at 1 degree of angle of attack. It is worth noting in this regard that during the optimization process of the wing and tail configuration, it was necessary to increase the wing's angle of attack at the root from 1.2 to 1.4 degrees to reduce the UAV's angle of attack in its cruise condition.

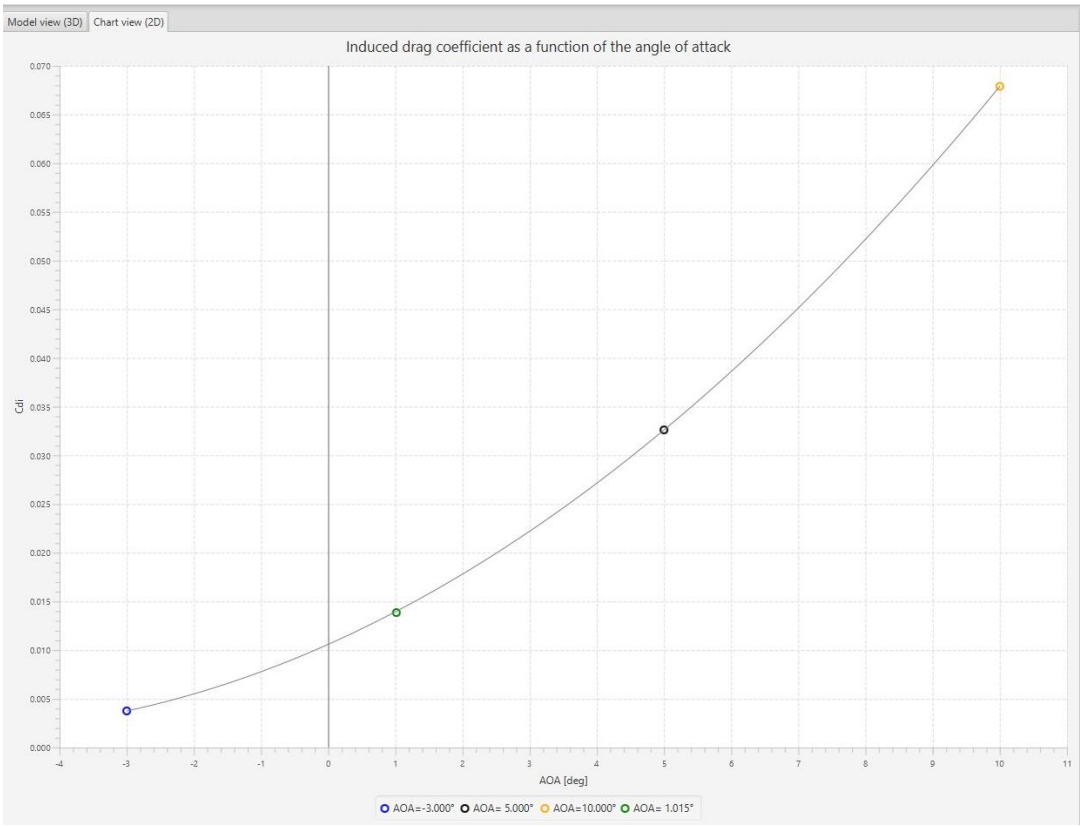

Figure 42. Induced drag Coefficient vs AOA for the UAV obtained in Aeolus

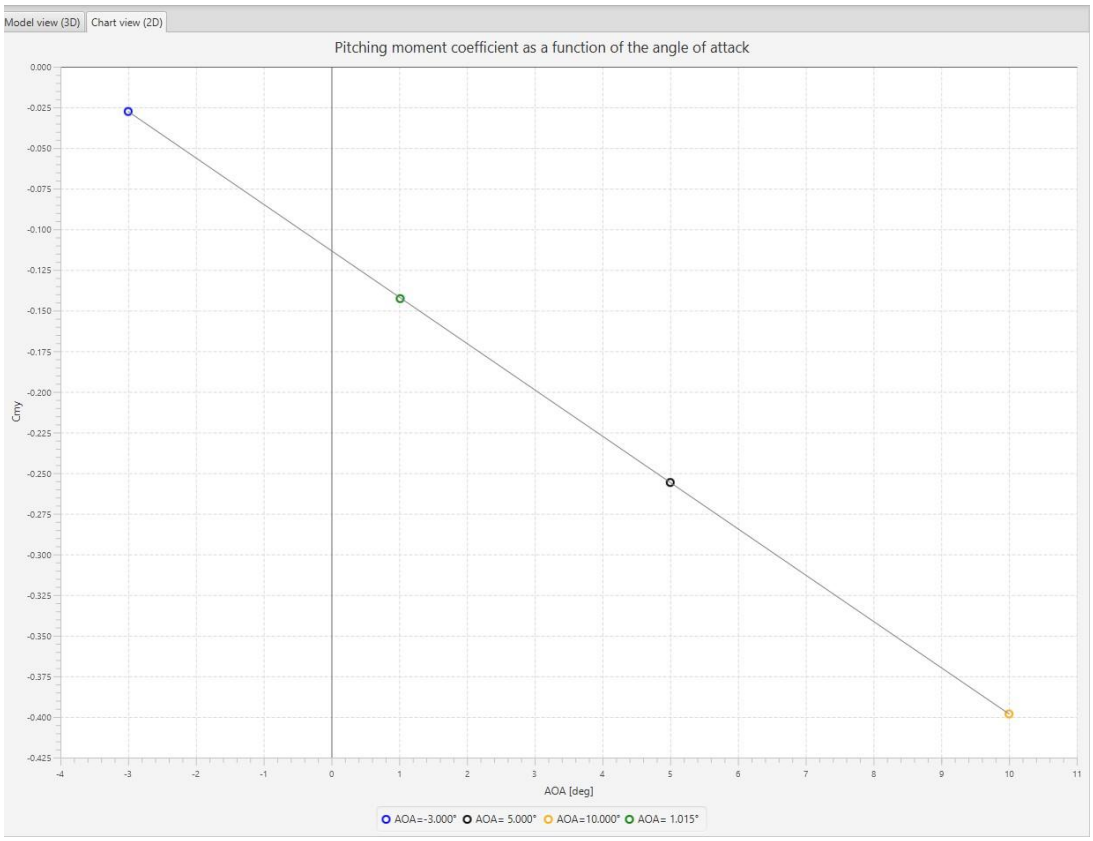

Figure 43. Pitching moment Coefficient vs AOA for the UAV obtained in Aeolus

As can be observed in Figure 43, the slope of the moment coefficient curve with respect to the angle of attack is negative, which is one of the criteria for longitudinal static stability. While it is true that there is no zero-moment coefficient for the flight angles of attack, it is worth noting in this regard that Aeolus does not take into account the position of the center of gravity, with which a position can be trimmed where the UAV's aerodynamic moment is zero. This will be done later in section 4.3.3. The relevant information provided by Aeolus is that the aircraft is stable regarding the slope of the moment coefficient curve.

In the Figure 44 can be seen the variation of the center of pressure and aerodynamic center.

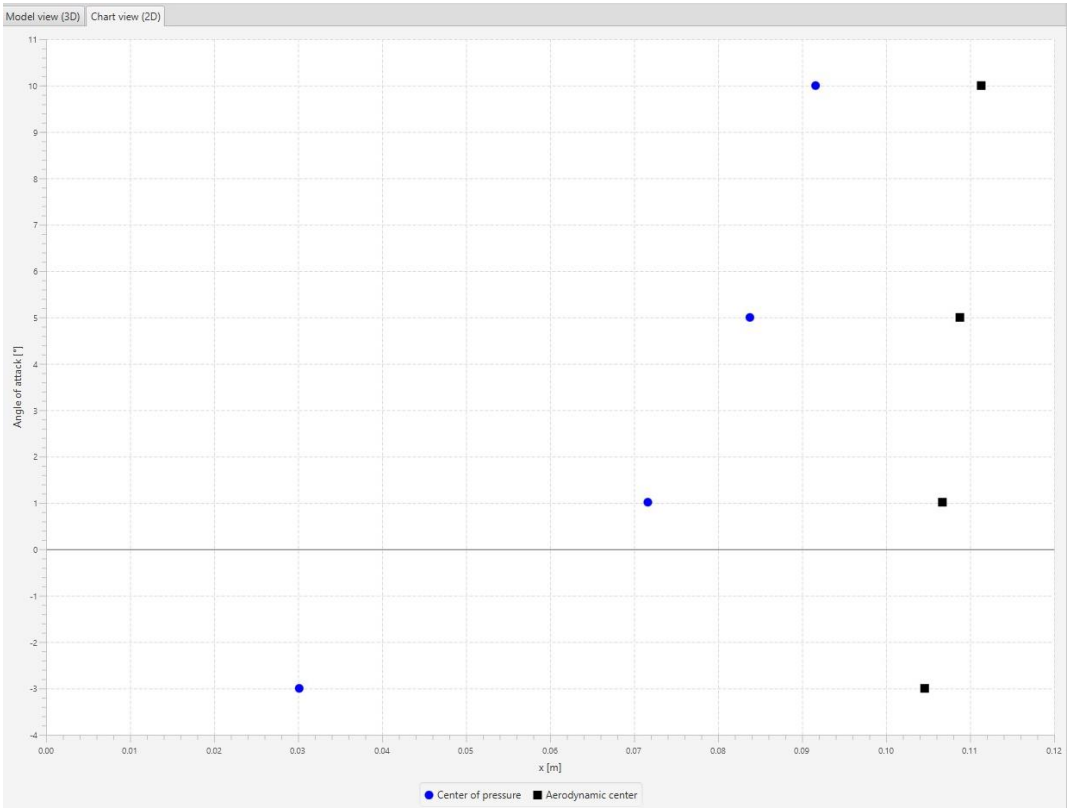

Figure 44. Center of pressure and Aerodynamic center variation with respect to AOA for the UAV obtained in Aeolus

The obtained aerodynamic efficiency value for the UAV in this simulation is 26.92. If we compare it with that of the wing formed by the AH21-7 airfoil, it is slightly lower (26.95). However, this represents a reduction in efficiency of only 0.1%. It should be noted that the efficiency obtained for the UAV includes the tail, and the angle of attack of the wing has been decreased from 4.1 degrees to 2.4 degrees (including the wing incidence angle of 1.4 degrees and the UAV angle of attack of 1 degree). Therefore, these results justify the changes made to the wing airfoil.

In the Figure 45, the aerodynamic efficiency is shown as a function of flight speed and altitude. As can be observed, the UAV design point is located in the region of maximum efficiency for the flight conditions of the intended mission.

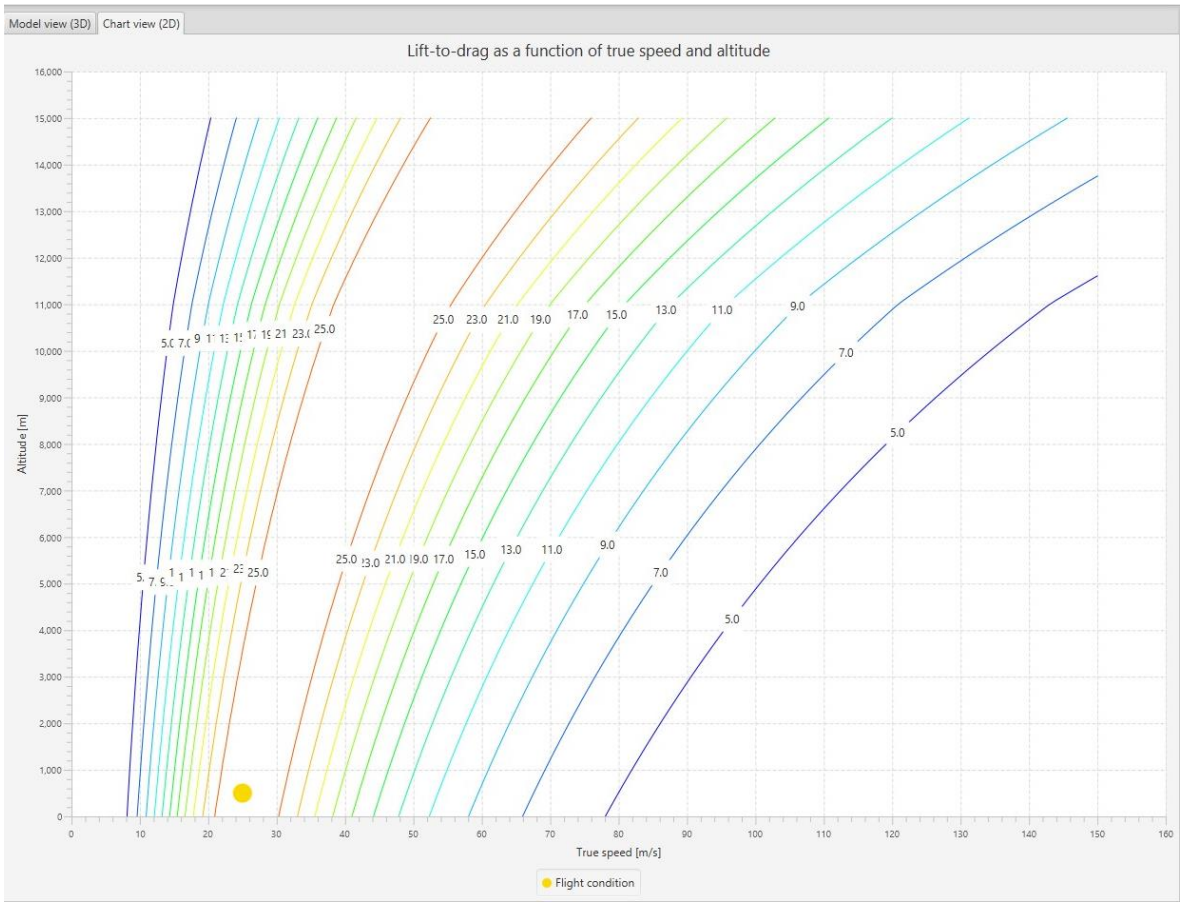

Figure 45. Efficiency as a function of true speed and altitude for the UAV obtained in Aeolus

Finally, the thrust required to maintain balanced flight for the UAV is 14.53 N. It is important to note in this regard that the required thrust refers solely to the aerodynamic drag caused by the wing and tail, and it has been obtained using a vortex method. More accurate results will be obtained later in the CFD analysis.

With these results obtained in the Aeolus software, the initial aerodynamic design of the UAV can be validated.

4.1.4 Aerodynamic validation using CFD-Fluent

In the realm of UAVs, ensuring optimal aerodynamic performance is paramount for achieving efficiency, stability, and mission success. Computational tools play a vital role in this process, allowing engineers to simulate and validate the aerodynamic behavior of UAV designs before physical prototypes are built. Fluent, a renowned Computational Fluid Dynamics (CFD) software developed by ANSYS, stands out as a versatile tool for such aerodynamic validations.

Fluent offers a comprehensive suite of tools and capabilities tailored specifically for aerodynamic simulations. Its advanced solver algorithms and robust meshing capabilities enable engineers to accurately predict airflow around complex UAV geometries and assess various aerodynamic parameters such as lift, drag, and stability coefficients. Additionally, Fluent provides the flexibility to simulate diverse flight conditions, including steady-state and transient regimes, as well as different atmospheric conditions and flight maneuvers.

Moreover, Fluent's post-processing features facilitate in-depth analysis of simulation results, allowing engineers to visualize flow patterns, identify areas of high aerodynamic loadings or inefficiencies, and iteratively refine UAV designs for optimal performance. Its seamless integration with other ANSYS tools further enhances the overall design process, enabling multidisciplinary optimization and comprehensive assessment of UAV performance across various engineering domains.

The aerodynamic analysis of the UAV in Fluent is conducted based on its geometry, defining a control volume where the airflow variables are analyzed. This control volume must be large enough so that the effect of its walls does not affect the flow around the UAV.

The UAV's geometry can be generated in Ansys or imported. While Ansys stands out as a versatile and effective analysis tool, when it comes to designing geometry, it does not have the same capabilities as specialized CAD design software.

The wing geometry entails some complexity, as its lateral part has a variable twist and is tapered, the airfoil of the wingtip and the one of the winglets are different, and the winglet has a morphology that is difficult to generate while maintaining smooth contours. CATIA is the software used for the detailed general design of the UAV, so the geometry will be generated first in this software and then imported into Ansys for aerodynamic design.

The wing geometry information generated in Aeolus can be used for its design in CATIA. The airfoils of each section can be modified based on the normalized modified airfoil so that they have their exact dimensions in the wing in CATIA. Likewise, their position can also be obtained from the Aeolus data. The same applies to the tail. In this way, the wing and tail obtained in Aeolus can be accurately represented.

In the Figure 46, you can see the semi-wing modeled in CATIA. In the Figure 47, you can see the complete UAV modeled in CATIA, which will be subsequently imported into Ansys for aerodynamic analysis and to validate the design with CFD.

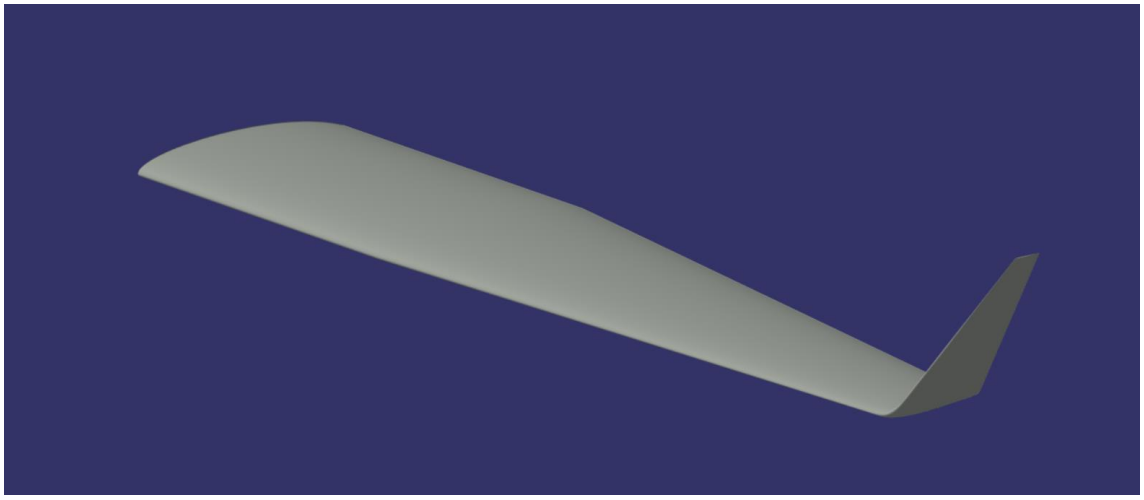

Figure 46. Semi-wing modelled in CATIA

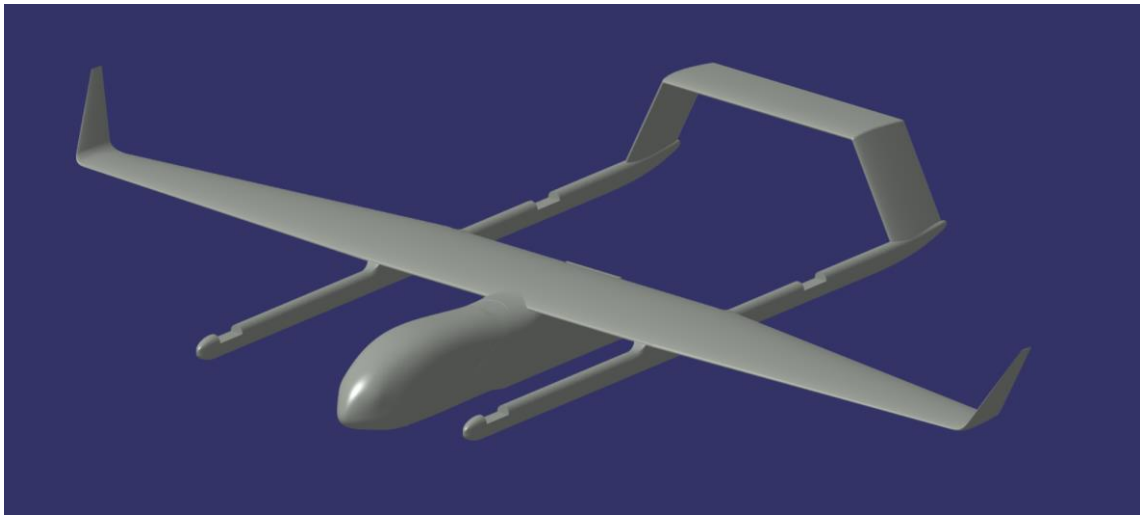

Figure 47. CATIA model of the UAV to be imported to Ansys

It is important to note that for this CFD analysis, some parts of the UAV that will generate non-negligible aerodynamic drag have been omitted. These elements are:

- Gimbal
- SAR
- Antennas
- Vertical thrust engines and their propellers
- Main engine and propeller

The gimbal will create significant drag, but it should not affect lift. Building the mesh to analyze the results, due to the gimbal geometry, could lead to some problems regarding mesh quality. In this regard, the gimbal's drag will be analyzed later when dimensioning the propulsion system. The same reasoning applies to the vertical thrust engines, their propellers, and the main engine. The main engine's propeller will be rotating in flight and producing thrust. That means there will be a suction force backwards at the end of the fuselage. Modeling this behavior in Ansys could be inefficient before validating the design in CFD, so it will not be evaluated for this study.

To save computational processes in the CFD analysis, results will be generated using symmetry. This means only half of the UAV will be analyzed, and the results will be extrapolated for the other half. In order to obtain aerodynamic coefficients as a function of angle of attack, the angle of attack of the UAV will be parameterized.

In the Figure 49, can be observed the mesh of the UAV. As shown, the number of elements on the surface of the UAV is considerably higher than that of the fluid volume, allowing for a greater amount of data to be obtained on this surface. This surface will produce the most changes in the fluid, thereby providing more reliable results.

The parameters to set the mesh are shown in Figure 48.

Defaults	
Physics Preference	CFD
Solver Preference	Fluent
Element Order	Linear
Element Size	0,5 m
Export Format	Standard
Export Preview Surface Mesh	No

Details of "Face Sizing" - Sizing	
Scope	
Scoping Method	Geometry Selection
Geometry	118 Faces
Definition	
Suppressed	No
Type	Element Size
Element Size	8,e-003 m
Advanced	
Defeature Size	Default (2,5e-003 m)
Influence Volume	No
Behavior	Hard
Capture Curvature	No
Capture Proximity	No

Figure 48. Mesh details

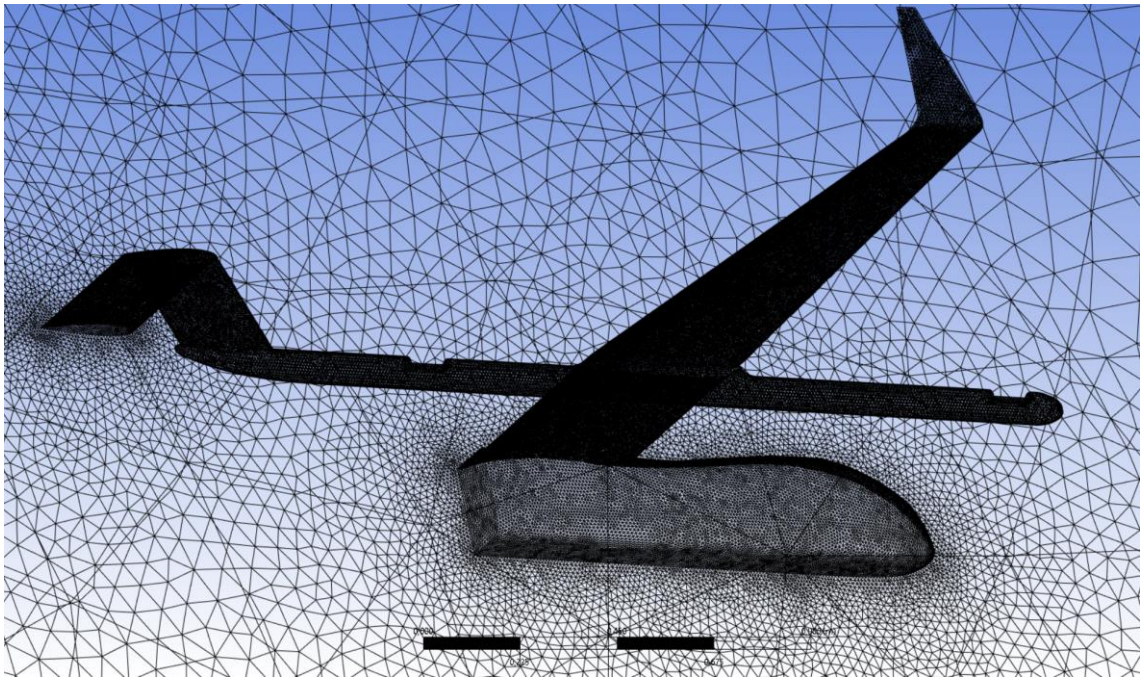

Figure 49. Detail of UAV mesh in Ansys

The average values of the main parameters of the quality of the mesh are shown below:

- Skewness: 0.21
- Orthogonal quality: 0.789
- Element quality: 0.85
- Aspect Ratio: 1.8

Number of elements and nodes of the mesh:

- Number of nodes: 704,115
- Number of elements: 4,034,783

Once the mesh is generated, the next step is to establish the simulation conditions:

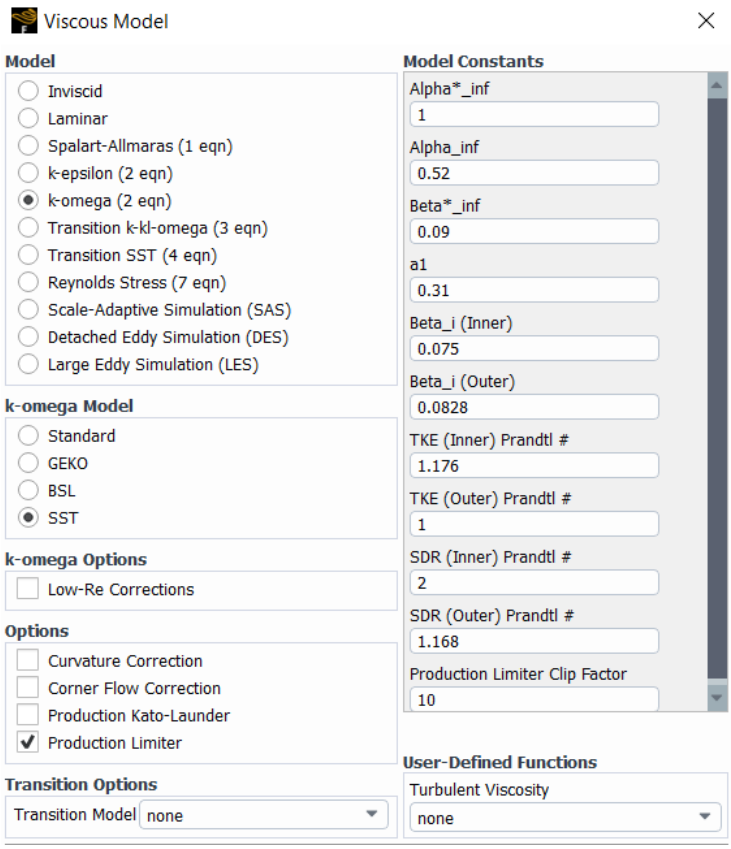

Figure 50. Viscous model set up in Fluent

Once the viscosity model is defined, the following parameters are set:

- Material: Air at sea level conditions
- Boundary conditions:
  - Inlet: Velocity inlet at 25 m/s
  - Outlet: Pressure outlet
  - Symmetry: Selecting the symmetry plane of the enclosure
  - Walls: Selecting the remaining sides of the enclosure plus the UAV surfaces

Figure 51 shows the initialization and calculation parameters.

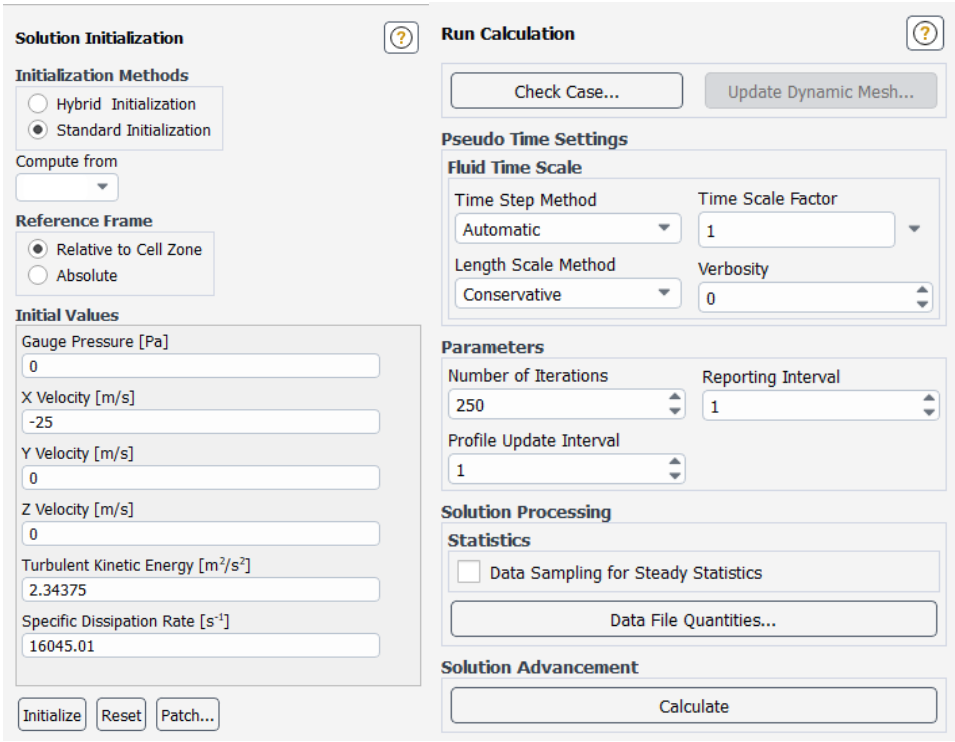

Figure 51. Initialization and calculation parameters definition in Fluent

With all parameters defined for the simulation, the next step is to proceed with the simulation. It's important to note that the angle of attack for these calculations is set at 0 degrees. Figure 52 shows the residuals of the solution.

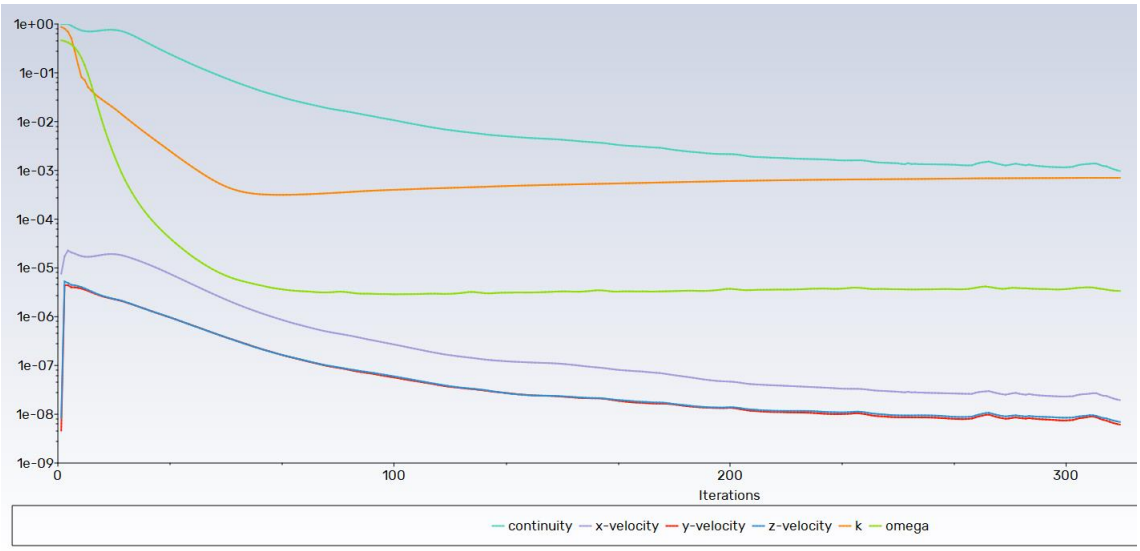

Figure 52. Residuals for 0 degree AOA UAV in Fluent

As it can be observed, the solution converged. Continuity reached a value of $1x10^{-3}$ order, so it can be said that simulation has run successfully.

In order to illustrate the results, it will be created three planes where magnitude contours will be plotted: symmetry plane, central wing-tail plane and lateral wing plane.

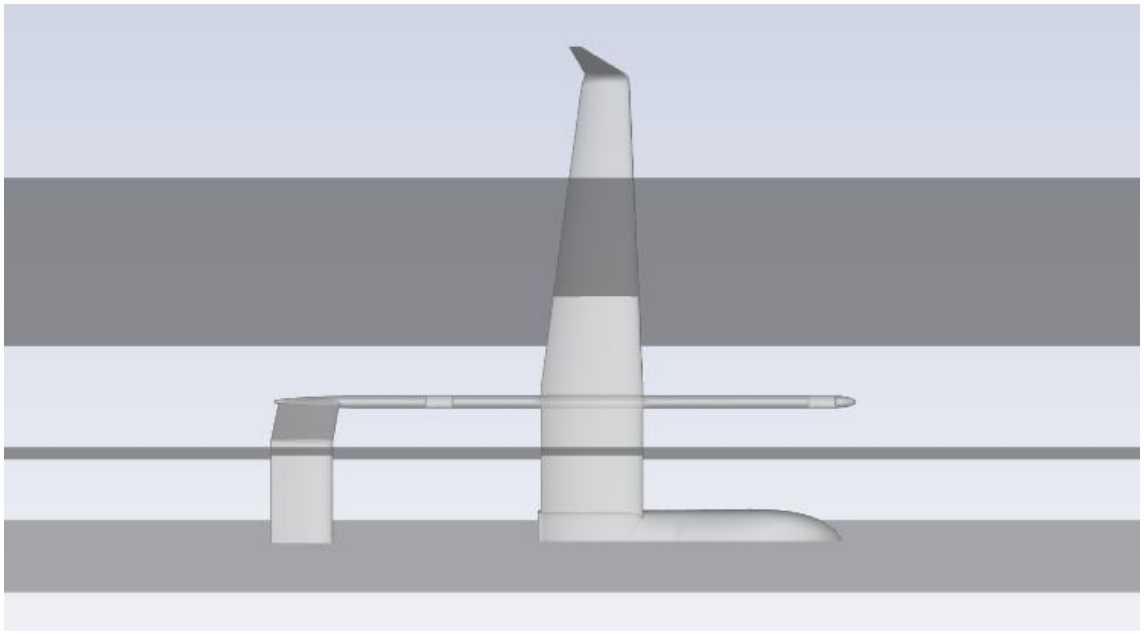

Figure 53. Plane's location to analyze the results obtained in Ansys

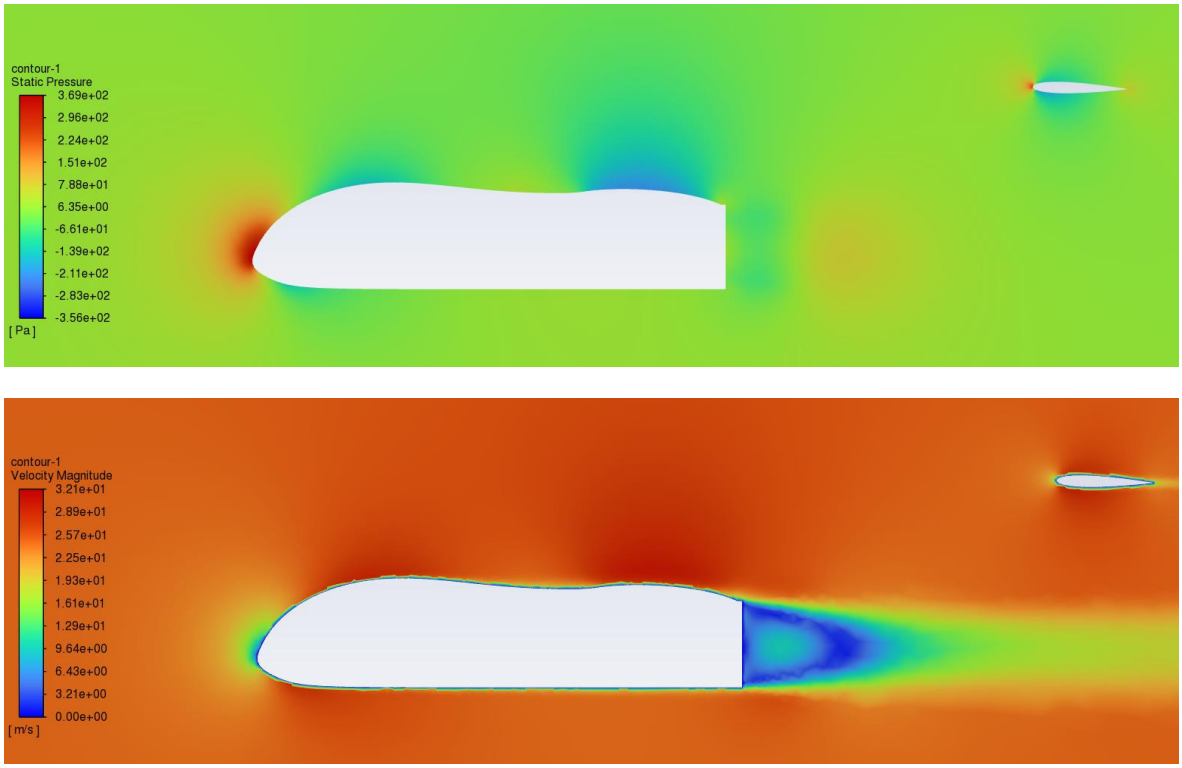

Figure 54. Static pressure (up) and Velocity (down) obtained for the symmetry plane

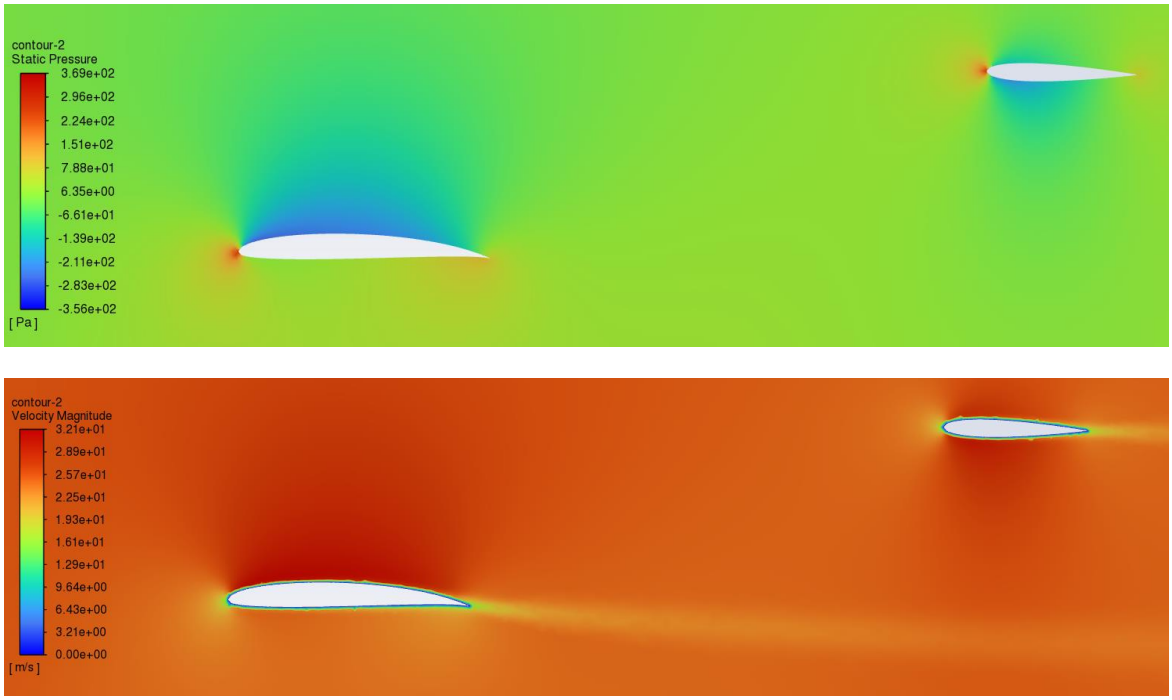

Figure 55. Static pressure (up) and Velocity (down) obtained for the central wing-tail plane

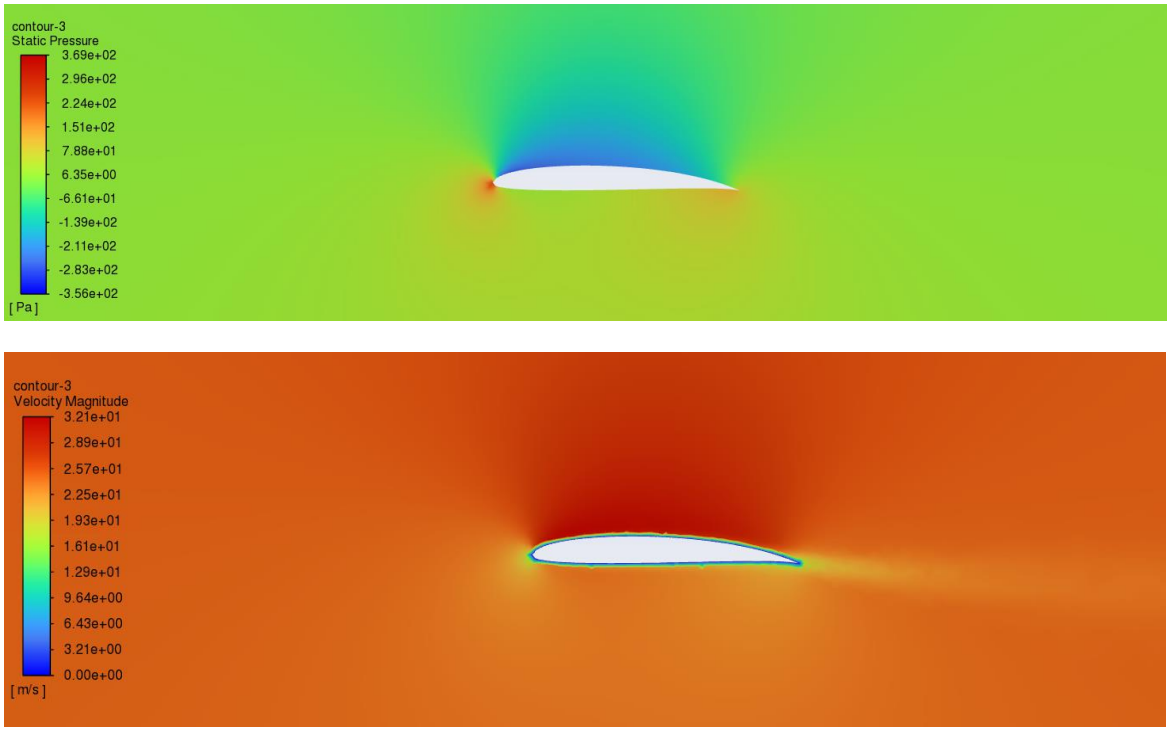

Figure 56. Static pressure (up) and Velocity (down) obtained for the wing plane

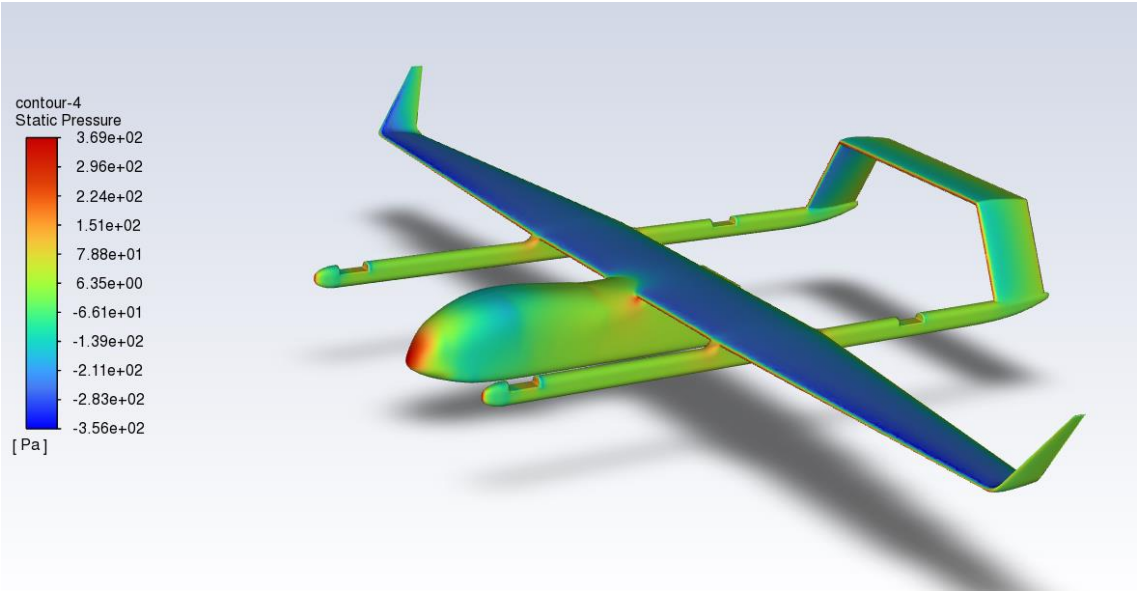

Figure 57. Static pressure distribution over UAV Surface

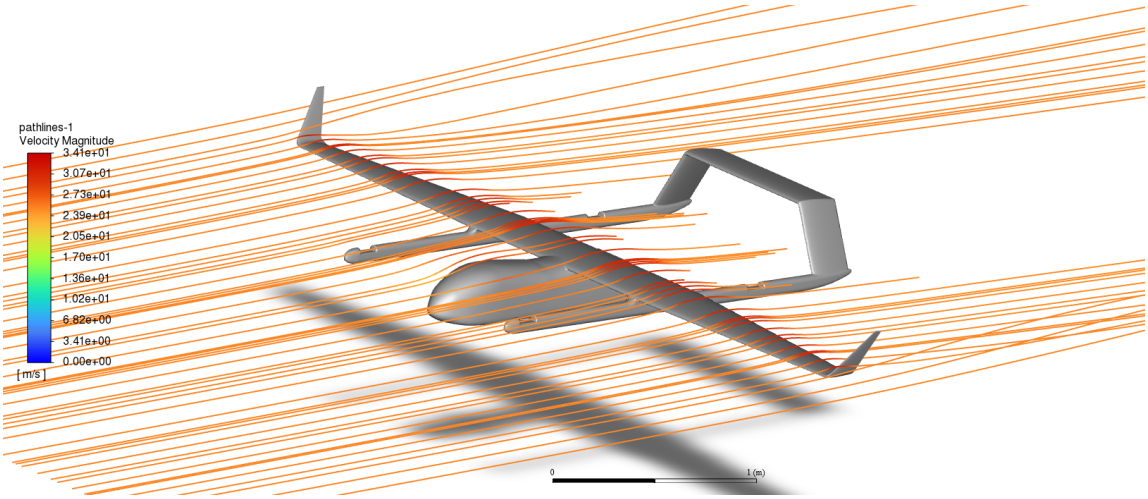

Figure 58. UAV path lines

Next, the resultant forces on the surface of the UAV are obtained to determine the values of lift and drag. It is important to remark that those values must be multiplied by two, since the simulation has been carried out for one half of the UAV.

- Lift: 308.04 N
- Drag: 21.5 N

The weight of the UAV is 392.4 N. Therefore, the lift obtained would be insufficient to support the weight of the aircraft. However, according to the data obtained in Aeolus, level flight was achieved at 1 degree angle of attack for 25 m/s. It should also be noted that in Aeolus the fuselage and arms were not included, so part of the central section of the wing is not providing lift as in the previous model. Additionally, the arms also affect the lift of the wing in the area where they attach to it.

Regarding the aerodynamic drag, the drag obtained in Fluent is significantly higher than that obtained in Aeolus. This is mainly due to the inclusion of the fuselage and arms. It is worth noting that, as the end of the fuselage has an abrupt and flat shape, it generates a low-pressure and high-recirculation zone (Figure 54), which significantly impacts the form drag.

The results obtained for 0 degrees angle of attack are satisfactory, and the solution has converged correctly. Next, the angles of attack will be parameterized from -5 degrees to 15 degrees in increments of 2.5 degrees. Lift and drag are set as output parameters. With that data, the next step is to plot the lift coefficient, drag coefficient and efficiency as a function of the angle of attack.

The next equations show how to obtain lift and drag coefficient as a function of the reference surface, density, velocity, lift and drag:

$$L = \frac{1}{2}\rho V^2 S C_L$$

$$D = \frac{1}{2}\rho V^2 S C_D$$

$$C_L = \frac{2L}{\rho V^2 S}$$

$$C_D = \frac{2D}{\rho V^2 S}$$

AOA	Lift (N)	Drag (N)	C_L	C_D
-10	-157,44	45,36	-0,29366	0,084607
-5	47,5	19,88	0,088599	0,037081
-2,5	175,88	19	0,328058	0,035439
0	308,04	21,5	0,574567	0,040103
5	529,08	36,94	0,986859	0,068902
7,5	573,4	48,96	1,069527	0,091322
10	561,02	72,62	1,046435	0,135453
12,5	549,02	96,44	1,024052	0,179883
15	473,16	125,9	0,882555	0,234833

Table 2. Lift, Drag and its coefficients as a function of AOA obtained in Fluent

In Table 2, the obtained results of lift, drag, and their coefficients from the Fluent simulation are shown. In the following images, the curves of the aerodynamic coefficients are displayed.

The values to obtain the aerodynamic coefficients are the next:

Velocity (m/s)	25
Density (kg/m^3)	1,225
Span (m)	4
MAC (m)	0,351
S (m^2)	1,4

Table 3. Reference values to obtain aerodynamic coefficients

From these points, the slope of the linear region of the lift coefficient curve with respect to the angle of attack can be calculated to obtain the necessary angle of attack for level flight. The following expression shows the relationship of the lift coefficient with respect to the angle of attack:

$$C_L(\alpha) = C_{L0} + \frac{dC_L}{d\alpha}\alpha$$

$$\alpha = \frac{C_L - C_{L0}}{\frac{dC_L}{d\alpha}}$$

The slope of the curve, $\frac{dC_L}{d\alpha}$, can be obtained by the next expression:

$$\frac{dC_L}{d\alpha} = \frac{\Delta C_L}{\Delta\alpha} = \frac{C_L(5) - C_L(0)}{5}$$

Zero lift coefficient, C_{L0}, is the lift coefficient obtained for AOA equal to zero. So, the expression for $C_L(\alpha)$ is as follows:

$$C_L(\alpha) = 0.574567 + (0{,}097193)\alpha$$

Then,

$$\alpha = \frac{C_L - 0.574567}{0{,}097193}$$

Lift coefficient required for level flight can be obtained from the lift expression, substituting the lift by the weight.

$$C_L = \frac{2W}{\rho V^2 S}$$

Lift coefficient required is equal to 0,7319. Substituting this value in the angle of attack expression, the angle for level flight is equal to 1,62 degrees.

This value is introduced again as an input parameter in Ansys to evaluate the results. Also, a value of -10 degrees for the angle of attack will be added to obtain the zero-lift angle of attack, since -5 degrees has shown to be not enough to obtain that point.

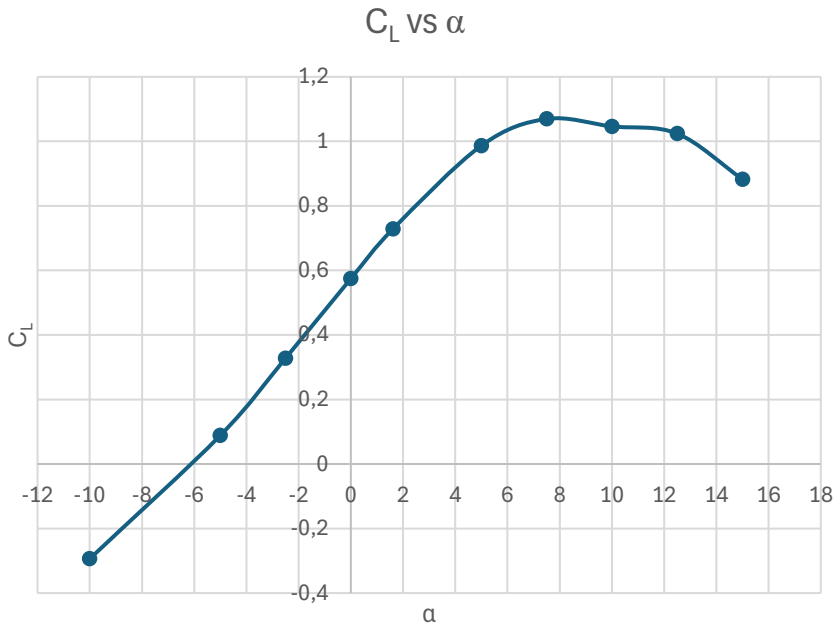

Figure 59. Lift coefficient vs AOA of the UAV obtained with Fluent

The obtained lift coefficient curve shows a smooth transition to stall, with a maximum lift coefficient at an angle of attack of 7.5 degrees. It is important to note that both the angle and the maximum coefficient might not be accurately represented, as more points would need to be plotted on the curve. However, the shape of the obtained curve supports the robustness of the results, as the lift coefficient values obtained in Aeolus (Figure 41) almost perfectly match those obtained in Fluent, except for the 10 degree angle of attack, at which the wing's boundary layer has already started to detach.

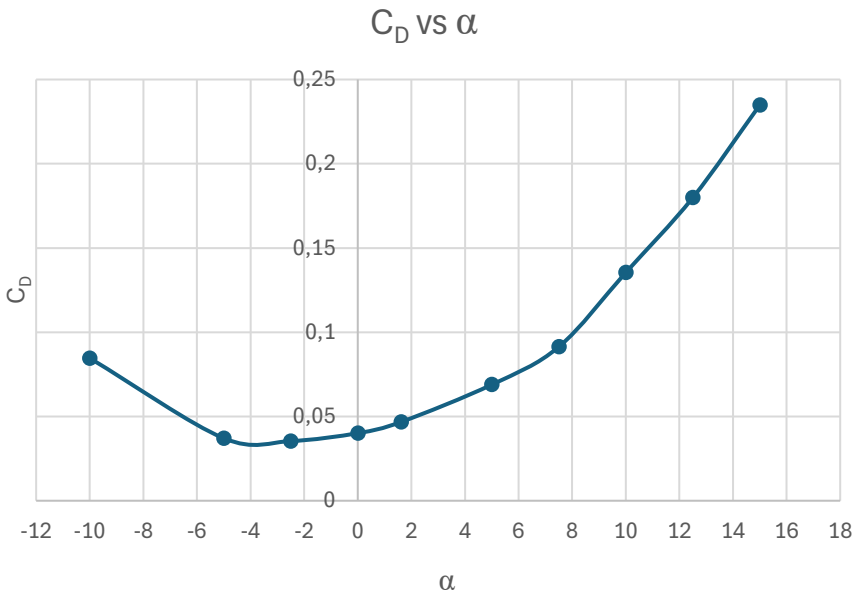

Figure 60. Drag coefficient vs AOA of the UAV obtained with Fluent

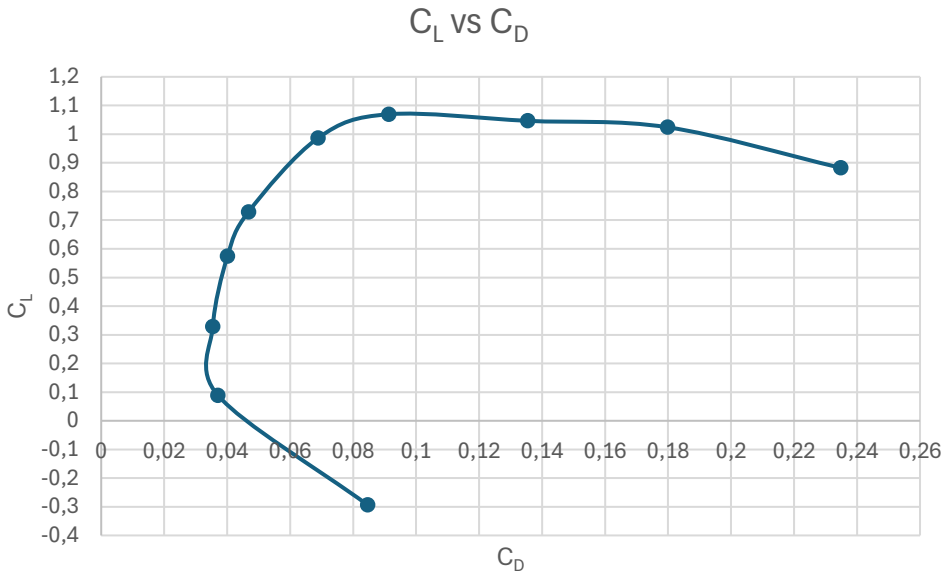

Figure 61. Lift coefficient as a function of drag coefficient of the UAV obtained with Fluent

Regarding the drag coefficient values compared to the lift coefficients, the difference between the data obtained in Fluent and those obtained in Aeolus is significantly greater. Nonetheless, this will be probably because of parasite drag contribution, not the induced drag. As previously mentioned, this was expected, since the Aeolus model did not include the fuselage or the arms.

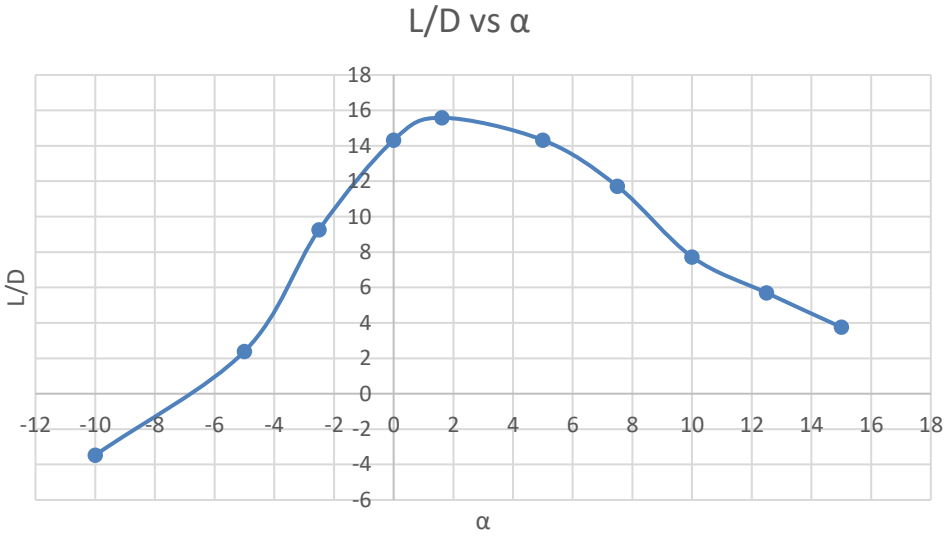

Figure 62. Efficiency vs AOA of the UAV obtained in Fluent

The results of efficiency as a function of the angle of attack show that the point of maximum efficiency for the UAV is during cruise flight, specifically at an angle of attack of 1.62 degrees at a speed of 25 m/s. This was the design intention, so in terms of efficiency, the obtained results validate the proposed solution.

Now that the lift coefficient curve has been obtained, the next step is to evaluate the stall behavior of the wing and the recirculation regions of the UAV. The objective of this analysis is to assess how the wing enters stall and to identify the sources of flow recirculation in order to determine which parts of the UAV generate the greatest aerodynamic inefficiencies. To do this, the velocity contours on the wing-tail plane will be observed from the angle of attack corresponding to the maximum lift coefficient (7.5 degrees) to the highest angle studied (15 degrees).

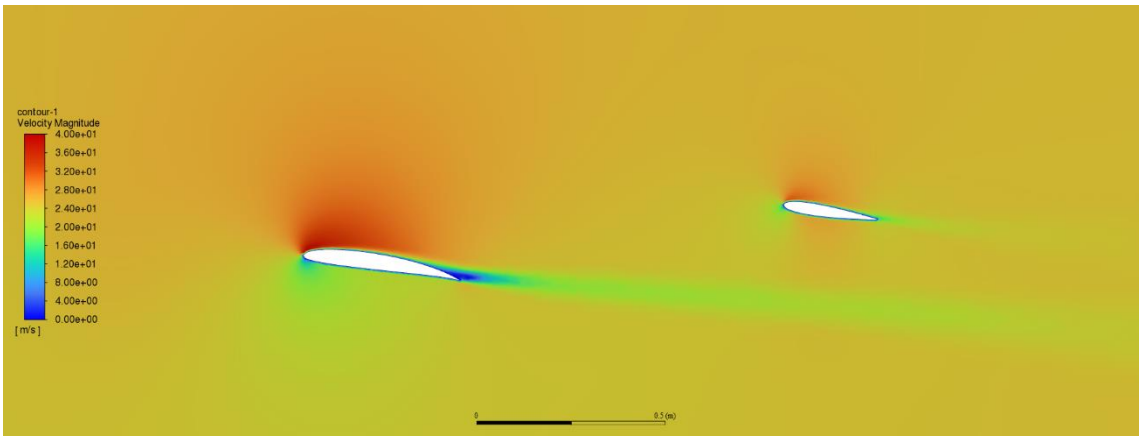

Figure 63. Velocity contour for 7.5 degrees AOA in wing-tail plane

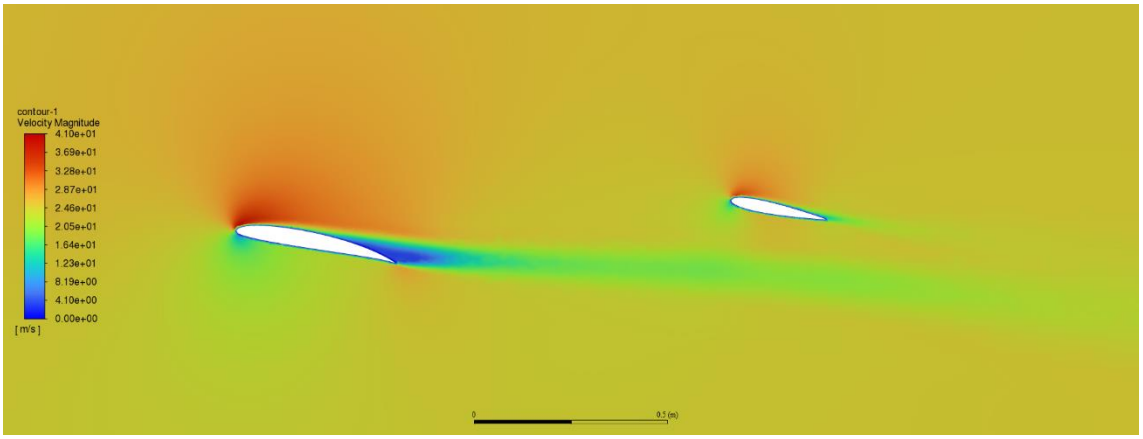

Figure 64. Velocity contour for 10 degrees AOA in wing-tail plane

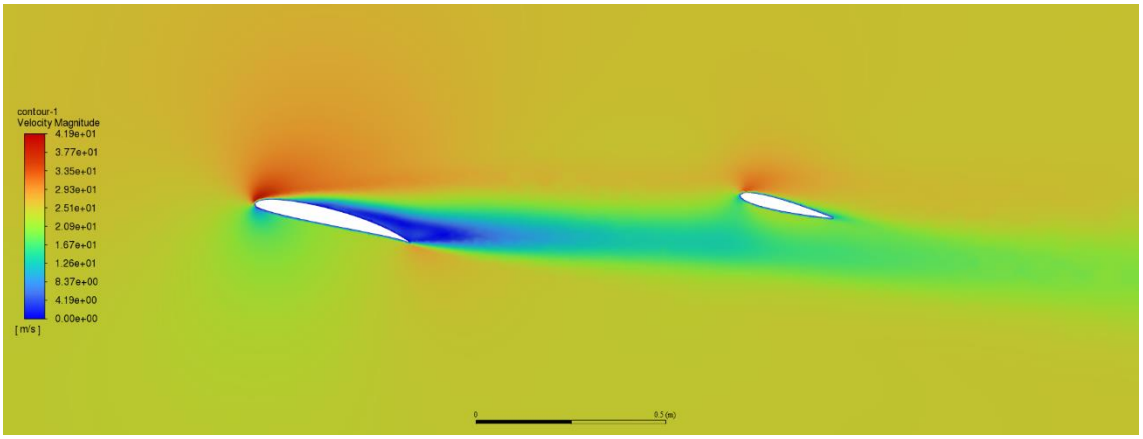

Figure 65. Velocity contour for 12.5 degrees AOA in wing-tail plane

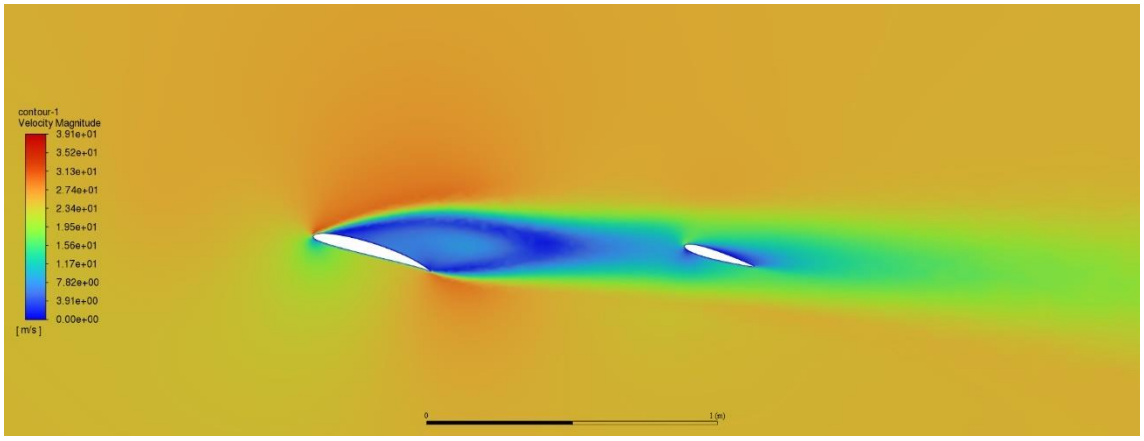

Figure 66. Velocity contour for 12.5 degrees AOA in wing-tail plane

As can be seen from Figure 63 to Figure 66 the wing stalls progressively. At 7.5 degrees angle of attack the boundary layer starts to separate at the trailing edge. At 10 degrees angle of attack the boundary layer detachment reaches about half of the airfoil. By 12.5 and 15 degrees the wing has stalled completely.

It is noteworthy that for both the 7.5 degree and 12.5 degree angles of attack, while the wing has stalled, the tail airfoil has not. This allows pitch control while the wing stalls and the ability to recover a lower angle of attack where the boundary layer remains attached to the wing airfoil, reinforcing the assumption that the UAV is longitudinally stable.

To evaluate the recirculation regions of the flow, the iso-surface tool in Fluent will be used. This tool allows the generation of surfaces formed by the points of the fluid that have a common property. Recirculation zones begin when the air flow in one direction changes its direction. That is, if an iso-surface is generated that gathers the points of the fluid with a velocity in the x-direction (flow direction in the simulation) of a negative value close to zero, the recirculation regions will be shown. To do this, the value for the iso-surface will be set to -0.1 m/s in the x-direction.

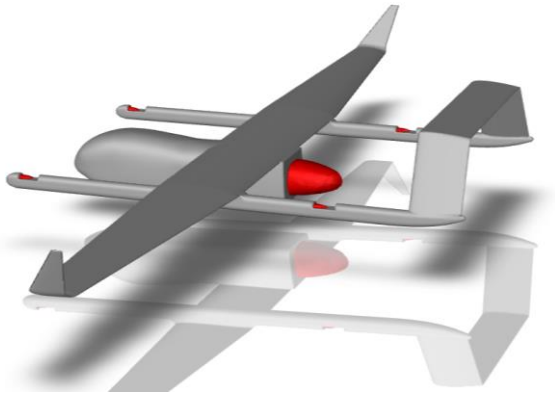

Figure 67. Recirculation for cruise (1.62 degrees AOA)

In Figure 67, the recirculation regions are shown in red. It can be observed that the recirculation regions in this flight condition are located at the end of the fuselage and in the cavities of the vertical thrust engines, as expected. It should be noted once again that the main engine will be located at the end of the fuselage, with its propeller generating suction force that will help reduce this effect.

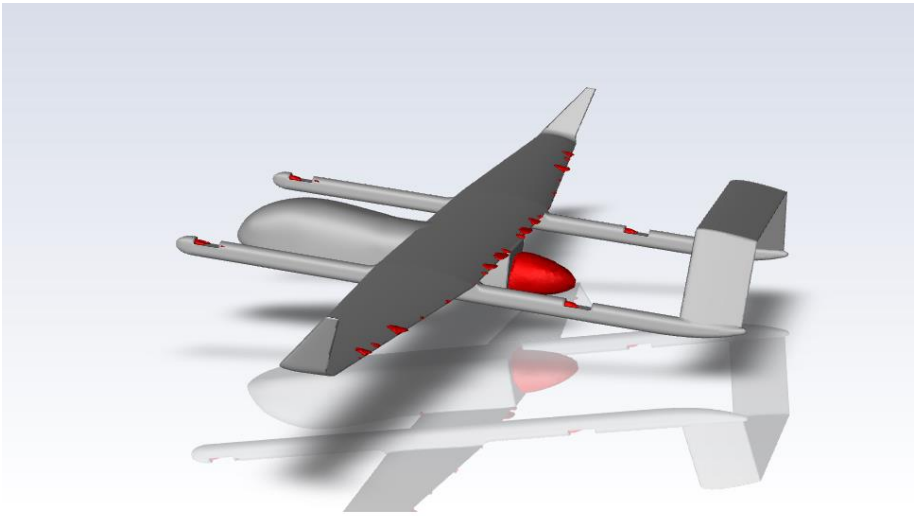

Figure 68. Recirculation for 7.5 degrees AOA

For an angle of attack of 7.5 degrees, flow recirculation regions begin to appear, but they are not extended along the entire wing.

Figure 69. Recirculation for 10 degrees AOA

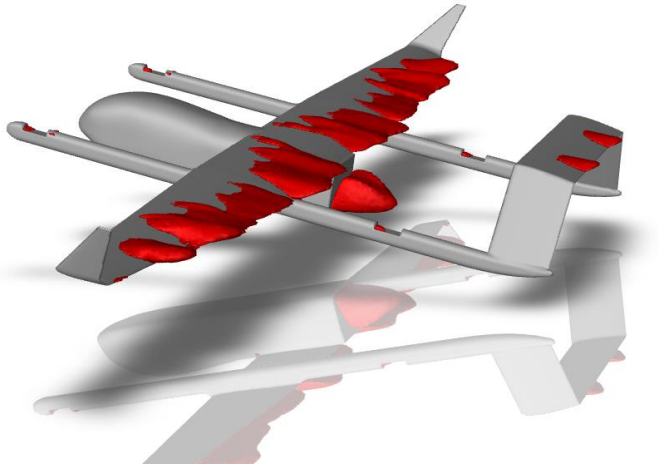

Figure 70. Recirculation for 12.5 degrees AOA

For 10 and 12.5 degrees of angle of attack, the recirculation zones are more clearly visible along the wing. They are not uniform but show how recirculation regions extend practically from the midsection of the airfoil to the trailing edge. However, it can be observed that these regions are not present on the horizontal stabilizer.

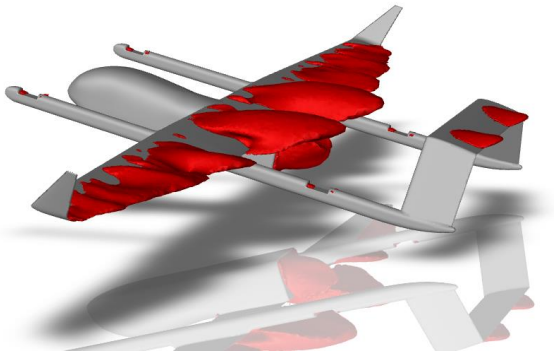

Finally, at 15 degrees of angle of attack, the entire wing exhibits recirculation regions, and the horizontal stabilizer also shows these regions.

4.2 Structures

In the realm of aerospace engineering, the structural design is key. The efficiency and performance of a UAV are heavily influenced by its structural integrity and weight. Consequently, achieving a delicate balance between minimizing weight and ensuring sufficient strength to endure flight loads is crucial.

This chapter delves into the structural design considerations for our UAV, highlighting the innovative approaches adopted to optimize weight savings while maintaining the requisite durability and resilience. Given the UAV's dismountable design, which facilitates ease of

transport and maintenance, the structural components must exhibit exceptional strength-to-weight ratios. This is where advanced composite materials come into play.

Carbon fiber composites have been selected as the primary material for the entire UAV structure, excluding the upper cover. This choice is driven by carbon fiber's superior strength-to-weight ratio, which significantly enhances the UAV's performance by reducing weight without compromising structural strength. The remarkable stiffness and tensile strength of carbon fiber composites make them ideal for withstanding the aerodynamic and operational stresses encountered during flight.

However, due to the electrically conductive nature of carbon fiber, which could interfere with the UAV's internal communication systems, the upper cover is constructed from glass fiber composites. Glass fiber, while slightly heavier than carbon fiber, offers the necessary transparency for electromagnetic signals, ensuring uninterrupted communication and control of the UAV's equipment.

Error! Reference source not found. shows the general arrangement of the structure in CATIA. In the next paragraphs different parts of the structure will be described in detail.

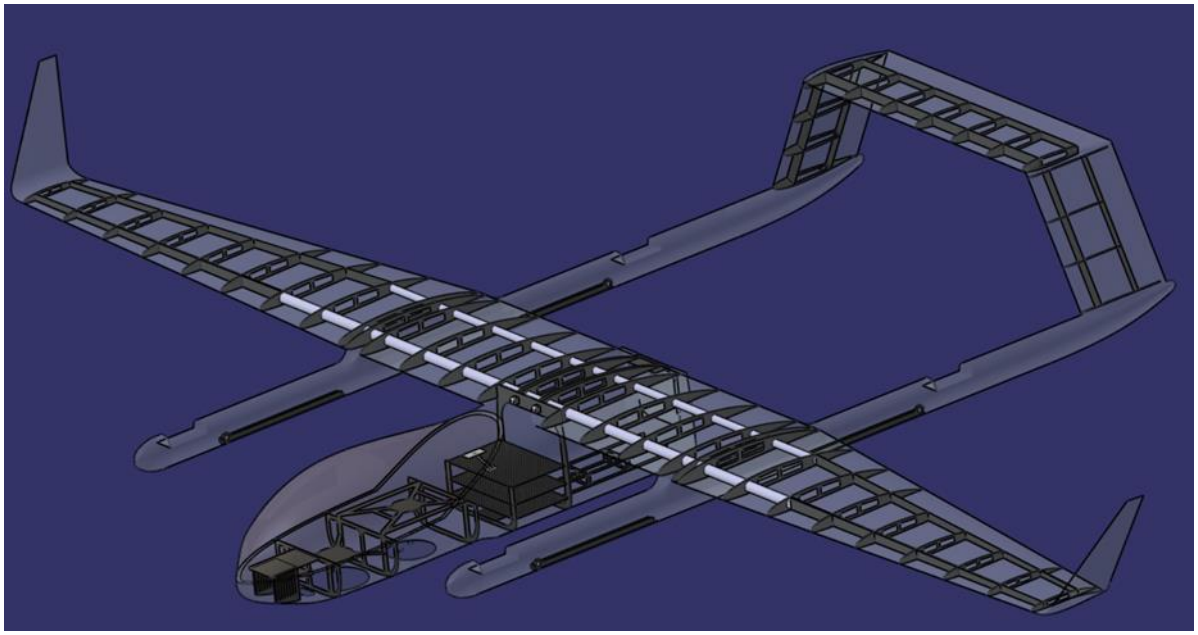

Figure 71. UAV structure

4.2.1 Fuselage structure

The fuselage of a UAV is a critical structural component, serving as the central body that houses the various systems and payloads while maintaining the overall integrity and aerodynamic efficiency of the aircraft. In this section, it will be explored the fuselage's structural design, focusing on the primary loads it must endure during flight.

The fuselage must withstand several key loads during flight, including:

- Aerodynamic loads: These are the forces exerted by the airflow over the fuselage, including lift, drag, and side forces. The fuselage must be aerodynamically efficient to minimize drag while providing sufficient structural support to manage these forces.
- Structural Loads: The fuselage experiences bending and torsional loads, particularly during maneuvers and turbulence. These loads require the fuselage to have adequate stiffness and strength to prevent deformation and ensure stability.
- Load Transfer from Wing: The lift generated by the wings is transferred to the fuselage, necessitating a robust central frame to distribute these forces effectively. This frame acts as the primary load-bearing structure, ensuring the fuselage can handle the concentrated loads without compromising its integrity.
- Operational Loads: These include the forces resulting from the payload, equipment vibrations, and impacts during landing. The fuselage must be designed to absorb and distribute these loads to protect the internal components and maintain structural integrity. Also, the vibrations induced by the combustion main engine must be withstand.

To address these requirements, the fuselage structure of our UAV employs a monocoque design. This design approach integrates the skin and frame into a single, load-bearing shell, optimizing weight efficiency and structural strength. The monocoque structure ensures that the external loads are uniformly distributed across the fuselage, enhancing its overall resilience.

A central frame is incorporated within the monocoque fuselage to effectively withstand and distribute the lift produced by the wings. This frame is crucial for maintaining structural integrity and ensuring the fuselage can handle the aerodynamic forces during flight.

Inside the fuselage, there is an internal support structure designed primarily to accommodate and secure the necessary equipment for the UAV's operations. While this internal structure is not a primary structural element (PSE), it plays a vital role in organizing and protecting the equipment, ensuring that the UAV's systems function optimally without interfering with the primary load-bearing functions of the fuselage. The fuselage also features several strategically placed holes to facilitate the UAV's functionality:

- Payload Openings: For the gimbal and 3D mapping sensor to extend and operate effectively.
- Antenna Ports: To ensure proper communication and signal transmission.
- Pitot Tube Opening: For accurate airspeed measurements.
- Range finder. To allow laser to be emitted and received.
- Engine Mounting Holes: To secure the main engine firmly in place.
- Harness Connection Port: Located on the upper part of the fuselage, this hole allows for the connection of the harness, which transmits data from the autopilot to the engines and servomotors, as well as power for the vertical thrust engines.

These features are integrated into the fuselage design to ensure that they do not compromise structural integrity while providing the necessary functionalities for the UAV's mission.

Figure 72 shows the fuselage structure.

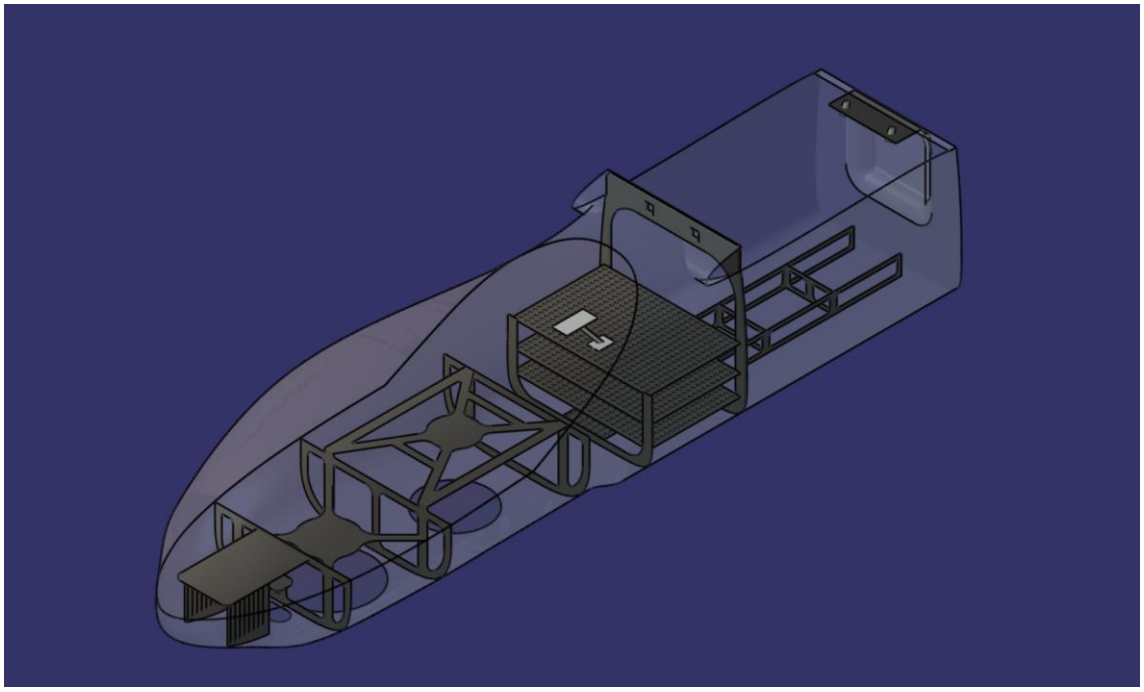

Figure 72. Fuselage structure

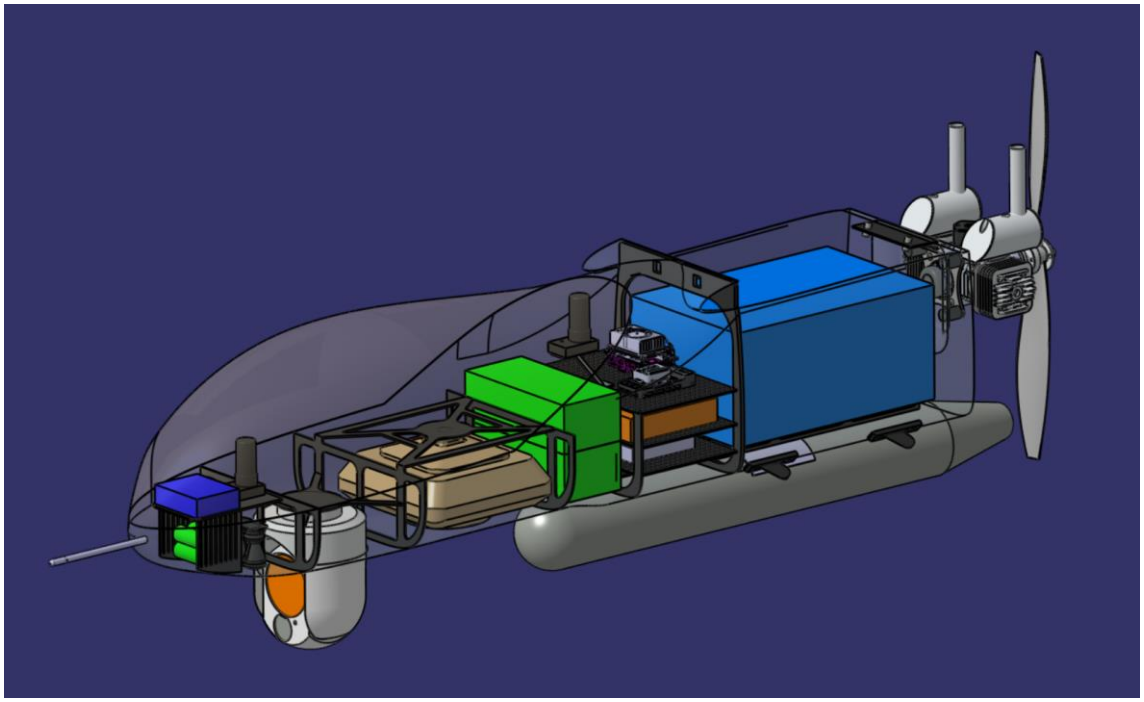

Figure 73. Fuselage equipped

4.2.2 Wing structure

The wing structure of the UAV is a pivotal component, designed to generate lift and maintain aerodynamic stability during flight. The design of the wing must balance the need for lightweight construction with the ability to endure significant aerodynamic and structural

loads. In this section, it will be described the components and materials used in the wing structure, emphasizing their roles and the rationale behind their selection.

The wing structure is composed of the following primary elements: skin, stiffeners, and ribs. Each of these components plays a crucial role in ensuring the wing's strength, durability, and functionality.

- Skin: The wing skin is the outer layer that covers the wing structure, providing a smooth aerodynamic surface to reduce drag. Constructed from carbon fiber composite, the skin offers excellent strength-to-weight ratio, which is essential for minimizing the overall weight of the UAV while maintaining structural integrity. The carbon fiber skin is designed to withstand the aerodynamic loads during flight and transfer these loads to the internal stiffeners and ribs.
- Spars: The wing incorporates two main spars (a front spar and a rear spar) both constructed from carbon fiber tubes. These spars provide longitudinal strength and rigidity to the wing, allowing it to endure bending and torsional loads effectively. A key feature of these spars is their extractable design, facilitating the dismounting and transportation of the UAV. At specific points along the wing, the stiffeners transition from carbon fiber tubes to carbon fiber plates. This design adjustment is strategically implemented to better withstand bending moments. The carbon fiber plates are oriented to maximize their resistance to bending, ensuring the wing maintains its structural integrity under various flight conditions.
- Ribs: The ribs are internal structural elements that run perpendicular to the stiffeners and skin. They provide the necessary shape and support to the wing, ensuring it retains its aerodynamic profile. The ribs distribute the loads from the skin and stiffeners, preventing localized stresses and deformation. The spacing and design of the ribs are optimized to balance weight savings with structural requirements, ensuring the wing's durability and performance.
- Winglets: The winglets, located at the wingtips, are designed to enhance aerodynamic efficiency by reducing wingtip vortices and drag. These components are made from a combination of carbon fiber skin and low-density polyamide. The carbon fiber skin provides the necessary structural strength, while the low-density polyamide core offers weight savings without compromising the winglet's performance. Given that the airfoil section of the winglets is symmetric, and they are not subjected to significant loads, this material combination effectively reduces weight while maintaining the required rigidity and durability.

In summary, the wing structure of the UAV is designed to balance the competing demands of weight savings and structural strength. The use of carbon fiber composites for the skin, stiffeners, and winglets ensures that the wing remains lightweight yet robust enough to endure the aerodynamic and operational loads encountered during flight. The strategic design of the stiffeners, transitioning from tubes to plates, further enhances the wing's ability to withstand bending moments, contributing to the overall reliability and performance of the UAV.

Below is a structural analysis of the wing. Given the complexity of the VTOL configuration at a structural level, the analysis would need to consider both the arms and the tail, as these hang from the wing. To simplify this analysis, only the lateral parts of the wing will be analyzed. The goal is to validate the dimensions and material chosen for the spars, skin, and ribs of the wing. Therefore, the structure of the winglets will not be analyzed either.

To analyze the behavior of the structure, Ansys software will be used. First, a 3D model of the lateral part of the wing will be introduced into Fluent to obtain the pressure distribution on its surface.

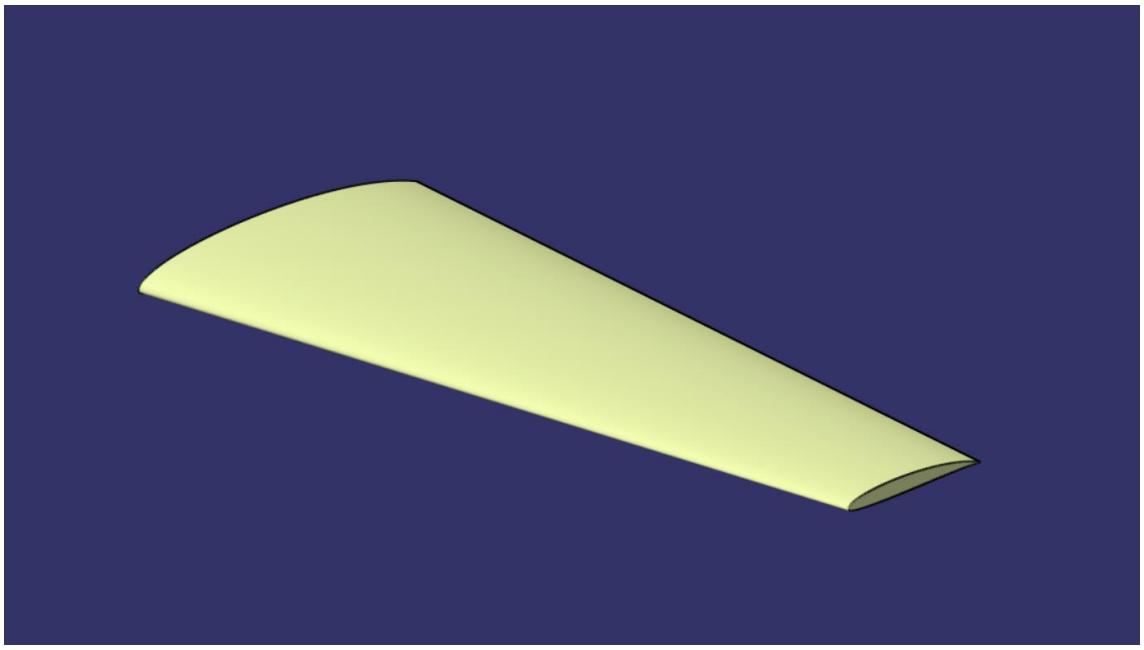

Figure 74. Lateral wing design in CATIA for Fluent analysis

Next, the wing model is imported into the Geometry Design Modeler to generate the appropriate enclosure for performing the simulation in Fluent. Also, it is given a rotation of 1.62º to the wing for representing the cruise conditions of angle of attack.

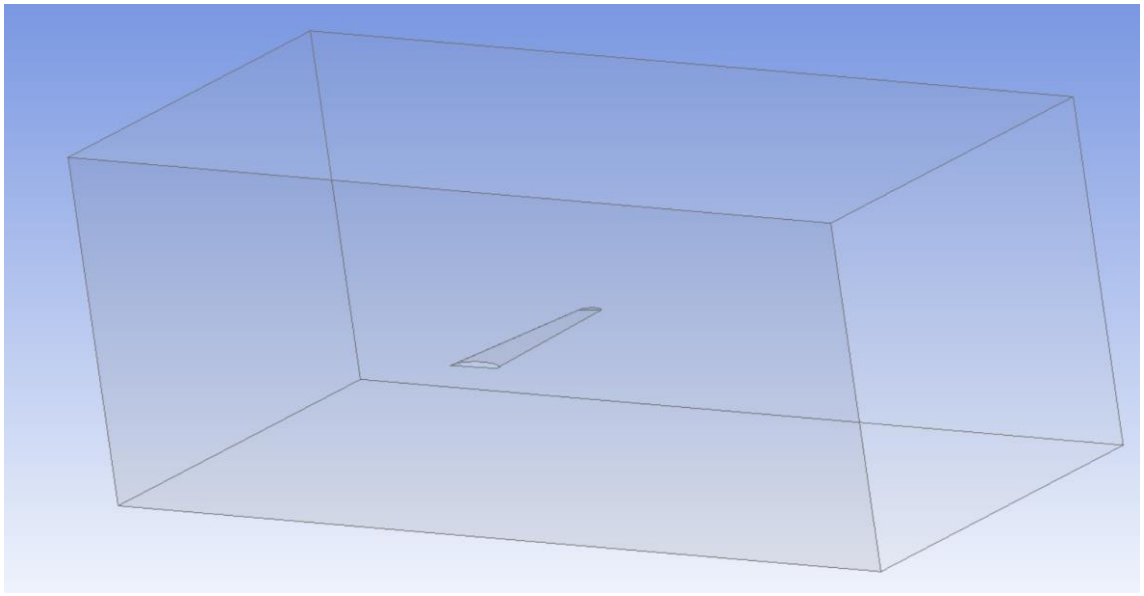

Figure 75. Wing enclosure in Geometry Design Modeler

Figure 76 shows the mesh of the wing before performing the simulation in Fluent.

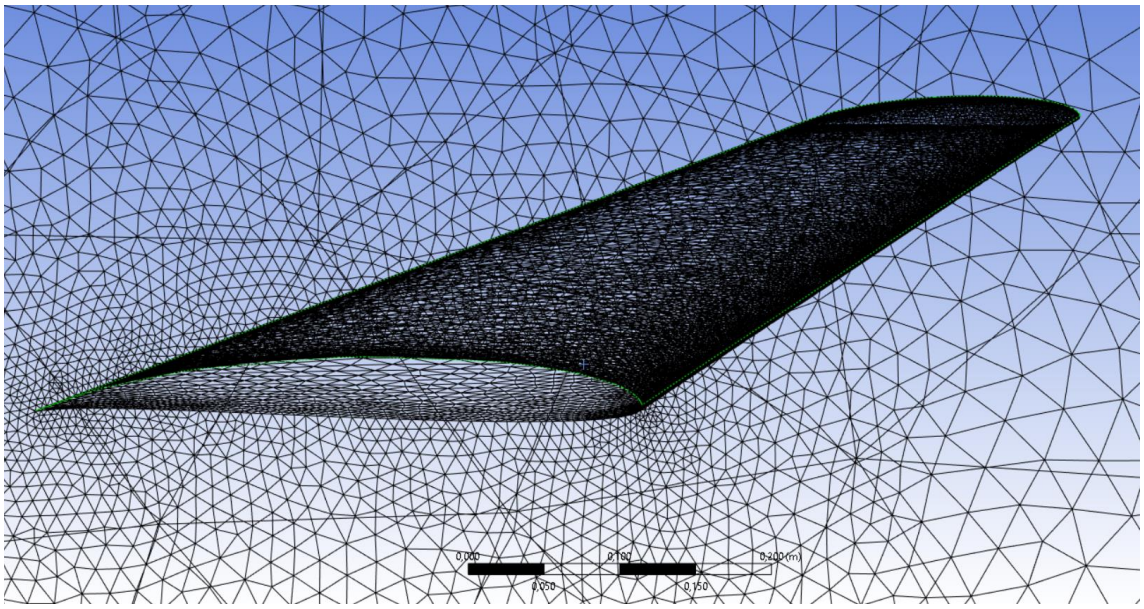

Figure 76. Detail of the lateral wing mesh

Average quality parameters of the mesh are as follows:

- Skewness: 0.21
- Orthogonal quality: 0.79

Next, the simulation parameters are defined in Fluent:

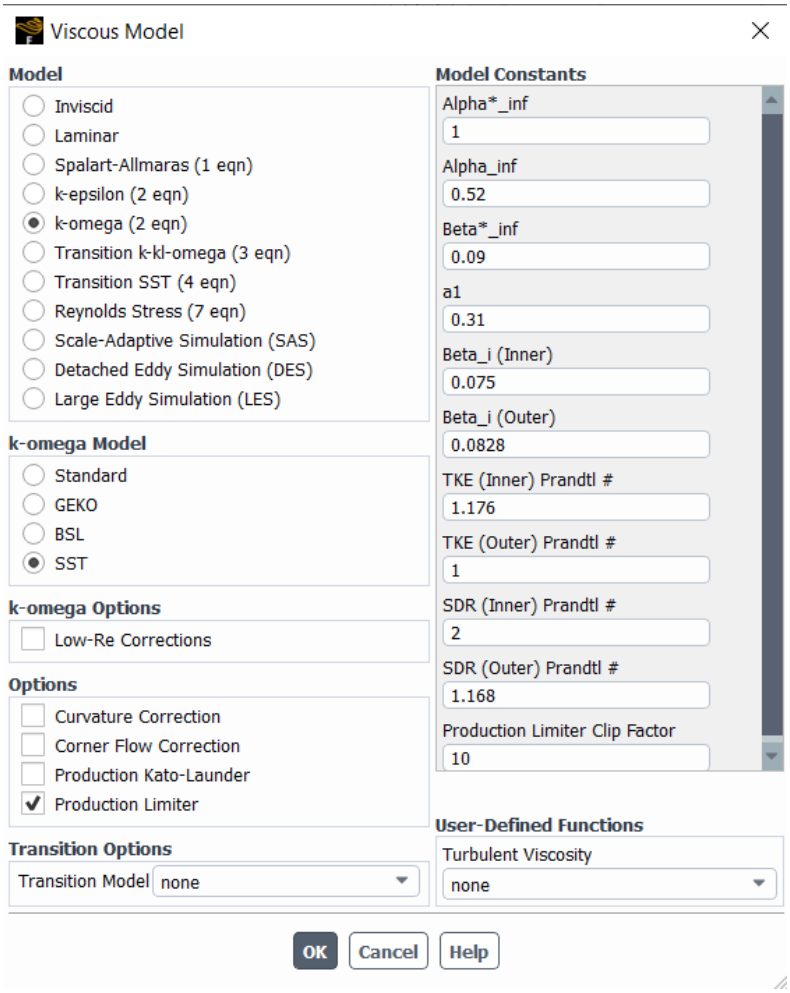

Figure 77. Viscous model set up for wing Fluent analysis

Velocity is set to 25 m/s, as the cruise flight condition. The model is simulated and shows the next residuals when finished:

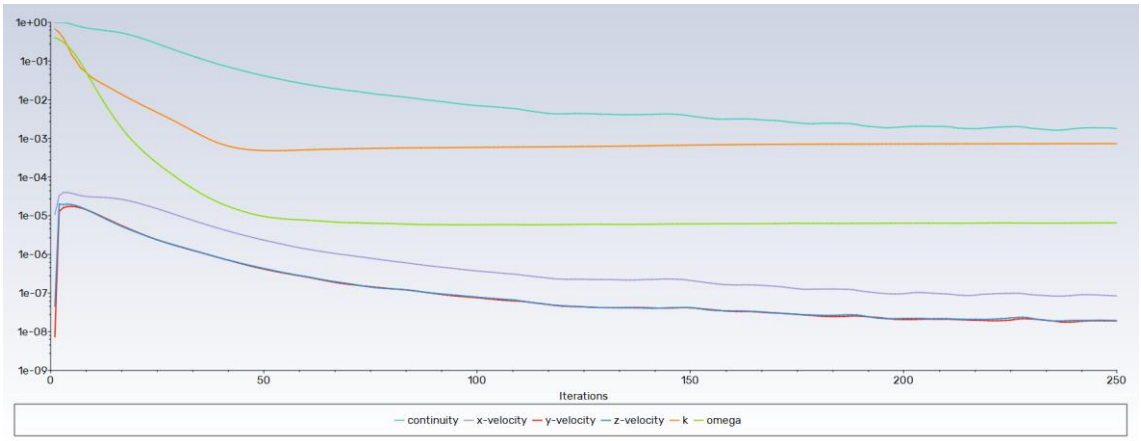

Figure 78. Residuals plot of the lateral wing Fluent simulation

As it can be seen in Figure 78, the solution converged, and continuity reaches a third order value. In Figure 79 and Figure 80 can be observed the pressure distribution along the skin, showing a lower pressure in the upper skin, providing lift.

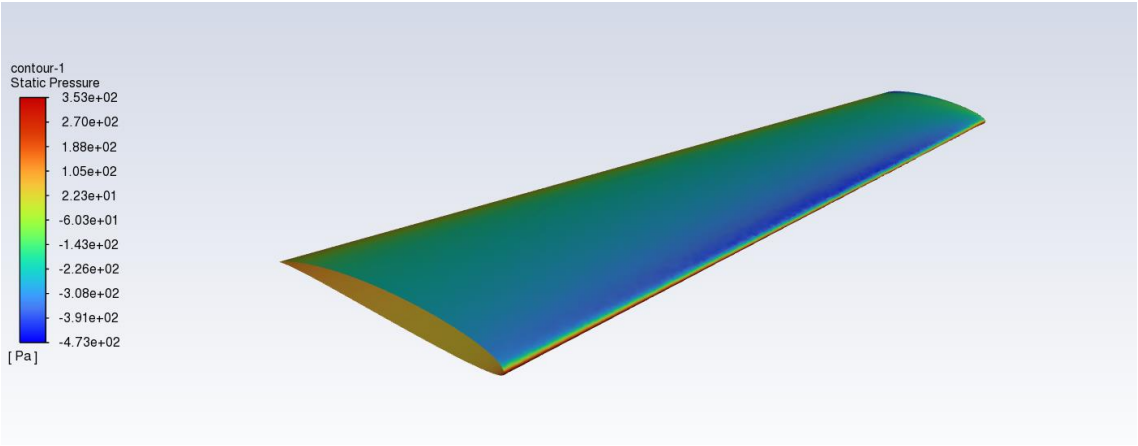

Figure 79. Static pressure distribution in upper skin

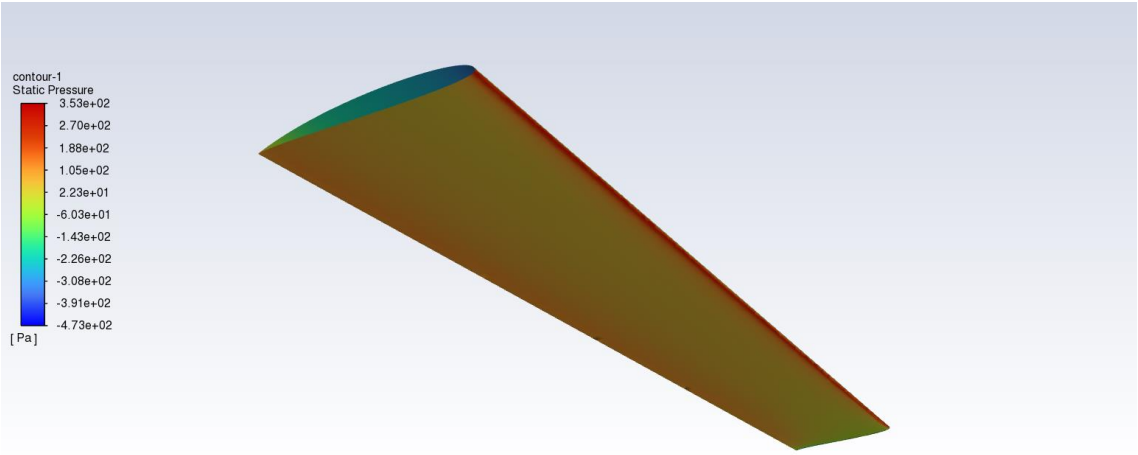

Figure 80. Static pressure distribution in lower skin

The main idea for conducting this analysis was to transfer the pressure distribution obtained in Fluent to the static structural module in order to accurately represent the load distribution on the wing under cruise conditions. However, when importing this load distribution, several errors appeared that prevented the data from being considered valid. Therefore, it was decided to obtain the resultant lift force of the wing and the moment produced around the y-axis to achieve results that are more representative of reality. The values obtained were as follows:

- Lift: 109 N
- Moment around y axis: 9.5 Nm

Figure 81 shows the skin and structure of the wing designed in CATIA. In this regard, it is noteworthy that the internal structure of the wing has been modelled to be as faithful as possible to the real manufacturing process. The spars and ribs would be manufactured by milling a 2 mm thick carbon fiber plate.

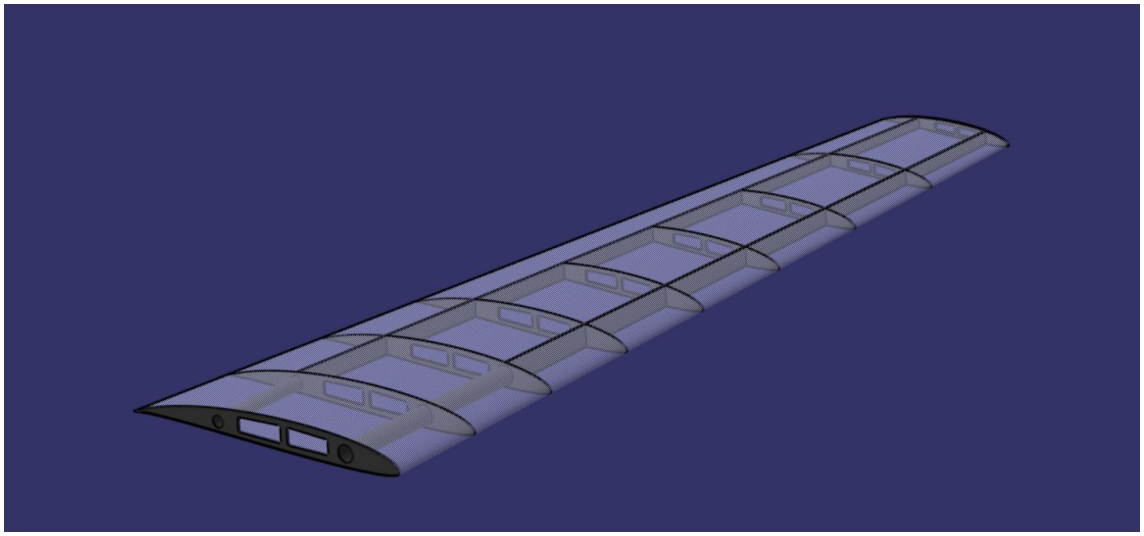

Figure 81. Skin and internal structure of the wing modelled in CATIA

As can be seen, there are three ribs that end at the rear spar and do not extend their geometry to the trailing edge of the wing. This is because the aileron is located in that region, and to allow for its rotation, they must have that shape.

Next, the skin and internal structure are imported into the Geometry Design Modeler of the static structural module in Ansys, and the setup is prepared to perform the simulation.

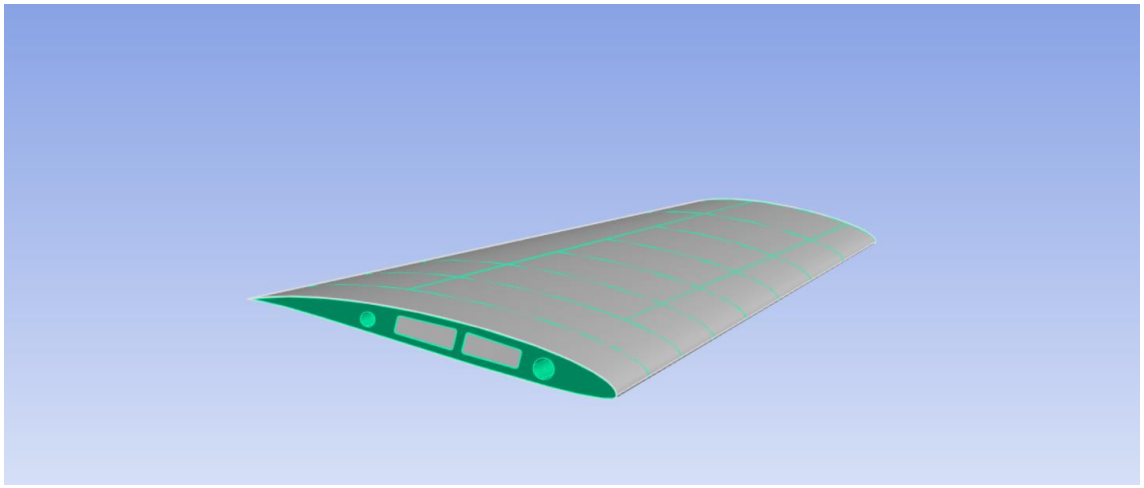

Figure 82. Skin and internal structure of the wing imported to Ansys

Both the skin and the internal structure of the wing use the material Epoxy Carbon Woven. The characteristics of this material are shown in Figure 83.

Epoxy Carbon Woven (230 GPa) Pre...

Density	1420,0	kg/m³
Structural		
Orthotropic Elasticity		
Young's Modulus X direction	6,134e+10	Pa
Young's Modulus Y direction	6,134e+10	Pa
Young's Modulus Z direction	6,9e+09	Pa
Poisson's Ratio XY	0,040000	
Poisson's Ratio YZ	0,30000	
Poisson's Ratio XZ	0,30000	
Shear Modulus XY	3,3e+09	Pa
Shear Modulus YZ	2,7e+09	Pa
Shear Modulus XZ	2,7e+09	Pa
Orthotropic Stress Limits		
Tensile X direction	8,05e+08	Pa
Tensile Y direction	8,05e+08	Pa
Tensile Z direction	5e+07	Pa
Compressive X direction	-5,09e+08	Pa
Compressive Y direction	-5,09e+08	Pa
Compressive Z direction	-1,7e+08	Pa
Shear XY	1,25e+08	Pa
Shear YZ	6,5e+07	Pa
Shear XZ	6,5e+07	Pa

Figure 83. Epoxy Carbon Woven material data

Before meshing these geometries, it is necessary to establish the contacts between the two bodies (skin and internal structure). As previously mentioned regarding the manufacturing process of the internal structure from carbon fiber plates, both the spars and ribs have faces that are perpendicular to each other. In Figure 84, it can be seen that the rib face, which must rest on the inner surface of the wing skin, forms a 90-degree angle with the face perpendicular to the spars' tubes. Due to the geometry of the wing, primarily the fact that it is tapered, it is impossible for the rib faces that need to rest on the inner skin and the inner skin itself to be tangent.

During the wing manufacturing process, this problem would be resolved by applying epoxy between the internal structure of the wing and the skin to ensure that both are bonded along the geometry and that loads can be transferred effectively. However, when performing this analysis, Ansys must assume that the structures are bonded even if they are not physically so. This fact must be taken into account when validating the results obtained from the simulation.

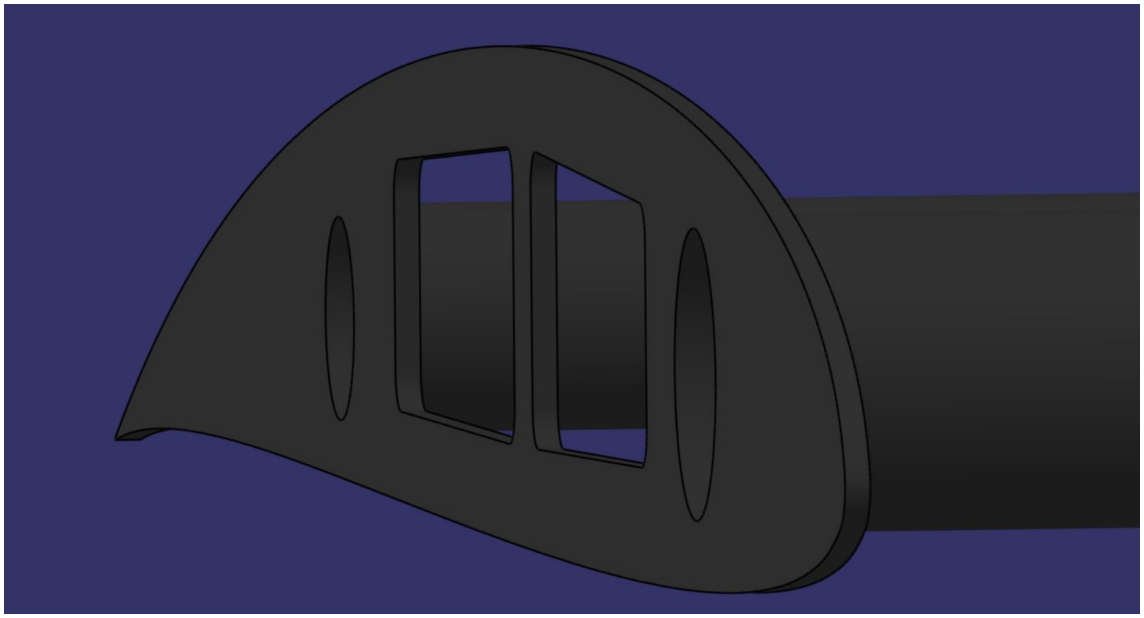

Figure 84. Detail of a wing rib

The contacts between the wing skin and the internal structure have been generated automatically. Figure 85 shows the surfaces of these contacts that has been successfully generated.

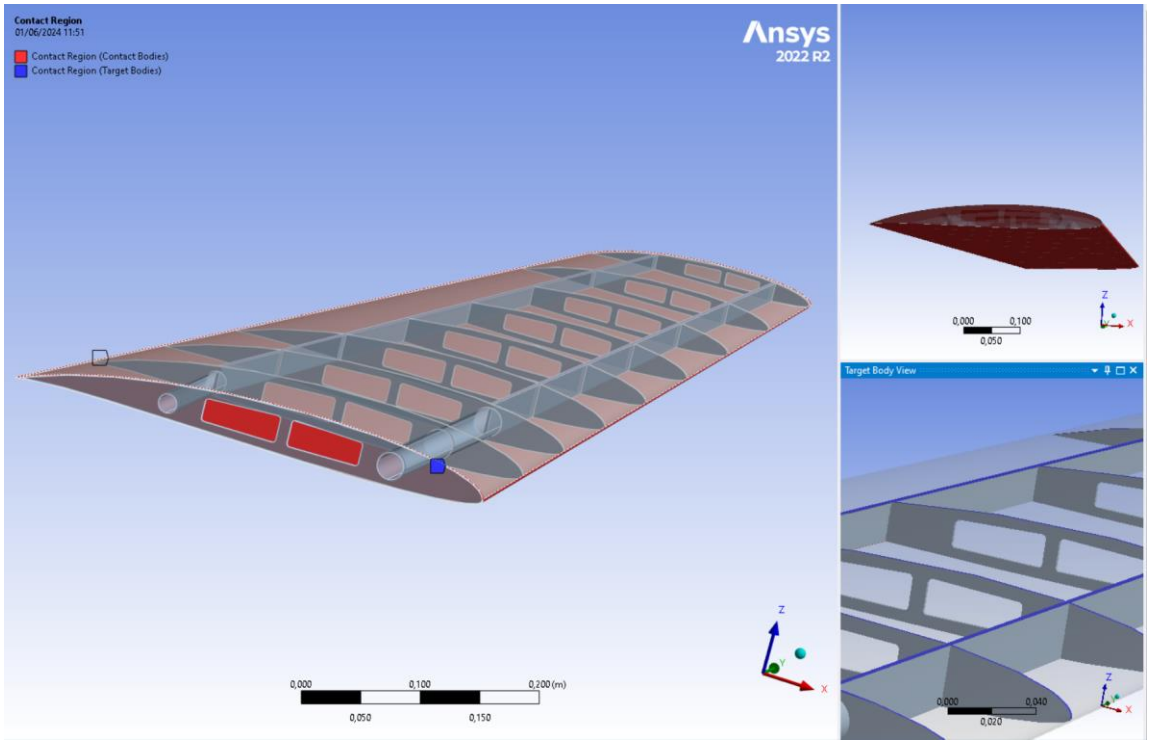

Figure 85. Contact definition between wing skin and internal structure

Figure 86 shows the details of the contact region.

Details of "Contact Region"	
Scope	
Scoping Method	Geometry Selection
Contact	4 Faces
Target	43 Faces
Contact Bodies	Skin_structure
Target Bodies	Wing_structure
Protected	No
Definition	
Type	Bonded
Scope Mode	Automatic
Behavior	Program Controlled
Trim Contact	Program Controlled
Trim Tolerance	3,2326e-003 m
Suppressed	No

Figure 86. Details of contact region

As it can be seen, the contact type is bonded, which means that surfaces in contact remains attached.

Figure 87 shows the mesh of the wing skin and internal structure.

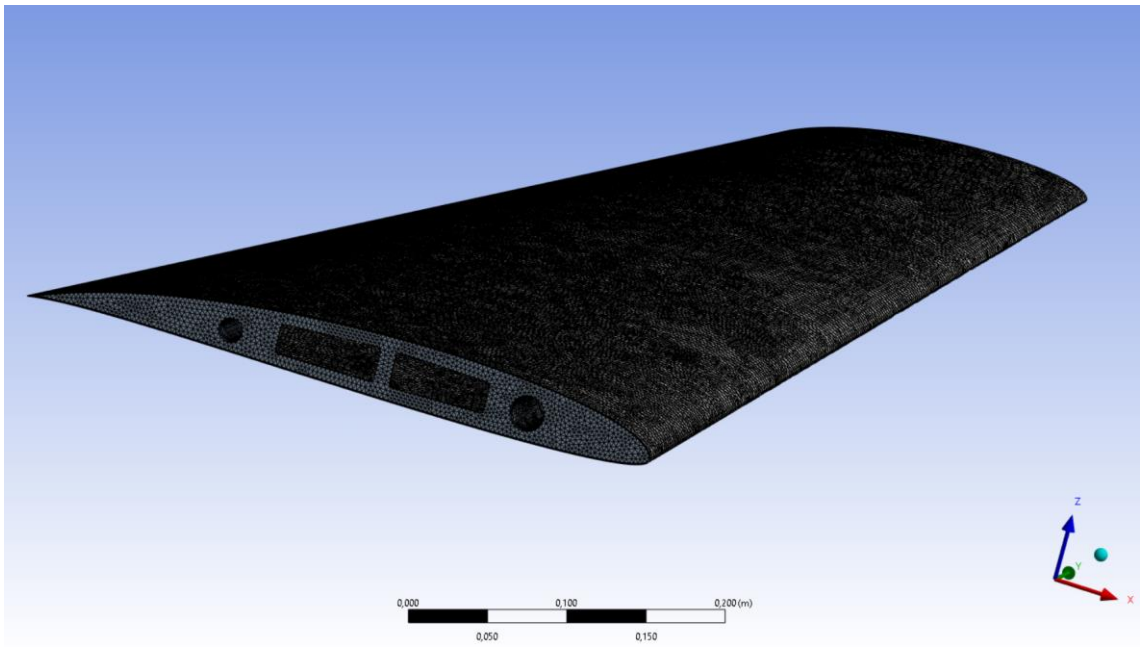

Figure 87. Detail of the wing skin and internal structure mesh

The next step is to establish the simulation conditions for the static structural module. First, the fixed supports are defined as shown in Figure 88 and Figure 89.

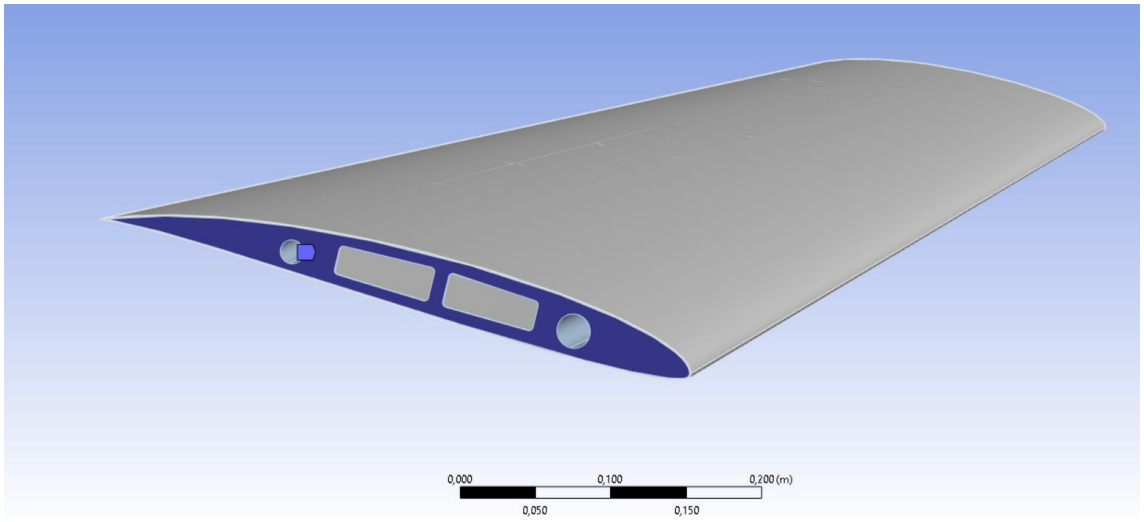

Figure 88. Fixed support definition of internal structure

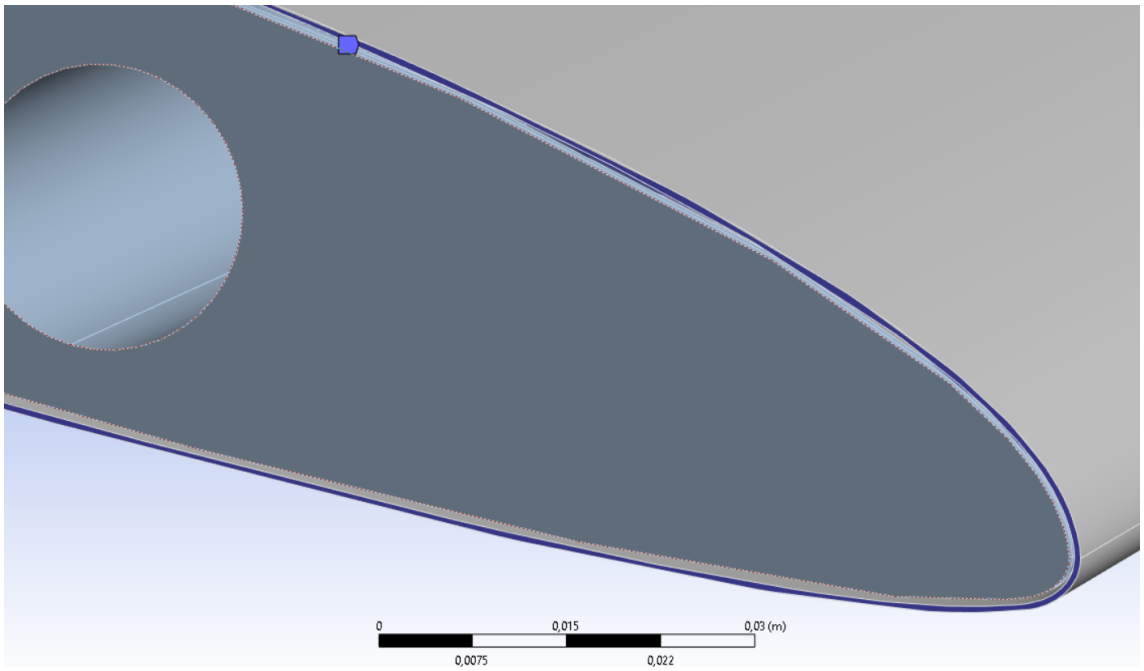

Figure 89. Fixed support definition for skin

Next, a lift force with the magnitude obtained in Fluent is applied to the outer surface of the wing skin. Figure 90 shows the details of this load application. Figure 91 shows how it has been applied using components.

Additionally, a moment is also applied to the same surface. Figure 92and Figure 93 show the details of this application.

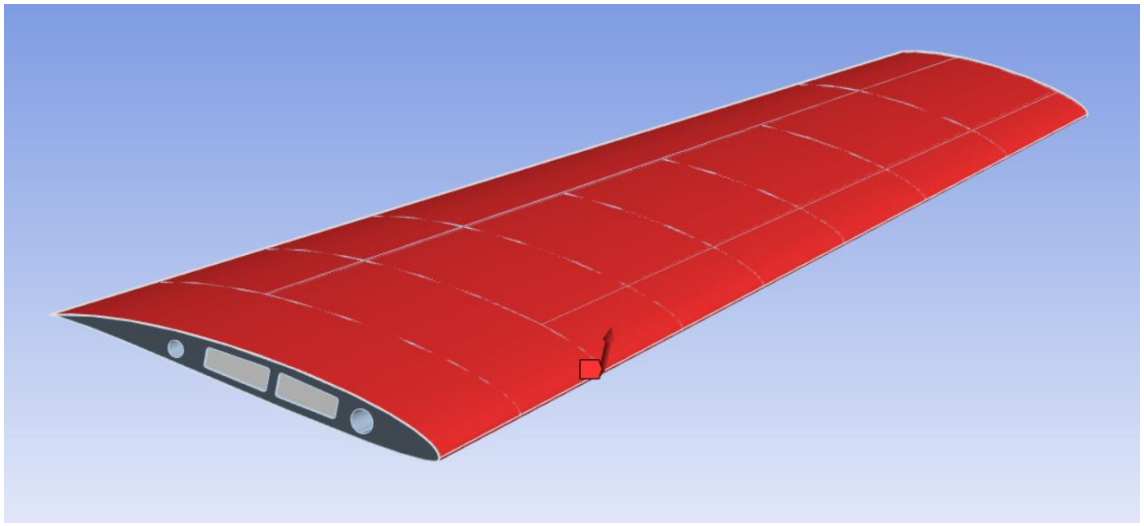

Figure 90. Detail of lift load application on wing skin surface

Details of "Force"

Scope	
Scoping Method	Geometry Selection
Geometry	2 Faces
Definition	
Type	Force
Define By	Components
Applied By	Surface Effect
Coordinate System	Global Coordinate System
X Component	0, N (ramped)
Y Component	0, N (ramped)
Z Component	109, N (ramped)
Suppressed	No

Figure 91. Details of lift force

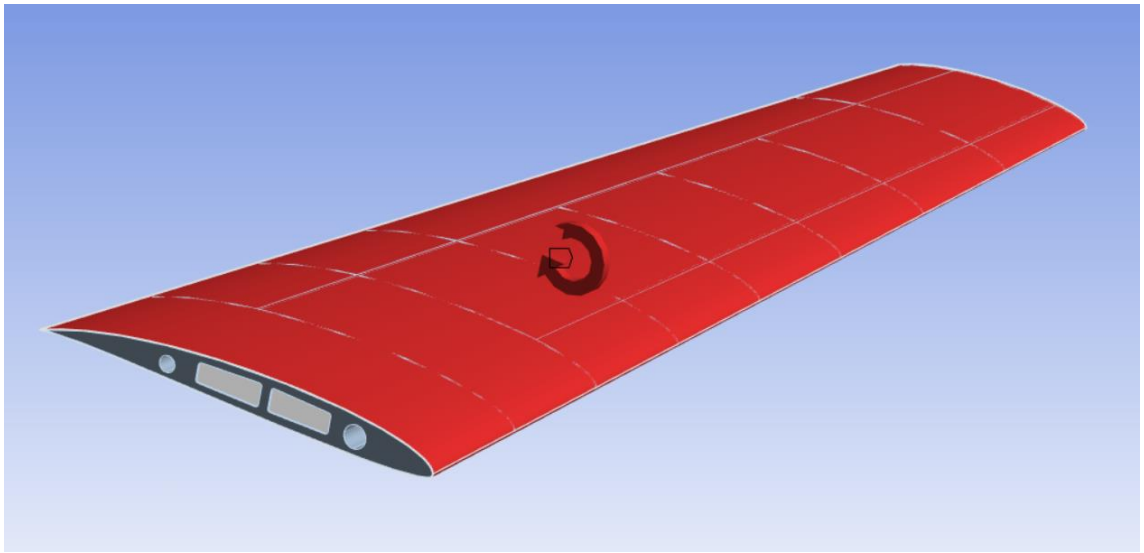

Figure 92. Detail of moment load applied on wing skin surface

Details of "Moment"

Scope	
Scoping Method	Geometry Selection
Geometry	3 Faces
Definition	
Type	Moment
Define By	Components
Coordinate System	Global Coordinate System
X Component	0, N·m (ramped)
Y Component	9,5 N·m (ramped)
Z Component	0, N·m (ramped)
Suppressed	No
Behavior	Deformable
Advanced	

Figure 93. Details of moment applied

With the simulation conditions established, the simulation is performed. The results obtained can be observed below:

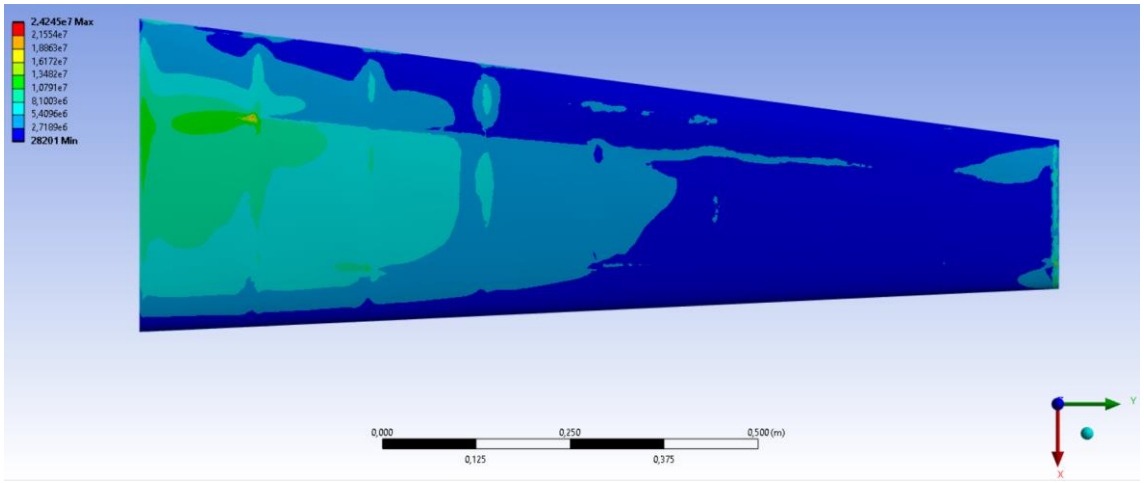

Figure 94. Upper skin stress distribution

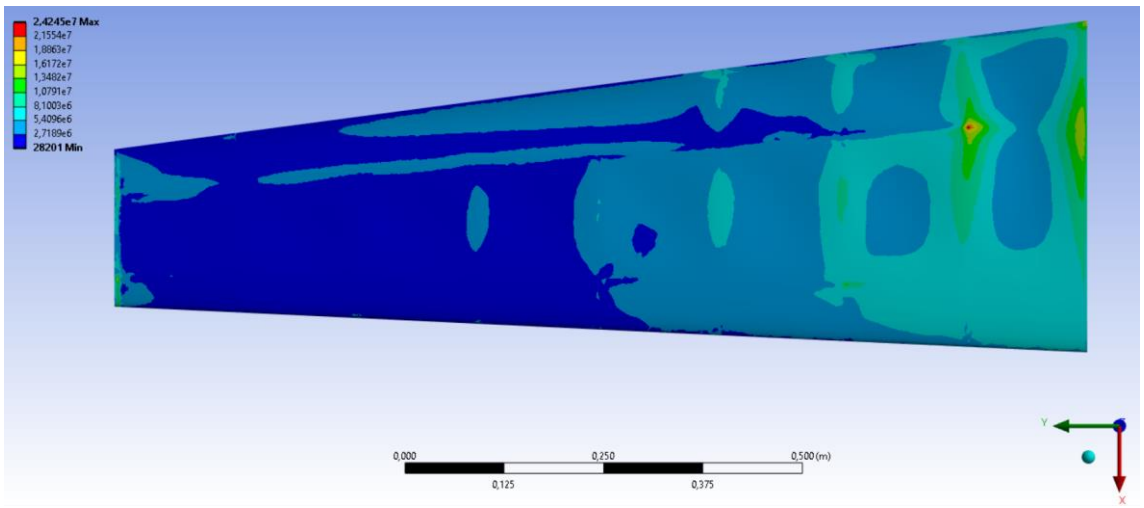

Figure 95. Lower skin stress distribution

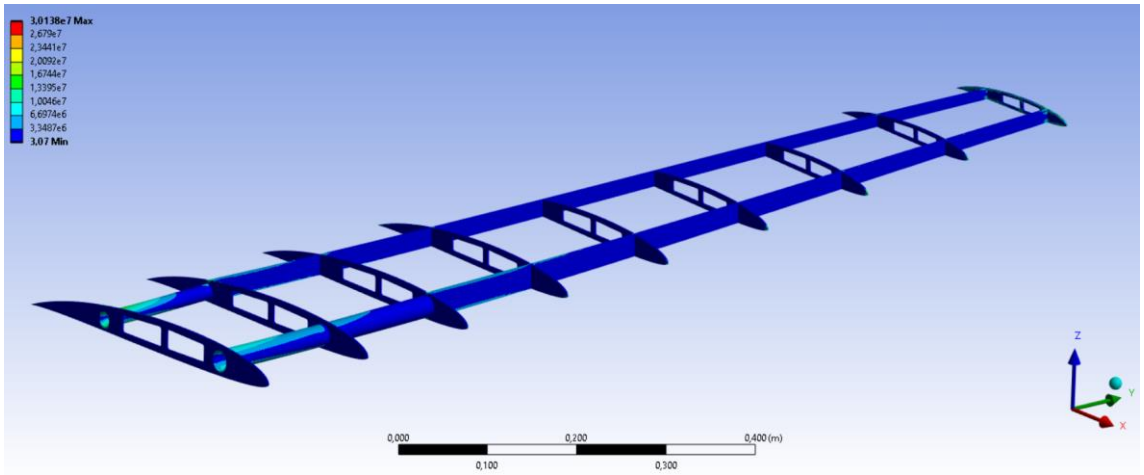

Figure 96. Ribs and Spars stress distribution

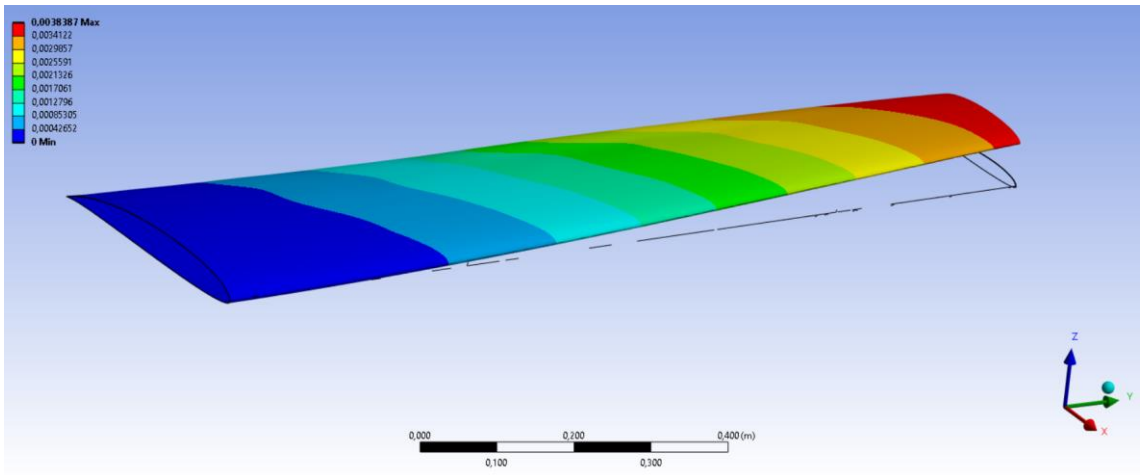

Figure 97. Skin total deformation

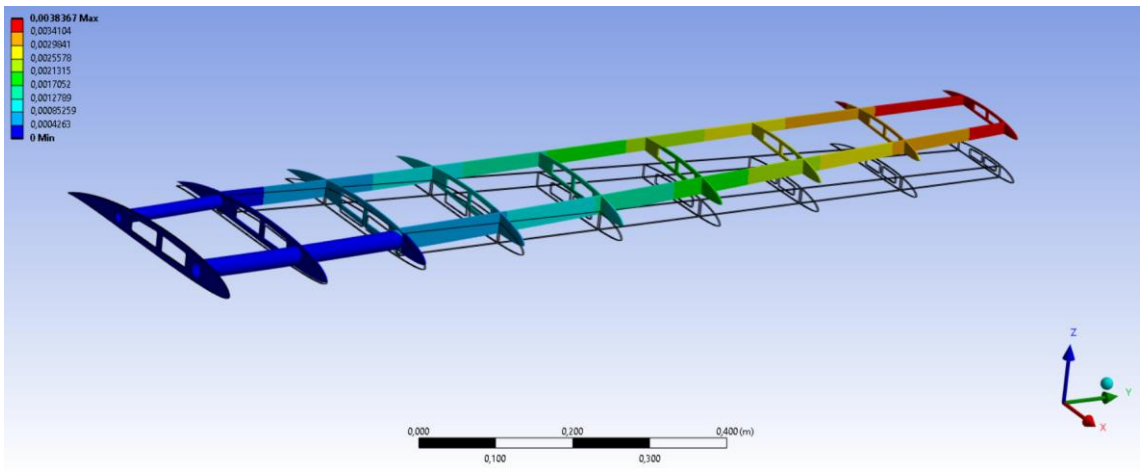

Figure 98. Ribs and spars total deformation

The results obtained show that the maximum stress value is 3.0138 x 10^7 Pa. Considering that the maximum stress value supported by the material is 8.05 x 10^8 Pa, the structure would withstand the cruise flight loads.

It is important to note that carbon fiber composite material has texture, meaning the maximum stress it can withstand depends on the direction of the applied load. The chosen material has the fibers oriented in the X and Y directions, allowing it to support the maximum load in these directions. This fact must be considered during the manufacturing of the internal structure, ensuring that the maximum loads are aligned with the fiber direction.

By applying a safety factor of 1.5 to the maximum load obtained, it would still be within the maximum load capacity of the material. Therefore, the structure has room for optimization and weight reduction.

On the other hand, the maximum deformation of the wing is found at the tip, as expected, and has a value of 3.8387 mm.

The entire semi-wing internal structure can be seen in Figure 99.

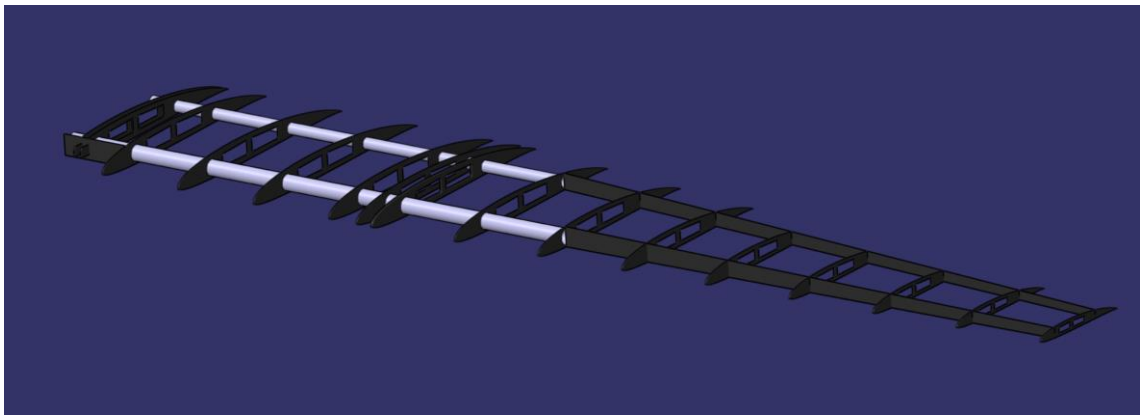

Figure 99. Semi-wing internal structure

As can be seen in Figure 100, the ribs in the central part and at the junction with the lateral part of the wing are placed at a shorter distance from each other. This is to reinforce the joint between the central wing and the side wing, as well as the joint with the boom. On the other hand, the way in which the lift is transmitted to the fuselage is through two bolts formed by two ribs each, which are shaped to fit into the main frame of the fuselage to transmit the load. On the other hand, the region near the trailing edge of the central part of the wing has two holes with inserts located in a carbon fiber sheet attached to the fuselage. This is how the center wing is attached to the fuselage: two bolts in the leading edge attachment region and two screws in the trailing edge attachment region.

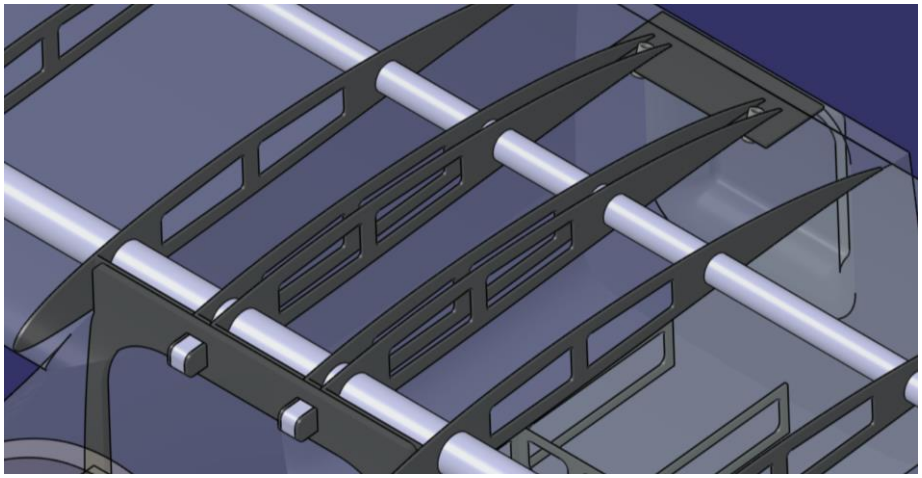

Figure 100. Detail of central wing and fuselage union

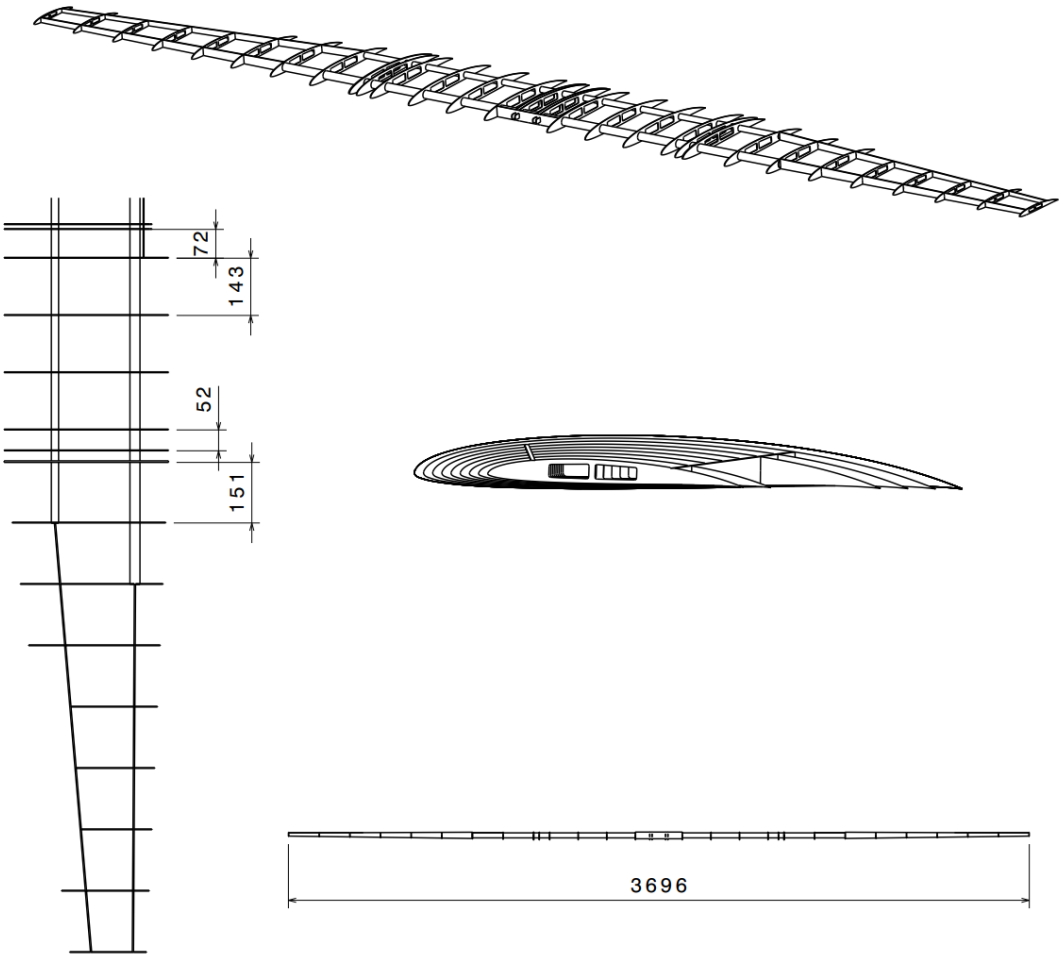

Figure 101. Wing structure drawing (all units are in mm)

4.2.3 Arms and landing gear structure

The arms are of great structural importance in the UAV. Their functions are as follows:

- Serve as support for the vertical thrust motors.

- Withstand the forces of the vertical thrust motors during the takeoff and landing phases.
- Allow the passage of signal and power wiring to the vertical thrust motors and the tail servomotors.
- House the landing gear.

The proposed structure for the arms is a carbon fiber monocoque. Figure 102 shows the arm in designed in CATIA.

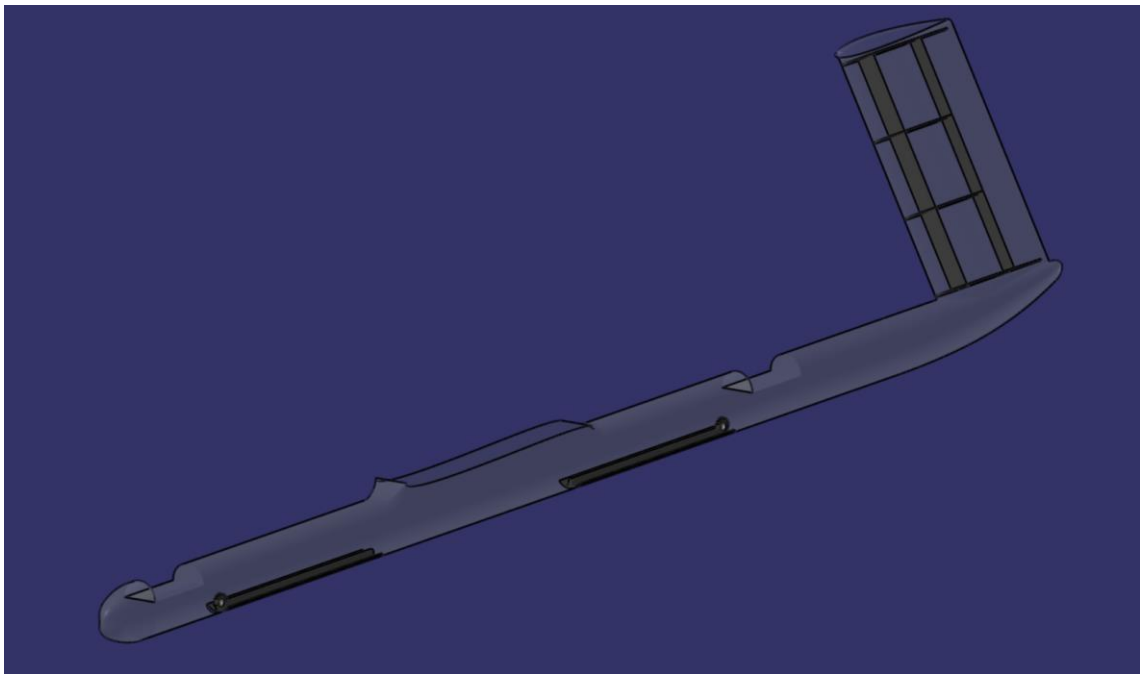

Figure 102. Arm structure

To reduce the number of parts that need to be assembled and to provide sufficient structural rigidity to the arm, the vertical stabilizer is attached to the arm.

Regarding the landing gear, it consists of four retractable legs. For the folding and unfolding mechanism, each leg has a gear that can be operated by a servomotor. This improves flight efficiency by reducing the aerodynamic drag that a fixed and exposed landing gear would generate.

The internal structure of the stabilizers consists of 4 ribs and two spars. Two of the ribs have been cut at the trailing edge to allow for the deflection of the rudder control surface.

Figure 103 shows the landing gear deployed. Notice that enough space has been provided to avoid both gimbal and main propeller to touch the ground.

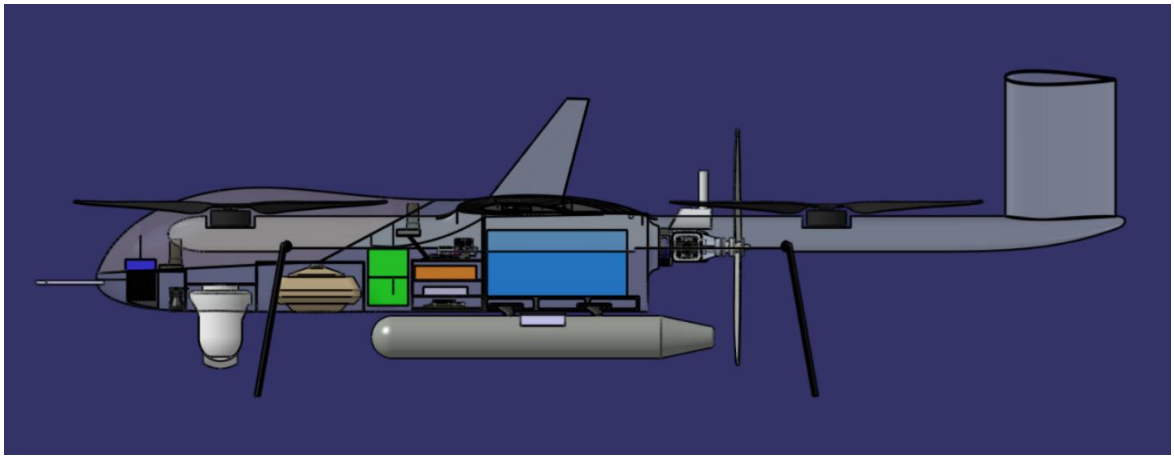

Figure 103.UAV with landing gear deployed

4.2.4 Horizontal tailplane structure

The structure of the HTP is very similar to that of the VTP. It is composed of a carbon fiber skin and an internal structure consisting of seven ribs and two spars. All the ribs are shortened at the trailing edge to allow for the deflection of the pitch control surface. In this regard, the elevator would be divided into two parts at the midpoint, to reduce the load that a single servomotor would have to exert to move it. Therefore, two servomotors are needed to control this surface.

Figure 104 shows the detail of the HTP structure. Notice that, as for the VTP, ribs are provided with holes with two purposes:

- Reducing weight.
- Allowing wires to pass from the arm to the servomotors.

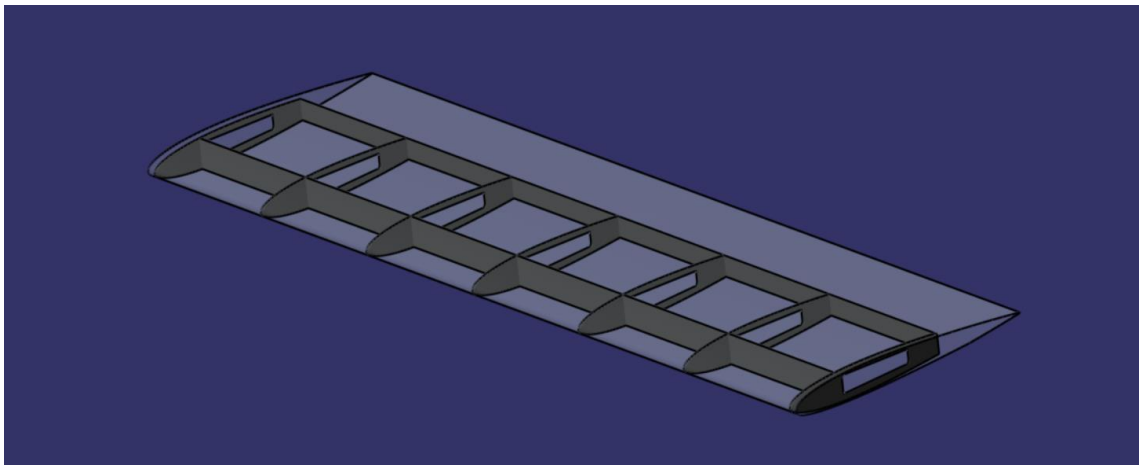

Figure 104. HTP structure

4.3 Flight mechanics

Flight mechanics is a fundamental discipline within aerospace engineering that deals with the forces and moments acting on an aircraft and its resulting motion. It encompasses the study of how aircraft perform under various flight conditions, including takeoff, cruising, maneuvering, and landing. The primary goal of flight mechanics is to understand and predict the behavior of

an aircraft in response to control inputs and external influences such as wind gusts or turbulence.

The core concepts in flight mechanics include the analysis of the aircraft's equations of motion, which describe how the aircraft moves in three-dimensional space. These equations consider the balance of forces, such as lift, weight, thrust, and drag, as well as the balance of moments, which affect the aircraft's rotational motion about its center of gravity. By solving these equations, it can be predicted how the aircraft will react to different flight conditions and control inputs.

Additionally, flight mechanics involves the study of performance metrics such as range, endurance, and maneuverability, which are critical for designing efficient and effective aircraft. Understanding these aspects helps engineers to optimize the aircraft's design for specific missions, ensuring it meets the required performance standards.

A critical component of flight mechanics is ensuring the aircraft's aerodynamic stability. Aerodynamic stability, particularly static and dynamic stability, plays a vital role in determining the aircraft's ability to maintain a steady flight path and respond predictably to disturbances. By linking flight mechanics with aerodynamic stability, engineers can design aircraft that are not only capable of achieving their performance goals but also provide safe and reliable operation under a variety of flight conditions.

4.3.1 Weight estimation

Knowing the weight of an aircraft is crucial for analyzing flight mechanics and stability because it directly influences the forces and moments acting on the aircraft, which in turn affect its performance and behavior in flight. The weight of an aircraft determines the magnitude of the gravitational force that must be counteracted by lift for the aircraft to maintain level flight.

Accurate knowledge of the aircraft's weight is essential for several reasons:

- Lift Calculation: The weight must be precisely balanced by the lift generated by the wings. Understanding the aircraft's weight allows engineers to determine the required lift, which influences wing design and the selection of appropriate flight speeds.
- Performance Analysis: The weight impacts key performance metrics such as takeoff distance, climb rate, cruising speed, and landing distance for typical fixed wing aircrafts. In the proposed design, heavier aircraft requires more thrust for takeoff and landing, since the vertical thrust engines must generate a lift force in their propellers higher than UAV’s weight to ascend.
- Center of Gravity (CG) Position: The weight distribution within the aircraft affects the location of the center of gravity, which is critical for maintaining stability. An improper CG position can lead to unstable flight conditions, making the aircraft difficult to control and potentially unsafe.
- Structural Integrity: Aircraft structures are designed to withstand specific loads. Knowing the weight ensures that the aircraft operates within its structural limits, preventing potential damage or failure.

- Fuel Efficiency: The weight of the aircraft impacts fuel consumption. Heavier aircraft require more fuel to achieve and maintain flight, affecting the overall efficiency and operational costs.

In summary, knowing the weight of an aircraft is fundamental to accurately analyze flight mechanics and stability, ensuring the aircraft can perform as expected while maintaining safety and efficiency throughout its operational envelope.

To address the weight estimation, these will be divided into different sections:

- Structural weight
- Payload weight
- Powerplant weight
- Systems required to fly weight

SUBSYSTEM	ÍTEM	Weight/u (g)	Quantity	Weight (g)	Weight/Subsystem (kg)
Structure	Fuselage skin	1492,42	1	1492,42	9,322
	Fuselage internal structure	708,58	1	708,58	
	Wing skin	3714,72	1	3714,72	
	Wing internal structure	1279,704	1	1279,704	
	Arm skin	840,64	1	840,64	
	Landing gear	66,53	4	266,12	
	VTP internal structure	146,0328	2	292,0656	
	HTP skin	576,52	1	576,52	
	HTP internal structure	151,656	1	151,656	
Payload	Gimbal	1270	1	1270	6,704
	3D mapping sensor	1300	1	1300	
	Spectrum analyzer	750	1	750	
	Spectrum analyzer antenna	32	2	64	
	SAR	3040	1	3040	
	Payload battery	280	1	280	
Powerplant	HT engine	2360	1	2360	19,880
	VT engine	800	4	3200	
	HT propeller	86	4	344	
	VT propeller	95	4	380	
	ESCs	279	4	1116	
	Fuel tank	6800	1	6800	
	Batteries for VT	2640	2	5280	
	Power distribution Board	400	1	400	
Systems required to flight	Autopilot	100	1	100	1,5460
	GPS	40	2	80	
	Computer onboard	250	1	250	
	Pitot tube	100	1	100	
	Rangefinder	30	1	30	
	Radio module	300	1	300	
	Radio module antennas	32	2	64	

	Satellital antenna	102	1	102	
	Servomotors for landing gear	52	4	208	
	Servomotor for control surfaces	52	6	312	
Wiring	Power transmission wiring	1000	1	1000	1,950
	Data wiring	700	1	700	
	Connectors	250	1	250	
Total weight	**39,402 kg**				

Table 4. Weight estimation

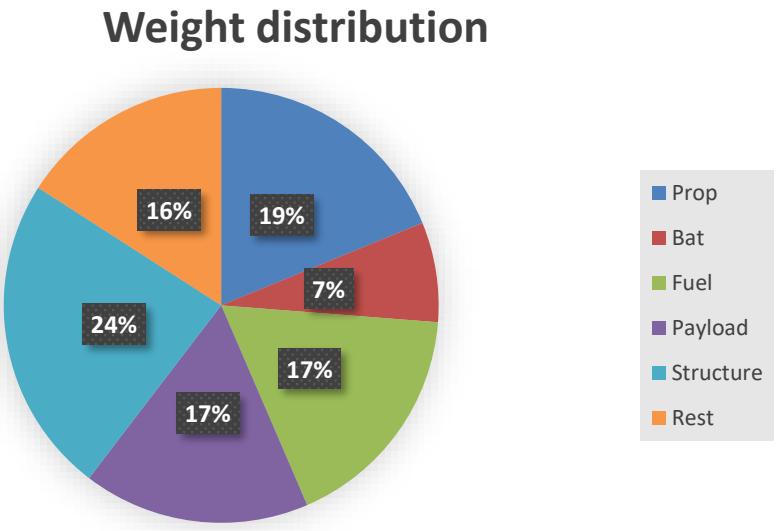

Figure 105. Weight distribution

4.3.2 Engine selection

Selecting an internal combustion engine (ICE) for a fixed wing UAV involves considering a variety of parameters to ensure optimal performance, efficiency, and reliability. Here are the main parameters to take into account:

- **Thrust Requirements**: Determine the required thrust to ensure the UAV can achieve and maintain its desired flight envelope, including takeoff, cruising, and maneuvers.
- **Engine Weight**: The engine's weight should be low enough to avoid excessive impact on the UAV's payload capacity and overall performance.
- **Specific Fuel Consumption (SFC)**: Measure of the fuel efficiency of the engine. Lower SFC means better fuel efficiency, which is critical for extended flight durations.
- **Fuel Type**: The type of fuel used (e.g., gasoline, diesel, or alternative fuels) impacts both the energy density and availability.
- **Horsepower (HP) or Kilowatts (kW)**: The engine must provide sufficient power to meet the UAV's performance requirements, considering factors like altitude, speed, and payload.
- **Power Curve**: How the engine's power output varies with RPM. A broad and flat power curve is often desirable for flexibility in different flight conditions.

- **Altitude Performance**: The engine's ability to perform efficiently at various altitudes, as air density affects engine power.

The required thrust is determined by the aerodynamic drag of the UAV. From the data obtained in Fluent, the necessary thrust for each angle of attack can be determined. However, the aerodynamic drags due to the vertical thrust motors, the EO/IR gimbal, and the SAR have not been taken into account in Fluent, so those increments in drag need to be added. Additionally, the engine must have enough power not only to maintain a cruising condition but also to gain altitude and maneuver.

To be able to dimension the total drag of the UAV, the first step is to obtain the drag coefficients of the bodies that have not been taken into account in Fluent. For this, the bodies will be assumed to be cylinders to approximate their drag coefficients.

$$C_{DgimbalEO/IR} = 1.1$$

$$C_{DSAR} = 0.5$$

$$C_{DVTOL\ engines} = 1.1$$

To be able to add these drag coefficients to that of the UAV, it is necessary to multiply by the reference area of each body and divide it by that of the UAV.

$$C_{DgimbalEO/IR_{UAV}} = C_{DgimbalEO/IR}\frac{S_{ref,gimbal\ EO/IR}}{S_{ref,UAV}} = 1.1\frac{0.016m^2}{1.4m^2} = 0.012$$

$$C_{DSAR_{UAV}} = C_{DSAR}\frac{S_{ref,SAR}}{S_{ref,UAV}} = 0.5\frac{0.007m^2}{1.4m^2} = 0.002$$

$$C_{DVTOL\ engines/IR_{UAV}} = C_{DVTOL\ engines}\frac{S_{ref,VTOL\ engines}}{S_{ref,UAV}} = 1.1\frac{0.006m^2}{1.4m^2} = 0.0047$$

The reference areas used were the wing surface area for the UAV and the cross-section for the bodies. For the VTOL engines, the cross-section of each motor was multiplied by the number of motors (4). Now that all the drag coefficients are applied to the same reference surface, they can be added to the UAV's drag coefficient to obtain the total drag coefficient of the UAV and its equipment.

$$C_{D\ UAV\ Total} = C_{D\ UAV} + C_{DgimbalEO/IR_{UAV}} + C_{DSAR_{UAV}} + C_{DVTOL\ engines/IR_{UAV}}$$

$$C_{D\ UAV\ Total} = 0.04678 + 0.012 + 0.002 + 0.0047 = 0.065$$

With the obtained drag coefficient, applying the cruise conditions, the aerodynamic drag for that condition can be calculated.

$V = 25\ m/s$

$\rho = 1.225\ kg/m^3$

$C_D = 0.065$

$S = 1.4\ m^2$

$$D = \frac{1}{2}\rho V^2 S C_D = 0.5 \cdot 1.225 kg/m^3 \cdot 25^2 m^2/s^2 \cdot 1.4 m^2 \cdot 0.065 = 35.093 N$$

The obtained aerodynamic drag is the thrust that the engine must provide to fly in cruise condition. It is noteworthy that it has significantly increased compared to the drag obtained in Fluent, specifically by 40%, with the EO/IR gimbal being the largest contributor to the drag. In Figure 106, a graph shows the drag contribution obtained from each piece of equipment.

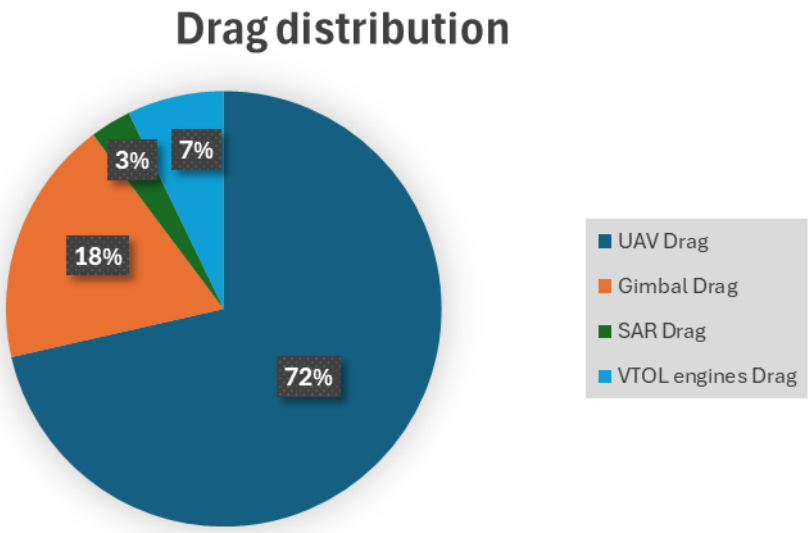

Figure 106. Drag distribution

As can be observed, the EO/IR gimbal is responsible for almost one-fifth of the total drag of the UAV, while the SAR and VTOL engines together account for one-tenth of the drag.

Once the required thrust is known, the engine can be selected considering the most relevant aspects mentioned earlier. By searching other UAVs in the market with similar characteristics to the proposed one, the combustion engine selected has the next characteristics:

- Max power: 7HP at 8500 RPM
- Static thrust: 15.2 kg
- Recommended propeller: 22x10 inches
- Weight including alternator: 2.36 kg
- Fuel consumption: 1.2 l/h
- Alternator power: 180W

Figure 107. ICE with alternator

The data provided for the manufacturer is quite minimal, so it will be necessary to make some assumptions.

It is noteworthy that the propeller plays a fundamental role in propulsion, as it is responsible for transforming the output power from the engine shaft into useful power for flight. This power transformation is achieved through a propulsive efficiency, which depends on the advance ratio J. This parameter depends on the diameter D of the propeller, the number of revolutions n of the engine, and the flight speed V.

$$J = \frac{V}{nD}$$

Brandt, John B., et al. from University of Illinois[5] have provided a database of propellers. Using the proposed propeller for the manufacturer and plotting the data the next graph is obtained:

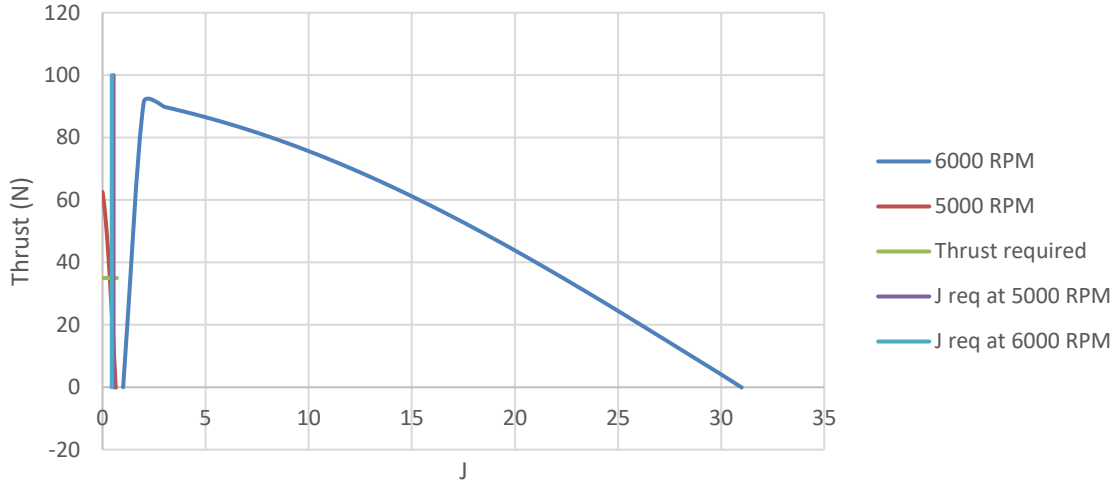

Figure 108. Propeller data

As can be seen in Figure 108, with the proposed propeller the required thrust would be achieved at a flight speed of 25 m/s at 6000 RPM. Regarding the combustion engine, there are no power curves for the shaft in relation to RPM nor specific fuel consumption. Therefore, it would be necessary to conduct tests on an engine test bench to perform these measurements. However, the fuel consumption provided by the manufacturer will be assumed, since the engine seems to have enough power to obtain the desired thrust.

Finally, it must be taken into account that alternator would subtract power from the engine to convert it into electricity.

4.3.3 Stability analysis

Stability is a critical aspect in the design and operation of aircraft, ensuring that the vehicle can maintain its intended flight path and respond predictably to control inputs and external disturbances. In aerodynamics, stability is broadly categorized into static and dynamic stability, both of which play essential roles in the overall behavior and safety of an aircraft.

[5] J. B. Brandt, R. W. Deters, G. K. Ananda, O. D. Dantsker, and M. S. Selig, "UIUC Propeller Database (Vols 1-4)," University of Illinois at Urbana-Champaign, Department of Aerospace Engineering

- Static stability refers to the initial tendency of an aircraft to return to its original state after a disturbance. If the aircraft tends to return to its original attitude, it is considered statically stable. This is an immediate and short-term response, typically assessed by examining the forces and moments acting on the aircraft when it is displaced from its equilibrium position. Static stability can be further divided into longitudinal, lateral, and directional stability, each addressing different aspects of the aircraft's orientation and response.
- Dynamic Stability, on the other hand, involves the aircraft's response over time following a disturbance. An aircraft with good dynamic stability will exhibit damped oscillations that gradually return it to its equilibrium state. This characteristic is essential for ensuring smooth and controlled flight, as it dictates how the aircraft behaves over longer periods following a disturbance.

For the purposes of this analysis, we will focus specifically on static longitudinal stability, which pertains to the stability of the aircraft about its lateral axis. This type of stability is concerned with the aircraft's ability to maintain its pitch angle and, consequently, its angle of attack. Static longitudinal stability is a crucial aspect in the preliminary design phase, as it directly affects the aircraft's ability to maintain a steady flight path without continuous control inputs from the pilot.

To achieve static longitudinal stability, the aircraft must be designed so that any nose-up or nose-down disturbance generates aerodynamic moments that tend to restore the original flight attitude. Key factors influencing this type of stability include the position of the center of gravity (CG) relative to the aerodynamic center, the design of the horizontal stabilizer, and the overall aerodynamic profile of the aircraft.

By focusing on static longitudinal stability, we can ensure that the aircraft exhibits favorable pitch characteristics, leading to safer and more predictable performance. This analysis will provide a foundational understanding that can be further expanded upon when considering the dynamic aspects of stability in future studies.

Based on the results obtained in Aeolus, it has been demonstrated that the aerodynamic moment on the aircraft decreases as the angle of attack increases. In other words, the slope of the moment curve with respect to the angle of attack is negative, which is necessary for the UAV to be longitudinally stable with fixed controls.

To adjust the center of gravity so that the resulting aerodynamic moment about the center of gravity is zero, Ansys simulation will be used in the cruise condition to obtain the aerodynamic moment at the leading edge. Knowing the weight of the aircraft, the distance from the leading edge where the weight must be applied to counteract the aerodynamic moment can be calculated.

$$M_{LE} = Wd$$

$$d = \frac{M_{LE}}{W}$$

The moment about the leading edge obtained is 31.58 Nm, pitching downwards. As result, center of gravity position is 8.3 cm measured from the leading edge downwards. Figure 109 shows the center of gravity position in the UAV.

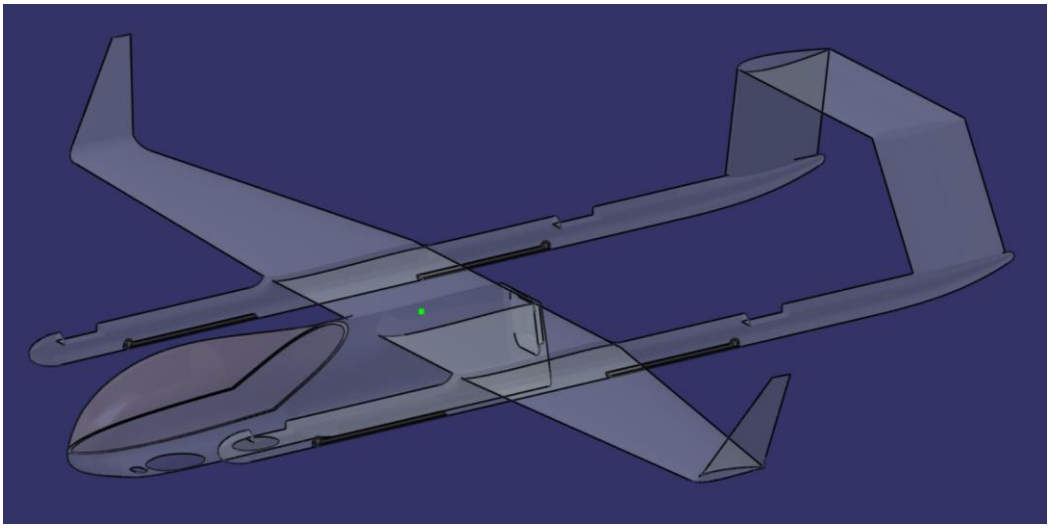

Figure 109. Center of gravity position (green dot) in the UAV

4.3.4 Range estimation

Since data on engine consumption as a function of the power delivered to the shaft is not available, the calculations for maximum range will assume the average consumption provided by the manufacturer. This is 1.2 l/h. Additionally, the preliminary range calculation will be performed by multiplying endurance by cruise speed. It is important to be cautious with the obtained values, as the fuel will decrease throughout the flight, resulting in less lift required as well as less thrust needed.

$$Endurance = \frac{Fuel\ capacity}{Fuel\ consumption} = \frac{10l}{1.2l/h} = 8.33h$$

$$Range = V_{cruise} Endurance = 25m/s \cdot 3.6s/h \cdot 8.33h = 750\ km$$

In this regard, it should be noted that UAV operations generally involve the UAV having to return to the landing site. Therefore, the range is reduced to half of that obtained, resulting in 375 km. In addition, these ranges are normally limited by the communications link, the range of the communications link being less than the operational range of the aircraft. The chosen communications system has a maximum range of 200 km, line-of-sight. Precisely for these reasons, it has been decided to incorporate a satellite antenna into the design, although, as mentioned above, this data link has a very low bandwidth, so that after 200 km from the take-off point, when the satellite communication comes into operation, there will be no capacity to obtain images from the payload sensors.

Chapter 5. CONCLUSIONS AND FUTURE WORK

5.1 Conclusions

The primary objective of this project was to perform a preliminary design a UAV specifically for ISR missions. The UAV was expected to meet several key requirements, including long endurance, sufficient payload capacity, real-time data transmission, autonomous operation, stealth capabilities, adaptability, and interoperability. Here are the main conclusions drawn from the project:

Design Achievement:

The designed UAV meets the primary objective of serving ISR missions effectively. It incorporates a VTOL fixed-wing configuration, which allows for versatile operations in confined spaces without needing auxiliary takeoff and landing systems.

The UAV's structure and systems have been optimized for ISR tasks, ensuring it can carry the necessary payloads such as EO/IR sensors, SAR systems, and SIGINT equipment.

Performance:

The aerodynamic analysis using CFD and Aeolus shows that the UAV achieves satisfactory performance in terms of lift and drag. Although the Fluent simulations indicated higher drag due to the inclusion of the fuselage and arms, the overall design supports stable flight characteristics at the desired speeds and angles of attack.

The UAV's stability analysis confirms that it possesses favorable static longitudinal stability, crucial for maintaining a steady flight path without continuous control inputs.

Payload and Systems:

The UAV is equipped with a modular payload bay that can accommodate various sensors and equipment necessary for ISR missions. This modularity ensures adaptability to different mission requirements.

The integration of advanced communication systems, including MANET and satellite datalink, ensures robust and secure data transmission, crucial for real-time intelligence gathering and dissemination.

Autonomy and Control:

The onboard computer and autopilot systems facilitate high levels of autonomy, enabling the UAV to perform complex missions with minimal human intervention. This includes capabilities for AI-based data processing and decision-making.

Stealth and Survivability:

The design incorporates features to reduce acoustic signature, enhancing the UAV's stealth capabilities. This is vital for operation in contested environments where detection avoidance is crucial.

5.2 Future work

While the project has successfully designed a UAV that meets the initial requirements, several areas require further investigation and optimization to enhance the UAV's performance and capabilities:

Dimension control surfaces

In this project ailerons, rudder and elevators has not been dimensioned. This should be accomplished in future works ensuring the controllability of the UAV.

Improve geometry in fuselage aft region

CFD results has proven that due to recirculation the airflow around the end of the fuselage drains energy, lowering the efficiency of the aircraft. To solve this problem, it is proposed to cover the hole engine, creating a geometry that eases the airflow to remain attached. Also, NACA intakes must be added to cooling down the engine.

Validate CFD results in wind tunnel

Aerodynamics results obtained must be validated by introducing a scaled UAV in a wind tunnel.

Perform an Aeroelastic Analysis:

Conduct comprehensive aeroelastic analysis to evaluate the interaction between aerodynamic forces and structural flexibility. This will help in understanding the impact of aerodynamic loads on the UAV's structural integrity and flight performance, particularly under varying operational conditions.

Optimize Structure:

Further structural optimization is necessary to reduce weight while maintaining strength and durability. Advanced materials and innovative design techniques should be explored to enhance the UAV's efficiency and payload capacity.

Analyze the Transition Phase in Detail:

A detailed analysis of the transition phase from vertical takeoff to fixed-wing flight and vice versa is essential. This phase is critical for mission success and requires precise control algorithms to ensure smooth and efficient transitions.

Obtain the Flight Envelope:

Establish the complete flight envelope of the UAV, defining its operational limits in terms of speed, altitude, and maneuverability. This will aid in planning and executing missions within safe and optimal performance parameters. In order to do that, it will be required to test ICE to gather data required to obtain flight envelope.

Integrate Other Payloads:

Explore the integration of additional payloads such as cargo deployment systems or mini UAV deployment mechanisms. This will extend the UAV's functionality beyond ISR, making it a versatile platform for various mission profiles, including logistics and tactical operations.

By addressing these areas, the UAV's design can be refined and its operational capabilities enhanced, ensuring it meets the evolving demands of modern ISR missions and beyond.

APPENDICES

APPENDIX 1 Electric motor data

Item No.	Prop	Throttle	Voltage (V)	Thrust (g)	Torque (N*m)	Current (A)	RPM	Inputpower (W)	Efficiency (g/W)	Operating Temperature ℃)
V807 KV170	G27*8.8	40%	47.76	4047	1.39	10.41	2732	497.06	8.14	107℃ (Ambient Temperature: 22℃)
		45%	47.69	5059	1.70	13.75	3021	655.50	7.72	
		50%	47.57	6445	2.17	19.81	3383	942.21	6.84	
		55%	47.42	7792	2.56	26.23	3699	1243.82	6.26	
		60%	47.30	9125	2.94	32.61	3993	1542.46	5.92	
		65%	47.06	10968	3.47	43.88	4362	2065.07	5.31	
		70%	46.90	12248	3.84	52.04	4602	2440.62	5.02	
		75%	46.69	13716	4.28	62.32	4867	2909.41	4.71	
		80%	46.49	14969	4.67	71.51	5077	3324.48	4.50	
		90%	46.04	17604	5.45	92.79	5445	4271.76	4.12	
		100%	45.52	19849	6.12	116.62	5785	5308.27	3.74	
	G28*9.2	40%	47.73	4372	1.56	11.04	2698	527.22	8.29	
		45%	47.65	5443	1.88	14.75	2988	702.90	7.74	
		50%	47.52	6915	2.37	21.39	3346	1016.23	6.81	
		55%	47.37	8307	2.77	28.13	3659	1332.57	6.24	
		60%	47.25	9702	3.17	34.67	3943	1637.97	5.92	128℃ (Ambient Temperature: 22℃)
		65%	47.09	11073	3.57	42.37	4199	1995.01	5.55	
		70%	46.82	12865	4.11	55.21	4538	2584.99	4.98	
		75%	46.61	14442	4.56	65.73	4784	3063.87	4.71	
		80%	46.40	15717	4.95	75.55	4983	3505.38	4.48	
		90%	45.93	18275	5.74	97.82	5345	4492.59	4.07	
		100%	45.34	20721	6.46	124.56	5649	5647.55	3.67	
	G29*9.5	40%	47.69	5070	1.87	12.97	2620	618.39	8.20	
		45%	47.59	6276	2.24	17.37	2897	826.77	7.59	
		50%	47.42	7916	2.84	25.28	3240	1199.04	6.60	
		55%	47.26	9558	3.34	33.51	3554	1584.03	6.03	
		60%	47.08	11083	3.82	42.40	3819	1996.30	5.55	
		65%	46.93	12433	4.23	49.99	4042	2346.17	5.30	HOT
		70%	46.62	14312	4.83	65.04	4338	3032.08	4.72	
		75%	46.33	15888	5.31	78.22	4552	3624.20	4.38	
		80%	46.09	17138	5.71	89.68	4727	4133.43	4.15	
		90%	45.54	19498	6.46	115.33	5024	5251.58	3.71	
		100%	44.71	20997	6.93	151.70	5200	6782.02	3.10	

Notes：Motor temperature is the motor surface temperature aftering running on 80% for 10 mins.
(Based on T-MOTOR test bench(es), all data are for reference only. T-MOTOR reserves the right of final interpretation.)

Figure 110. Electric motor data

APPENDIX 2 UAV CFD Residuals

-5 º AoA

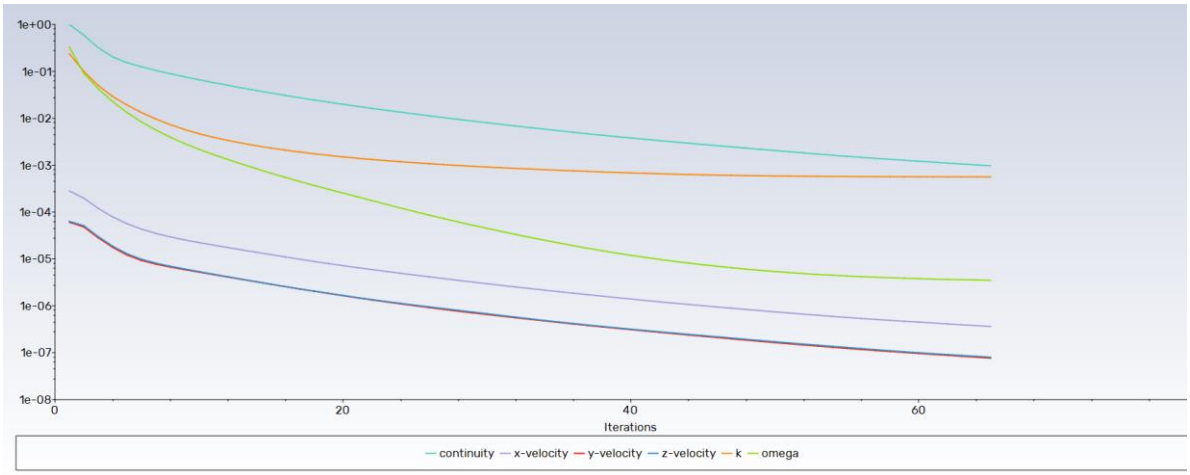

Figure 111. Residuals -5º AoA

-2.5 º AoA

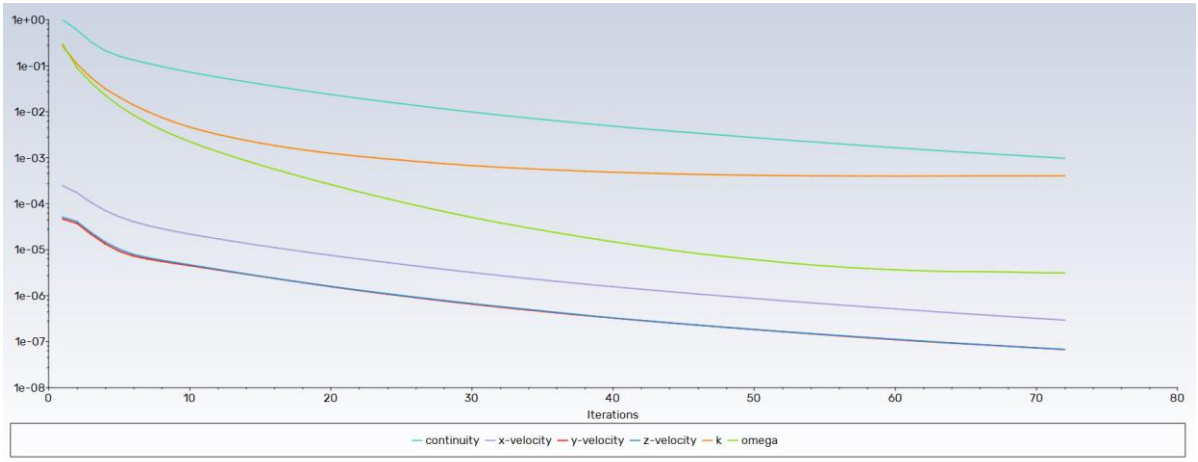

Figure 112. Residuals -2.5º AoA

1.62 º AoA

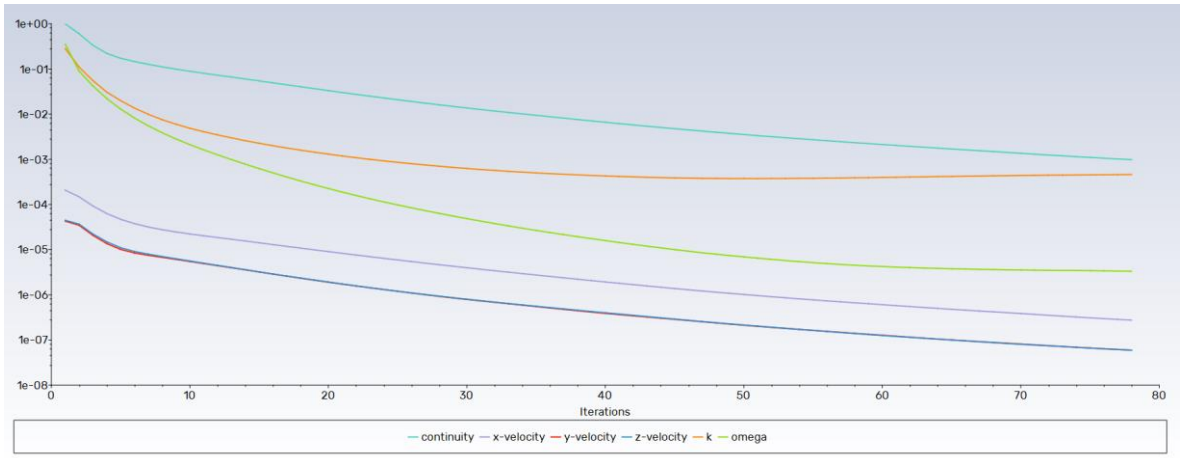

Figure 113. Residuals 1.62º AoA

5º AoA

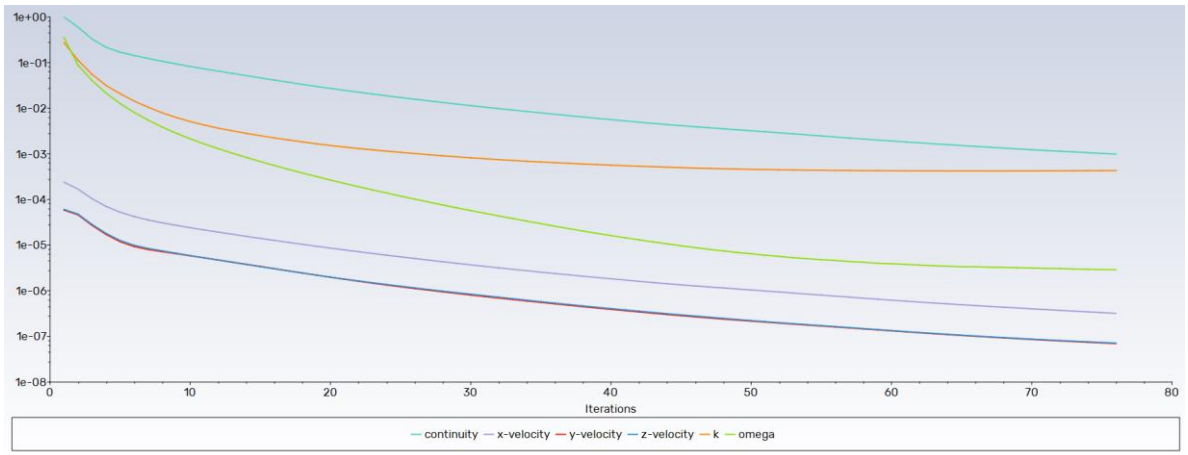

Figure 114. Residuals 5º AoA

7.5º AoA

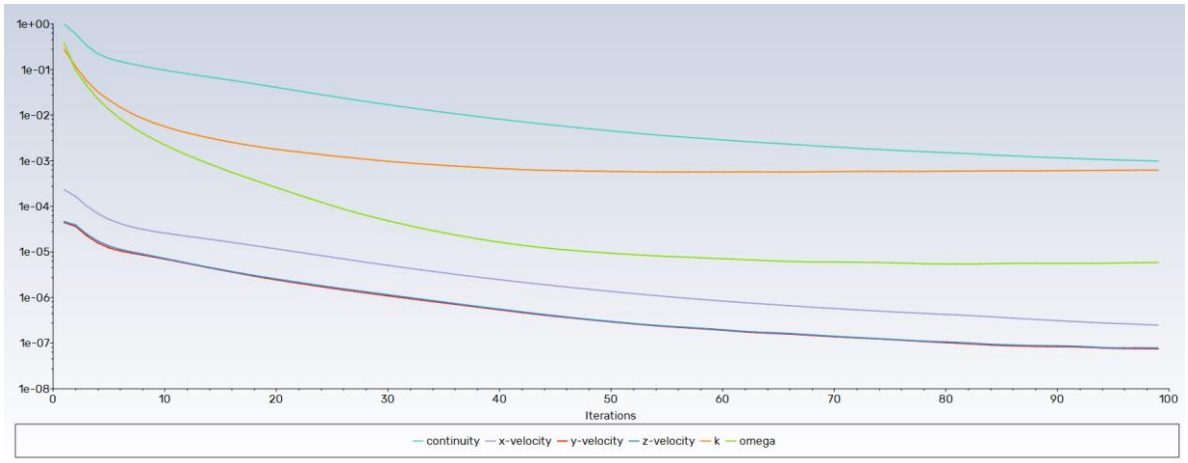

Figure 115. Residuals 7.5º AoA

10º AoA

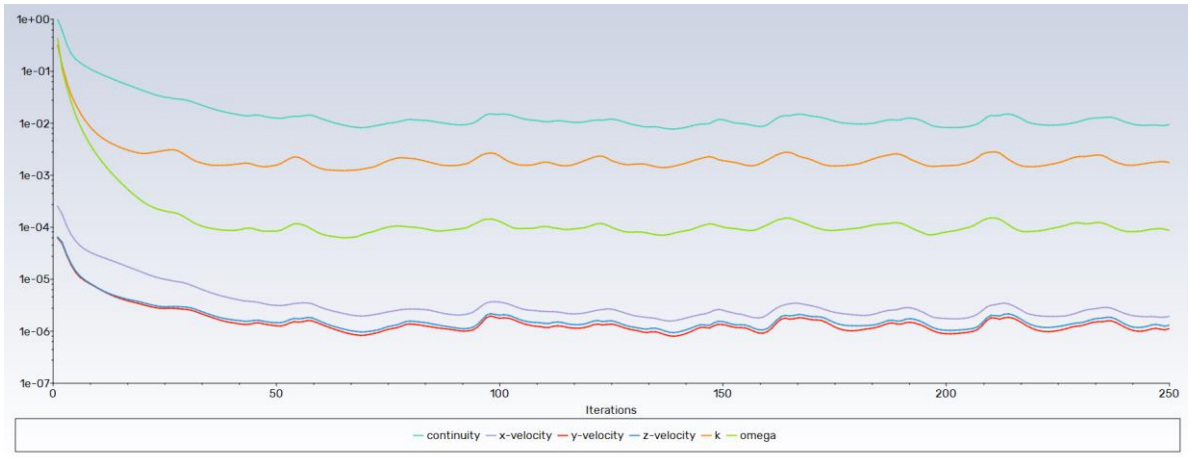

Figure 116. Residuals 10º AoA

12.5º AoA

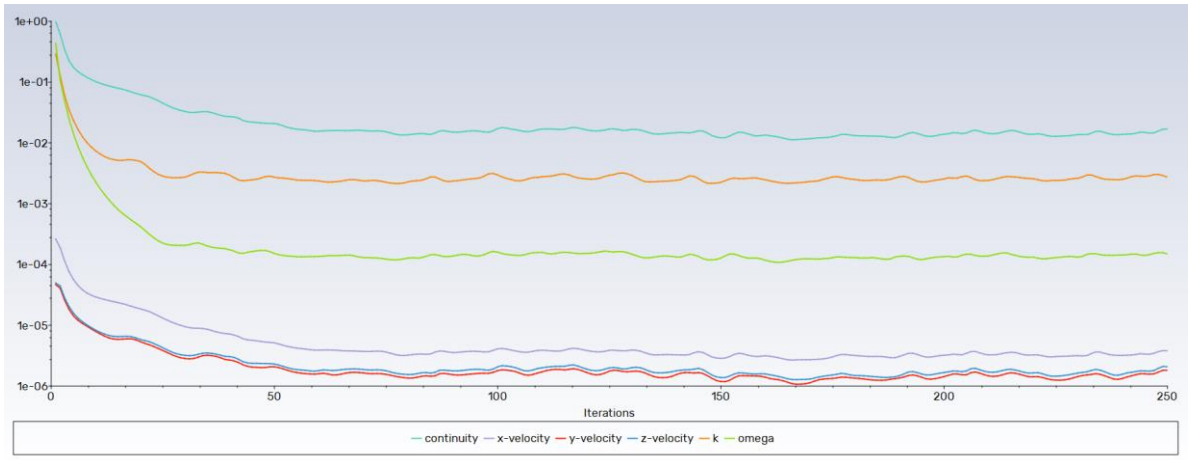

Figure 117. Residuals 12.5º AoA

15º AoA

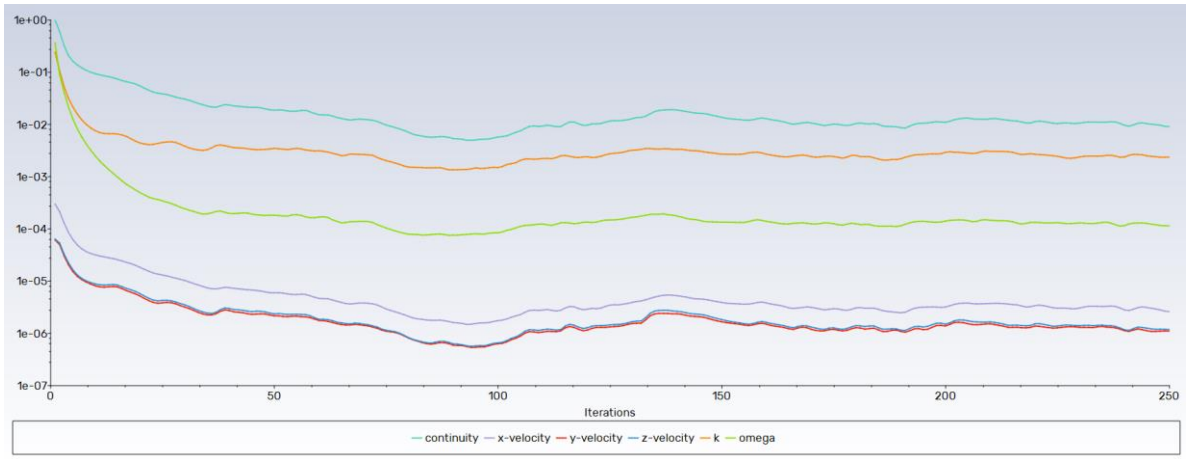

Figure 118. Residuals 15º AoA

APPENDIX 3 Propeller 22x10 Data

6000 RPM

V	J	Pe	Ct	Cp	PWR	Torque	Thrust	PWR2	Torque3	Thrust4	THR/PWR	Mach	Reyn	FOM
(mph)	(Adv_Ratio	-	-	-	(Hp)	(In-Lbf)	(Lbf)	(W)	(N-m)	(N)	(g/W)	-	-	-
0	0	0	0,0764	0,0222	1,992	20,929	20,522	1485,718	2,365	91,281	6,265	0,52	227139	0,757
2,76	0,0221	0,0734	0,0751	0,0226	2,028	21,299	20,195	1511,962	2,406	89,828	6,058	0,52	227263	0,7261
5,53	0,0442	0,142	0,0738	0,023	2,06	21,643	19,838	1536,38	2,445	88,241	5,857	0,52	227397	0,6957
8,29	0,0664	0,2058	0,0724	0,0233	2,09	21,954	19,45	1558,462	2,48	86,515	5,661	0,52	227543	0,6659
11,06	0,0885	0,2652	0,0708	0,0236	2,116	22,225	19,03	1577,714	2,511	84,644	5,471	0,52	227701	0,6365
13,82	0,1106	0,3204	0,0691	0,0239	2,137	22,45	18,575	1593,634	2,536	82,622	5,287	0,52	227870	0,6077
16,59	0,1327	0,3715	0,0673	0,024	2,153	22,62	18,086	1605,734	2,556	80,448	5,109	0,52	228052	0,5795
19,35	0,1548	0,4188	0,0654	0,0242	2,164	22,731	17,563	1613,585	2,568	78,121	4,937	0,52	228246	0,5518
22,12	0,1769	0,4626	0,0633	0,0242	2,168	22,776	17,006	1616,798	2,573	75,644	4,771	0,52	228454	0,5247
24,88	0,1991	0,5029	0,0611	0,0242	2,166	22,751	16,417	1615,029	2,57	73,022	4,611	0,52	228675	0,4982
27,65	0,2212	0,54	0,0588	0,0241	2,156	22,652	15,795	1607,971	2,559	70,258	4,455	0,52	228909	0,4723
30,41	0,2433	0,574	0,0563	0,0239	2,139	22,474	15,144	1595,344	2,539	67,359	4,305	0,53	229158	0,4469
33,18	0,2654	0,605	0,0538	0,0236	2,115	22,214	14,463	1576,892	2,51	64,331	4,16	0,53	229420	0,422
35,94	0,2875	0,6332	0,0512	0,0232	2,082	21,868	13,755	1552,378	2,471	61,18	4,019	0,53	229697	0,3975
38,7	0,3096	0,6586	0,0484	0,0228	2,04	21,435	13,02	1521,579	2,422	57,915	3,881	0,53	229989	0,3735
41,47	0,3318	0,6812	0,0456	0,0222	1,99	20,909	12,262	1484,289	2,362	54,54	3,747	0,53	230295	0,3499
44,23	0,3539	0,7011	0,0427	0,0216	1,931	20,29	11,48	1440,316	2,292	51,064	3,615	0,53	230616	0,3267
47	0,376	0,7181	0,0397	0,0208	1,863	19,574	10,677	1389,484	2,211	47,492	3,485	0,53	230953	0,3038
49,76	0,3981	0,7323	0,0367	0,0199	1,786	18,759	9,854	1331,631	2,119	43,833	3,357	0,53	231305	0,281
52,53	0,4202	0,7433	0,0335	0,019	1,699	17,843	9,013	1266,618	2,016	40,092	3,228	0,53	231672	0,2584
55,29	0,4423	0,7508	0,0303	0,0179	1,602	16,825	8,156	1194,328	1,901	36,277	3,097	0,53	232054	0,2359
58,06	0,4645	0,7543	0,0271	0,0167	1,495	15,702	7,283	1114,672	1,774	32,395	2,963	0,53	232452	0,2133
60,82	0,4866	0,7529	0,0238	0,0154	1,378	14,476	6,397	1027,6	1,635	28,453	2,824	0,53	232866	0,1905
63,59	0,5087	0,7452	0,0205	0,014	1,251	13,145	5,5	933,105	1,485	24,462	2,673	0,53	233296	0,1672
66,35	0,5308	0,729	0,0171	0,0124	1,115	11,71	4,593	831,231	1,323	20,429	2,506	0,53	233741	0,1432
69,12	0,5529	0,7003	0,0137	0,0108	0,968	10,172	3,679	722,089	1,149	16,365	2,311	0,53	234203	0,1182
71,88	0,575	0,6514	0,0103	0,0091	0,812	8,535	2,761	605,867	0,964	12,283	2,067	0,53	234680	0,0916
74,65	0,5972	0,5663	0,0069	0,0072	0,647	6,802	1,842	482,831	0,768	8,195	1,731	0,53	235172	0,0627
77,41	0,6193	0,4029	0,0034	0,0053	0,474	4,976	0,925	353,251	0,562	4,113	1,187	0,53	235678	0,0304
80,17	0,6414	-0,0137	-0,0001	0,0032	0,285	2,997	-0,018	212,753	0,339	-0,081	-0,039	0,53	236123	0

Table 5. 22x10 propeller data for 6000RPM

5000 RPM

V	J	Pe	Ct	Cp	PWR	Torque	Thrust	PWR	Torque	Thrust	THR/PWR	Mach	Reyn	FOM
(mph)	(Adv_Ratio	-	-	-	(Hp)	(In-Lbf)	(Lbf)	(W)	(N-m)	(N)	(g/W)	-	-	-
0	0	0	0,0754	0,0222	1,149	14,482	14,063	856,704	1,636	62,554	7,446	0,44	189296	0,7447
2,3	0,0221	0,0727	0,0741	0,0225	1,169	14,73	13,835	871,363	1,664	61,536	7,201	0,44	189399	0,7144
4,61	0,0442	0,1407	0,0728	0,0229	1,187	14,96	13,586	884,993	1,69	60,429	6,963	0,44	189511	0,6845
6,91	0,0664	0,204	0,0713	0,0232	1,203	15,169	13,315	897,309	1,714	59,227	6,731	0,44	189632	0,655
9,22	0,0885	0,2628	0,0698	0,0235	1,218	15,35	13,023	908,029	1,734	57,926	6,505	0,44	189763	0,6261
11,52	0,1106	0,3175	0,0681	0,0237	1,23	15,499	12,708	916,875	1,751	56,525	6,286	0,44	189903	0,5977
13,82	0,1327	0,3682	0,0663	0,0239	1,239	15,613	12,37	923,579	1,764	55,02	6,075	0,44	190054	0,5698
16,13	0,1548	0,415	0,0643	0,024	1,244	15,686	12,008	927,896	1,772	53,413	5,87	0,44	190215	0,5425
18,43	0,177	0,4583	0,0623	0,024	1,247	15,715	11,624	929,608	1,775	51,705	5,672	0,44	190388	0,5158
20,74	0,1991	0,4982	0,0601	0,024	1,245	15,696	11,218	928,522	1,773	49,899	5,48	0,44	190571	0,4895
23,04	0,2212	0,5348	0,0578	0,0239	1,24	15,628	10,791	924,462	1,766	47,998	5,294	0,44	190766	0,4639
25,34	0,2433	0,5683	0,0554	0,0237	1,23	15,506	10,343	917,267	1,752	46,006	5,114	0,44	190972	0,4387
27,65	0,2654	0,5987	0,0529	0,0235	1,216	15,329	9,876	906,791	1,732	43,926	4,94	0,44	191190	0,414
29,95	0,2875	0,6263	0,0503	0,0231	1,197	15,094	9,39	892,896	1,705	41,765	4,77	0,44	191421	0,3898
32,26	0,3097	0,651	0,0476	0,0226	1,174	14,799	8,886	875,453	1,672	39,525	4,604	0,44	191663	0,366
34,56	0,3318	0,673	0,0448	0,0221	1,146	14,442	8,366	854,344	1,632	37,212	4,442	0,44	191918	0,3426
36,87	0,3539	0,692	0,042	0,0215	1,112	14,022	7,831	829,458	1,584	34,831	4,282	0,44	192185	0,3196
39,17	0,376	0,7082	0,039	0,0207	1,074	13,535	7,281	800,691	1,529	32,385	4,124	0,44	192465	0,2968
41,47	0,3981	0,7214	0,036	0,0199	1,03	12,982	6,718	767,953	1,467	29,88	3,968	0,44	192757	0,2743
43,78	0,4203	0,7312	0,0329	0,0189	0,981	12,36	6,142	731,163	1,396	27,32	3,81	0,44	193063	0,2518
46,08	0,4424	0,7374	0,0298	0,0179	0,926	11,668	5,555	690,253	1,318	24,71	3,65	0,44	193381	0,2295
48,39	0,4645	0,7394	0,0266	0,0167	0,865	10,906	4,958	645,175	1,232	22,055	3,486	0,44	193713	0,207
50,69	0,4866	0,7362	0,0233	0,0154	0,799	10,073	4,353	595,9	1,138	19,36	3,313	0,44	194057	0,1843
52,99	0,5087	0,7264	0,02	0,014	0,727	9,169	3,739	542,424	1,036	16,632	3,127	0,44	194415	0,1613
55,3	0,5309	0,7076	0,0167	0,0125	0,65	8,195	3,12	484,773	0,926	13,876	2,919	0,44	194786	0,1375
57,6	0,553	0,6757	0,0134	0,0109	0,567	7,151	2,496	423,011	0,808	11,1	2,676	0,44	195170	0,1127
59,91	0,5751	0,6231	0,01	0,0092	0,479	6,039	1,869	357,244	0,682	8,312	2,373	0,44	195568	0,0865
62,21	0,5972	0,5338	0,0067	0,0074	0,386	4,862	1,241	287,622	0,549	5,521	1,957	0,44	195978	0,0582
64,51	0,6193	0,368	0,0033	0,0055	0,287	3,623	0,615	214,296	0,409	2,734	1,301	0,44	196400	0,0272
66,82	0,6415	-0,0314	-0,0002	0,0035	0,18	2,272	-0,032	134,399	0,257	-0,141	-0,107	0,45	196760	0

Table 6. Propeller data 5000 RPM

REFERENCES

[1]. M. S. Selig, "Getting started in XFOIL," University of Sheffield. [Online]. Available: https://digitalmedia.sheffield.ac.uk/media/2.+Getting+started+in+XFOIL/1_po90vnfv.

[2]. J. B. Brandt, R. W. Deters, G. K. Ananda, O. D. Dantsker, and M. S. Selig, *UIUC Propeller Database (Vols 1-4)*, University of Illinois at Urbana-Champaign, Department of Aerospace Engineering, 2017.

[3]. M. S. Selig, *UIUC Airfoil Coordinates Database*, University of Illinois at Urbana-Champaign, 2024. [Online]. Available: https://m-selig.ae.illinois.edu/ads/coord_database.html.

[4]. A. Phan and D. Moldovan, "An investigation on the aerodynamic performance of wings with winglets," *Polish Journal of Environmental Studies*, vol. 30, no. 5, pp. 2373-2380, 2021. [Online]. Available: https://psssj.eu/index.php/ojsdata/article/view/137/163.

[5]. M. E. Mirzaei, S. K. H. Ghodsi, and H. Shadmehri, "Improving the aerodynamics of wind turbine blades using CFD simulations," *Journal of Physics: Conference Series*, vol. 2716, no. 1, p. 012056, 2021. [Online]. Available: https://iopscience.iop.org/article/10.1088/1742-6596/2716/1/012056/meta.

[6]. R. Smith, "Systems engineering for the development of UAVs," *Systems*, vol. 11, no. 8, p. 400, 2023. [Online]. Available: https://www.mdpi.com/2079-8954/11/8/400.

[7]. T. Brown and J. Lee, "Advanced UAV navigation systems," *Aerospace*, vol. 8, no. 9, p. 256, 2021. [Online]. Available: https://www.mdpi.com/2226-4310/8/9/256#B21-aerospace-08-00256.

[8]. R. Wendell, "Russia's UAVs and UCAVs: ISR and Future Strike Capabilities," Jamestown Foundation, 2023. [Online]. Available: https://jamestown.org/program/russias-uavs-and-ucavs-isr-and-future-strike-capabilities/.

[9]. F. Götten, D. F. Finger, M. Havermann, C. Braun, M. Marino, and C. Bil, "Full configuration drag estimation of short-to-medium range fixed-wing UAVs and its impact on initial sizing optimization," *CEAS Aeronautical Journal*, vol. 12, pp. 589–603, 2021. [Online]. Available: https://link.springer.com/article/10.1007/s13272-021-00522-w.

[10]. "Unmanned Aerial Vehicles Market," MarketsandMarkets, 2024. [Online]. Available: https://www.marketsandmarkets.com/Market-Reports/unmanned-aerial-vehicles-uav-market-662.html.

[11]. "UAV Market Industry Analysis," Technavio, 2024. [Online]. Available: https://www.technavio.com/report/uav-market-industry-analysis.

[12]. "Unmanned Aerial Vehicles Market Share," Research and Markets, 2024. [Online]. Available: https://www.researchandmarkets.com/reports/4515744/unmanned-aerial-vehicles-market-share.

[13]. T. Brown and J. Lee, "Advanced UAV navigation systems," *Aerospace*, vol. 8, no. 9, p. 256, 2021. [Online]. Available: https://www.mdpi.com/2226-4310/8/9/256.

[14]. G. Hoffmann, H. Huang, S. L. Waslander, and C. J. Tomlin, "Quadrotor Helicopter Flight Dynamics and Control: Theory and Experiment," Stanford University, 2007.

[15]. "Ansys Academic Learning Resources," Ansys, 2024. [Online]. Available: https://www.ansys.com/academic/learning-resources.

[16]. U. Schuster, "Aeolus ASP User Guide," Aeolus Aero, 2023. [Online]. Available: https://aeolus-aero.com/wp-content/uploads/2023/04/UserGuide-Aeolus-ASP.pdf.

[17]. U. Schuster, "Aeolus ASP IR17-01," Aeolus Aero, 2023. [Online]. Available: https://aeolus-aero.com/wp-content/uploads/2023/09/IR17-01.pdf.

[18]. "UAV Market Industry Analysis," Technavio, 2024. [Online]. Available: https://www.technavio.com/report/uav-market-industry-analysis.

[19]. "Unmanned Aerial Vehicles Market," MarketsandMarkets, 2024. [Online]. Available: https://www.marketsandmarkets.com/Market-Reports/unmanned-aerial-vehicles-uav-market-662.html?gad_source=1&gclid=Cj0KCQjwpZWzBhC0ARIsACvjWRMiBPwY1FDcVNODUTrLperEvC20BlHzAgetYR5hHbASWRDZbioBLMMaAqlEEALw_wcB.

[20]. U. Schuster, "Comparison of Aeolus ASP for a Boxwing aircraft," Aeolus Aero, 2024. [Online]. Available: https://aeolus-aero.com/asp/benchmark-study/.

[21]. J. D. Anderson, *Fundamentals of Aerodynamics*, 6th ed. New York, NY, USA: McGraw-Hill Education, 2017.

[22]. S. Gudmundsson, *General Aviation Aircraft Design: Applied Methods and Procedures*, 1st ed. Burlington, MA, USA: Butterworth-Heinemann, 2013.

[23]. W. F. Phillips, *Mechanics of Flight*, 2nd ed. Hoboken, NJ, USA: John Wiley & Sons, 2010.

[24]. GUDMUNDSSON, “APPENDIX C4 – DESIGN OF SAILPLANES,” in *GENERAL AVIATION AIRCRAFT DESIGN*, 2013.